# EOCENE PALEOGEOGRAPHY OF THE ABIQUIU EMBAYMENT IN NORTH-CENTRAL NEW MEXICO

AN INVESTIGATION OF THE STRATIGRAPHIC AND STRUCTURAL CONTROLS INFLUENCING THE PALEO-CHAMA RIVER SYSTEM

---

A Thesis Presented to the

Faculty of the Department of Earth and Atmospheric Sciences

University of Houston

---

In Partial Fulfillment

of the Requirements for the Degree

Master of Science

---

By

Jason Damiañ Kegel

May 2015

**EOCENE PALEOGEOGRAPHY OF THE ABIQUIU EMBAYMENT IN NORTH-CENTRAL NEW MEXICO**

AN INVESTIGATION OF THE STRATIGRAPHIC AND STRUCTURAL CONTROLS INFLUENCING THE PALEO-CHAMA RIVER SYSTEM

____________________________________

Jason Kegel

APPROVED:

____________________________________

Dr. Michael Murphy, Chairman

____________________________________

Dr. William Dupre

____________________________________

Dr. Timothy Lawton

____________________________________

Dr. Peter Copeland

____________________________________

Dean, College of Natural Sciences and Mathematics

# ACKNOWLEGMENTS

First, I would like to thank my committee members for working with me and helping me to accomplish this task. I particularly thank Michael Murphy for working with me in the field and helping me develop my early ideas and knowing when to move on to new ideas. The field work would never have been accomplished without the help and friendship of Kevin O'Keeffe, as well as my dedicated field assistants Bartholomew and Dustin. I would also like to give special thanks to my children Claudia and Kailea for always making me happy even on the worst of days. Lastly, I would like to thank to my wife Eliza, without whom this never would have been possible. She has believed in me every step of the way and I could never have accomplished this without her help. Thanks babe, I love you.

**EOCENE PALEOGEOGRAPHY OF THE ABIQUIU EMBAYMENT IN NORTH-CENTRAL NEW MEXICO**

AN INVESTIGATION OF THE STRATIGRAPHIC AND STRUCTURAL CONTROLS INFLUENCING THE PALEO-CHAMA RIVER SYSTEM

---

An Abstract of a Thesis

Presented to

the Faculty of the Department of Earth and Atmospheric Sciences

University of Houston

---

In Partial Fulfillment

of the Requirements for the Degree

Master of Science

---

By

Jason Damiañ Kegel

May 2015

## ABSTRACT

Geologic models describing Cenozoic uplift and erosion of the southern Rocky Mountains predict a topographic inversion in the Four Corners region (i.e., present day basins were previously topographic highs and vice versa) during the transition from the Laramide orogeny to Rio Grande rifting. This predicts a change in the flow directions of rivers, as well as a distinct change in the sources from which basin sediments were derived. This process is investigated in the Abiquiu Embayment that lies at the junction of the modern Chama and Espanola Basins. The embayment is bound to the northeast by the Tusas-Brazos Uplift and to southwest by the Nacimiento Uplift. The Cañones Fault zone and Embudo Transfer zone bound the embayment along its width. The two studied sedimentary units exposed in the embayment include the Eocene El Rito formation, which unconformably overlies Precambrian to Cretaceous units and was deposited during the waning stages of shortening, and the syn-rift Oligocene Ritito Conglomerate that unconformably overlies the El Rito and was deposited between 25.1 Ma to 27.0 Ma. These two units record the transition from Laramide shortening to Rio Grande extension both directly, through their sedimentology, and indirectly, through their underlying unconformities. Outcrops of these units are located on the Colorado Plateau to the west at an elevation of 2600 m, in the Tusas-Brazos Mountains to the east at 2730 m, and within the rift valley near the Chama River at 1900 m.

This study investigates the unconformity at the base of the Eocene El Rito Formation. Detailed field work addressing the sedimentology, paleoflow, and provenance of the El

Rito is used in conjunction with a digital reconstruction of the unconformity to build a new paleogeographic map. The results show that Eocene canyons trend in the same direction as the modern ones, but are slightly wider and are inset into similar basement rock sequences. This indicates that the modern landscape is mimicking the Eocene geography. I interpret this to result from structural inversion whereby rifting drives reactivation of reverse faults, associated with Laramide basement-cored uplifts, resulting in inversion of the hanging wall to the Tusas-Brazos Laramide thrust fault into a footwall to a normal fault. This implies that structural/topographic high and lows switch places resulting in a minor modification to the landscape.

# CONTENTS

# 1. INTRODUCTION

## 1.1. INVESTIGATING THE EOCENE UNCONFORMITY

This study investigates the El Rito Formation to gain insight into the structural and depositional processes prevalent during and immediately following a widespread Eocene erosional event in north-central New Mexico.  To do this it is necessary to gain an understanding of the paleogeographic setting of the Eocene El Rito Formation that lies stratigraphically above this unconformity. Geologic models (Bauer and Kelson, 2004; and Goteti et al., 2013) describing Cenozoic uplift and erosion of the southern Rocky Mountains predict a topographic inversion in the Four Corners region (i.e., present days basins were previously topographic highs and vice versa) during the transition from the Laramide orogeny to Rio Grande rifting. This predicts a change in the flow directions of rivers, as well as a distinct change in the source from which basin sediments were derived. This process is investigated in the Abiquiu Embayment that lies at the junction of the modern Chama and Espanola Basins and contains geologic features that record the Late-Cretaceous through Cenozoic deformation and sedimentation history. This study investigates the unconformity at the base of the Eocene El Rito Formation. Detailed field work addressing the sedimentology, paleoflow, and provenance of the El Rito is used in conjunction with a digital reconstruction of the unconformity to build a new paleogeographic map

# 2. GEOLOGIC SETTING

## 2.1. REGIONAL OVERVIEW

North-central New Mexico contains a rich geologic history that has been interpreted to reveal the tectonic and depositional systems occurring along the western margin of the North American craton since the Proterozoic (Cather et al., 2006). The area of focus (Figure 1) along the eastern margin of the Colorado Plateau has been influenced by Late Cretaceous to Early Cenozoic Laramide contraction overprinted by Cenozoic rift extension. Variation in age, type of sedimentation, and style of deformation are used by Woodward (1974) to divide the region into three primary physiographic provinces: the Southern Rocky Mountains, the Colorado Plateau, and the Rio Grande Rift.

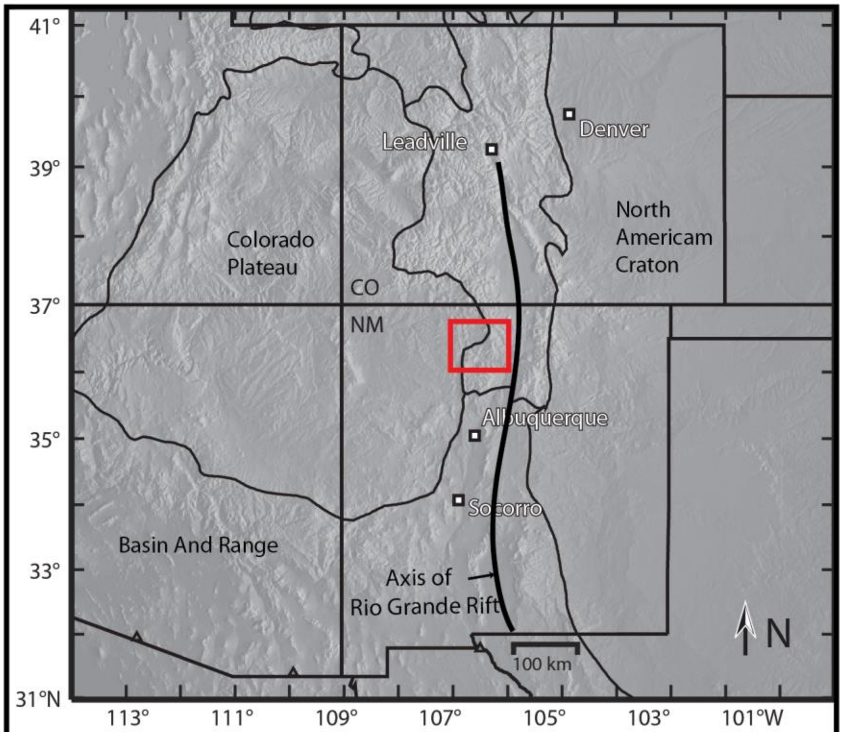


Figure 1: Map of the four corners region of Colorado, New Mexico, Arizona, and Utah illustrating the geographic relationship between the Colorado Plateau the Rio Grande Rift, and the North American Craton. Study area is marked by the red box. Modified from Berglund et al. 2011.

The Tusas-Brazos and Nacimento Uplifts of the Southern Rocky mountains (Figure 2) as well as the Gallina-Arthuleta Arch, the San Juan Basin, and the Chama Basin of the Colorado Plateau developed during the Laramide orogeny (Woodward, 1974). Features related to the Rio Grande Rift overprint the Laramide structures beginning in the Oligocene (Blakey and Ranney, 2008). Although the timing of rift initiation is debated (Kelley, 1979; Chapin and Cather, 1994; Kelley et al., 2013), age variation along the rift has been shown to young to the north (Baldridge et al., 1994). Volcanic and volcanoclastic rocks were deposited in the area beginning in the Late Eocene-Early

Oligocene driven by the San Juan volcanic cluster to the north and the Ortiz and Latir volcanic fields to the east (Cavazza, 1986; Ingersoll and Cavazza, 1991). Volcanism in the Jemez area initiated in the Miocene after development of the rift producing large volumes of extrusive igneous rocks that unconformably overlie the southern Chama Basin and the eastern Nacimiento Uplift (Woodford, 1967).

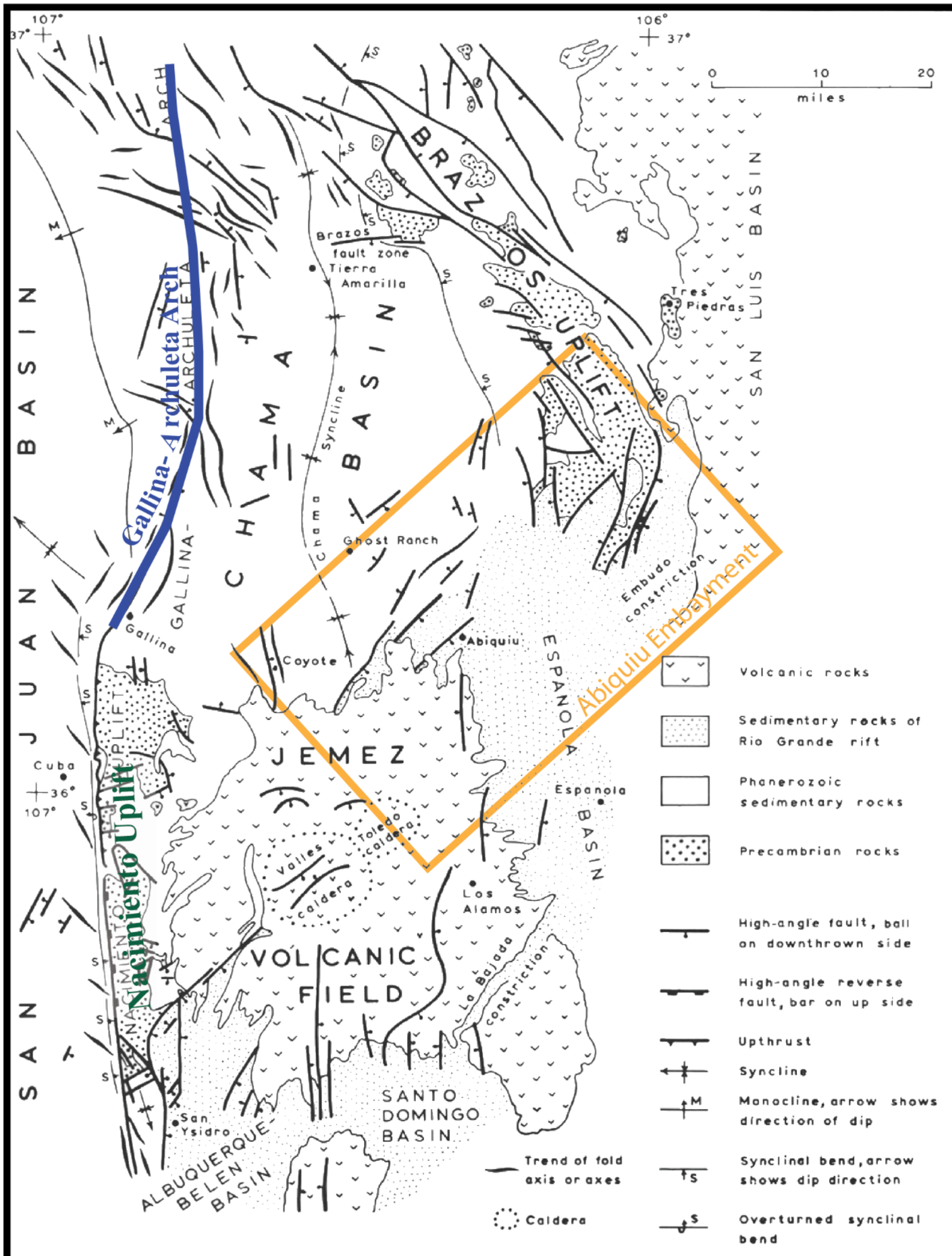


Figure 2: Simplified geologic map of north-central New Mexico modified from Woodward (1974), Abiquiu Embayment and study area highlighted in orange

### 2.1.1 Geology of north-central New Mexico

North-central New Mexico contains many geologic features that provide qualitative and quantitative evidence for numerous depositional, structural, and magmatic case studies (Woodward et al., 1972; Woodward, 1974; DeCelles and Giles, 1996; Seager et al., 1997; Yin and Ingersoll, 1997; Erslev, 2001; Bauer and Kelson, 2004; Cather, 2004; DeCelles, 2004; Tomlinson et al., 2013;). One of the key features influencing the geologic dynamics of the region throughout the Cenozoic is the Colorado Plateau (Cather, 2004). Recently, there has been a debate on the age of the Grand Canyon and how this age can help to constrain the uplift history of the plateau (Karlstrom et al., 2012; Flowers and Farley, 2012). The Colorado Plateau encompasses a large area centered around the Four Corners area of Arizona, New Mexico, Colorado, and Utah (Figure 1 and 3), it is a thick crustal block of relatively high relief that has not experienced the same magnitude deformation as the surrounding terrains (Cather et al., 2008; Moucha, 2008). The eastern portion of the Colorado Plateau within northwest New Mexico is divided into the Chama and San Juan Basins, which are separated by the Gallina-Archuleta Arch.

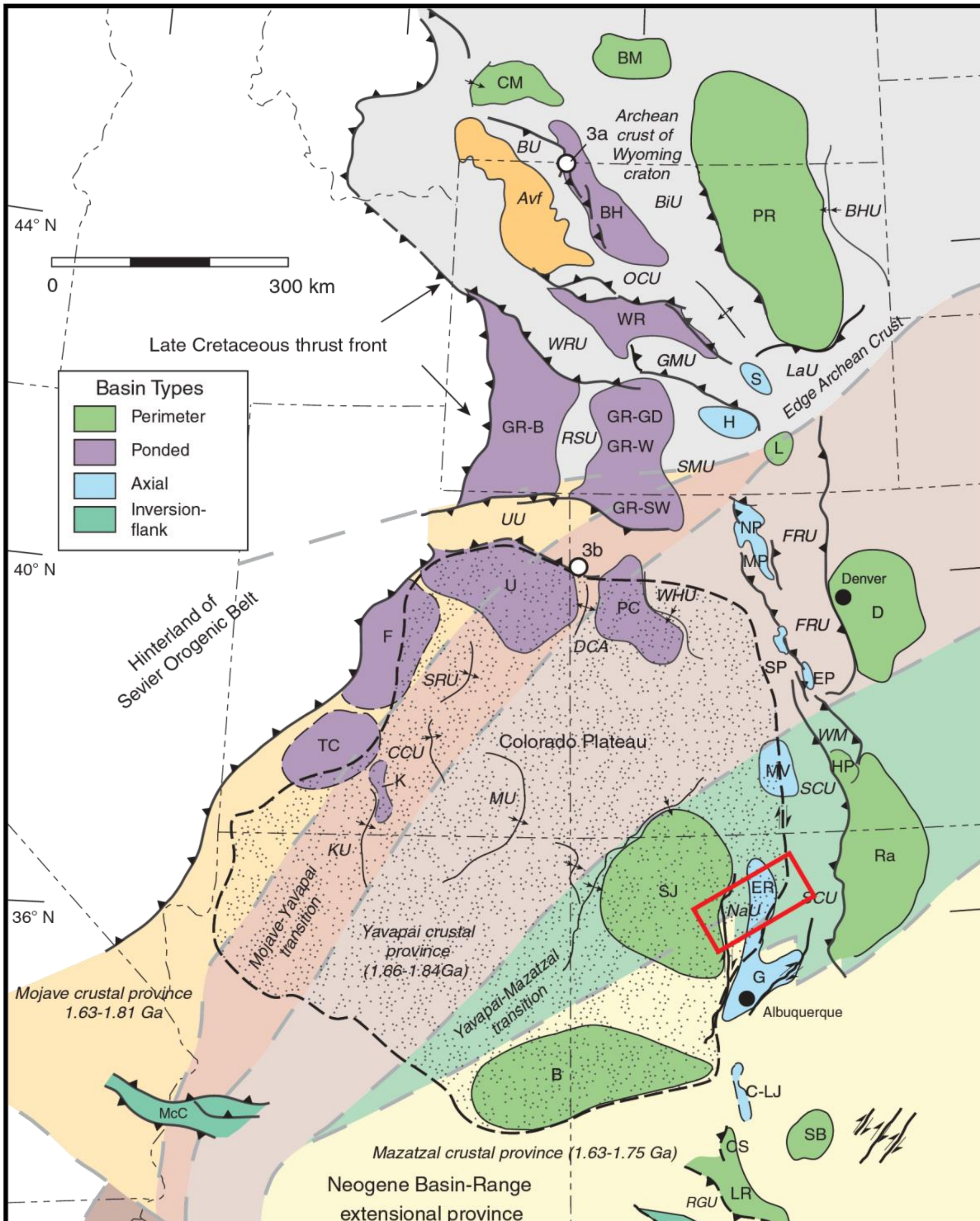


Figure 3: Map of Four Corners area showing Laramide uplifts, basins, and lineaments related to crustal provences. Red outline signifies study area. Modifed from Lawton (2008)

The Chama Basin is a synclinal structure located between the Gallina-Archuleta Arch and the Tusas-Brazos Uplift. The basin is roughly 10 km long in the north-south direction and is about 30 km at its widest point east-west. The highest points of the Tusas-Brazos Uplift and Gallina-Archuleta Arch are 2,133 meters and 457 meters, respectively, above of the lowest point of the Chama Basin (Woodward, 1974). In the northern Chama Basin Cenozoic sedimentary and volcanic rocks overlie Late Paleozoic and Mesozoic sedimentary strata (Smith, 2004); the southernmost portion of the basin contains only Late Paleozoic and Mesozoic sedimentary strata. To the southeast the Chama Basin is separated from the down-dropped Espanola Basin by a set of northeast-striking extensional faults of Neogene age that dip primarily to the southeast (Figure 2). The northeastern margin of the Chama Basin is flanked by steep, west-dipping faults that form the boundary between the Tusas-Brazos Uplift and the Chama Basin.

The Gallina- Archuleta Arch form the western edge of the Chama Basin. It is a north trending monoclinal structure that separates the Chama Basin from the San Juan Basin. The forelimb of the west trending monocline dips steeply towards the San Juan Basin to the west, the back limb gradually dips into the Chama Basin to the east (Woodward, 1974). Structural relief between the Gallina-Archuleta Arch and the San Juan Basin is approximately 2600 meters, slightly less than that between the Gallina-Archuleta Arch and the Nacimiento Uplift bordering the eastern margin of the Colorado Plateau, south of

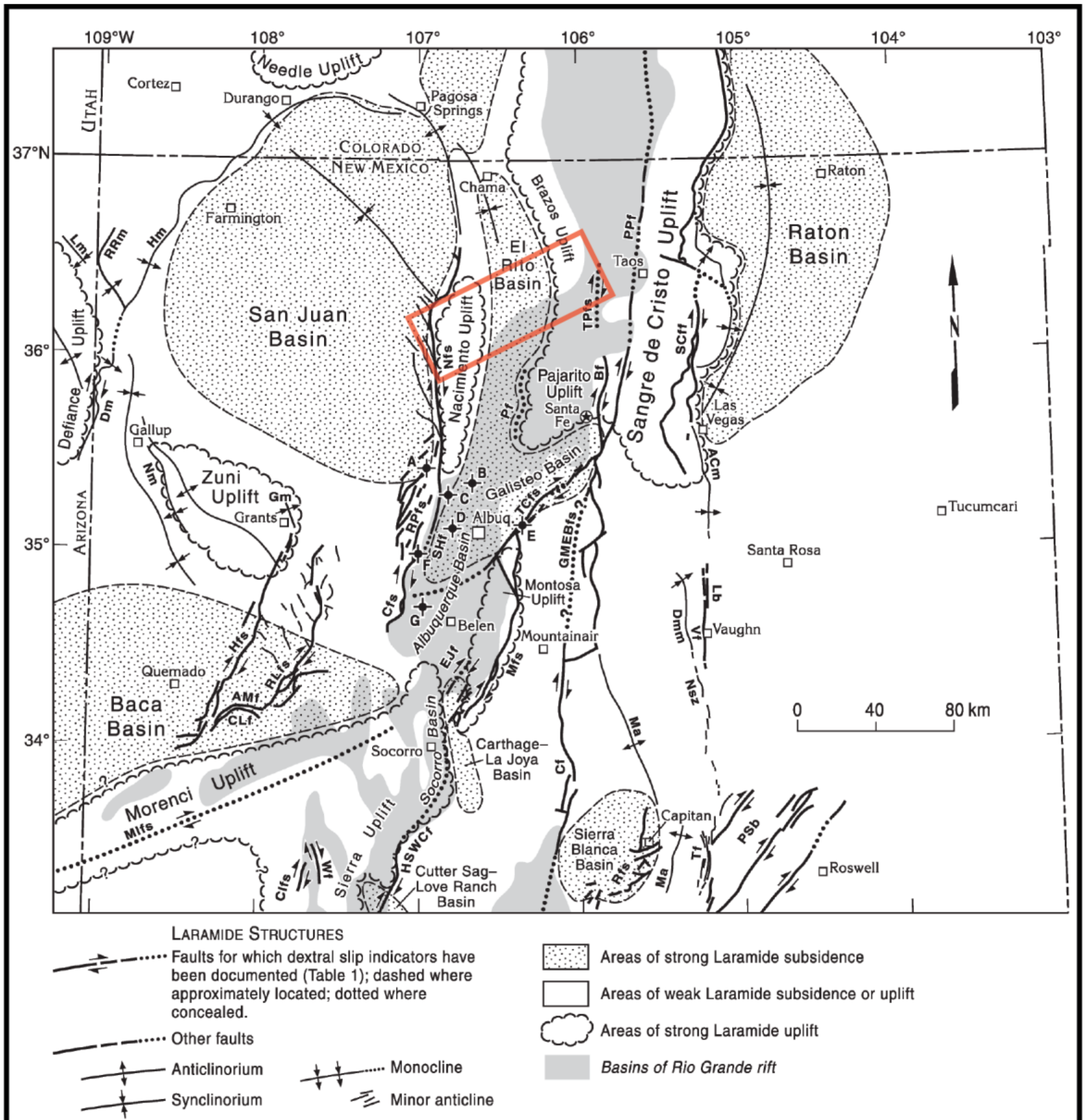


Figure 4: Laramide structures along the northern New Mexico - Colorado boarder from Cather (2004). Study area in red box.

the Chama Basin (Woodward, 1974). The arch and Nacimiento Uplift are interpreted, both from differential thickening of the Lewis Shale (Cather, 2004) and apatite fission track measurements (Kelley and Chapin, 1995), to have begun initial uplift in the Late Campanian. However, the majority of uplift did not occur until the Paleogene during the second stronger phase of Laramide uplift (Formento-Trigilio and Pazzaglia, 1998; Cather, 1999; Cather, 2004).

The San Juan Basin is an asymmetrical synclinal structure with an arc-shaped axis that arcs toward the northwest (Figure 4). This basin initiated as part of Western Interior Basin from widespread tectonic loading derived from the Cordilleran thrust belt to the west between 95 and 80 Ma (Cather, 2004). It has a diameter of approximately 160 km with a shallow southern limb and a steep northern limb. The basin is bordered on its southeastern margin by the Nacimiento Uplift, with a structural relief of roughly 3,050 meters, and on its northeastern margin by the Gallina-Archuleta Arch (Cather, 2004).

Within the Southern Rocky Mountains of the study area, Late Cretaceous to Early Cenozoic Laramide contractional deformation occurred along the eastern flank of the Colorado Plateau resulted in the Nacimento and Tusas-Brazos Uplifts (Figure 4). East of the San Juan Basin the Nacimiento Uplift trends north-south, creating a structural high covering an area approximately 80 km long and 10-16 km wide. It is composed primarily of east-dipping Proterozoic and younger rocks (Woodward et al., 1972). Extrusive volcanic rocks from the Jemez Volcanic Field cover the east-dipping strata along the eastern margin of the Nacimiento Uplift. The northern portion of the Nacimiento Mountains trend into the Gallina-Archuleta Arch where a north-plunging faulted anticline is responsible for uplift (Woodward, 1974). Steeply east-dipping reverse faults that flatten at depth are exposed near the surface and are interpreted to be responsible for uplift of the central and southern portions of the Nacimiento Uplift (Karlstrom and

Daniel, 1993). The kinematics of the faulting associated with the Nacimiento Uplift remain controversial. Some workers propose that dip-slip motion is primary while others suggest large amounts of strike slip (Cather, 2004).

From northern New Mexico to southern Colorado the Tusas-Brazos Uplift extends 80 kilometers northwest-southeast and is about 40 km wide. It is comprised of Proterozoic basement rocks and overlain in areas by Tertiary volcanic and clastic rocks. To the south the uplift is segmented by Neogene extensional faulting associated with Rio Grande rifting (Koning et al., 2013). Structural relief between the Tusas-Brazos Uplift and basins to the east associated with Rio Grande rifting is estimated to be 3,658 meters (Shaffer, 1970). The long-lived Tusas-Picuris Fault records multiple slip events dating back to 1.2-0.8 Ga (Cather et al., 2006), and bounds the eastern margin of the uplift.

In north-central New Mexico the Espanola Basin and San Luis Basins within the Rio Grande Rift have overprinted extensional deformation associated with shortening within the southern Rocky Mountains (Woodward, 1974). The Espanola Basin is bounded on the northwest by southeast-dipping normal faults of Neogene age associated with the northeast-dipping Pajarito Fault zone creating a northwest-dipping half graben. This half graben defines the Espanola Basin which is elongate north-south covering an area 65-80 km in length with a width of 30-65 km (Woodward 1974). The basin is filled by syn-rift sedimentary rocks of Eocene, Oligocene, and Miocene age, as well as Cenozoic igneous and volcaniclastic rocks derived from the San Juan, Latir, and Jemez volcanic fields. The sediments of the Espanola Basin overlie older Triassic and Jurassic rocks that exhibit folding from earlier tectonism (Cavazza, 1986). The San Luis Basin is east of the Tusas-Brazos Uplift and north of the Espanola Basin. It is elongate north-south and covers an area 196 km in length and 119 km in width. The basin is composed of Eocene and younger clastics and volcanics that sit directly on granitic basement (Golombek at al., 1983), indicating the San Luis Basin was part of a Laramide uplift prior to inversion due to Neogene Rio Grande Rift extension. The San Luis Basin tilts primarily to the east bound by the west-dipping Sangre de Cristo Fault zone. The Espanola and San Luis Basins are separated by the northeast-southwest-striking Embudo transfer zone that connects the west-dipping Sangre de Cristo Fault zone the east-dipping Pajarito Fault zone (Aldrich and Dethier, 1990).

### 2.1.2. Laramide Orogeny

The Laramide orogeny is defined by both a structural style and an age range. The age range definition for the Laramide is a Late Cretaceous to Early Cenozoic event within the Rocky Mountain involving basement style deformation (Lawton, 2008). The "Laramide" used as a structural style term refers to specific compression-related basement-cored uplifts and adjacent basins that formed in the region during the Late Cretaceous to Paleogene. In this paper the Laramide orogeny will be referred to within the context of the structural style definition. The basins and uplifts encompassing the Laramide orogeny encircle the less deformed Colorado Plateau (Figure 1 and 3) and extend north from Sonora, Mexico to Central Montana (Lawton, 2008). The structures of the Laramide Province are dominated by moderate-high-angle reverse faulting and back-thrusts that uplift Proterozoic crystalline and younger sedimentary and volcanic rocks. Primarily north-south-trending basins that were the locus of Late Cretaceous to Eocene, fluvial, alluvial, and lacustrine sedimentation are interspersed between uplifts (Yin and Ingersoll, 1997; DeCelles, 2004). The Laramide orogenic belt is ~800-1200 km inboard of its paleo-arc location, offering evidence for a shallow subduction angle of the Farallon plate as it moved beneath North America (Dickinson et al., 1988).

### 2.1.3. Rio Grande rifting

The Rio Grande Rift is a Cenozoic age continental rift extending from central Colorado to Northern Mexico over a distance of more than 1000 km (Baldridge et al., 1994) (Figure 5). The rift narrows northward from a broad extended region in the south, encompassing numerous horsts and grabens, to a narrow graben in Colorado (Figure 5). The rift marks the boundary between the deformed, topographically high Colorado Plateau and the low lying mid-continent plains of the United States. Some of the basins of the Rio Grande Rift are asymmetric half-grabens, averaging 50 km in width and 5-6 km of sediment thickness (Chapin and Cather 1994). Rifting is interpreted to be episodic and produced records of various events from the late Cenozoic to the Quaternary, with the most amount of sediment deposited in the middle to late Miocene (Ingersoll, 2001). The spatial extent of rifting was minimal in the late Oligocene to early Miocene where sediments were mainly composed of volcaniclastic material (Smith et al., 2002).

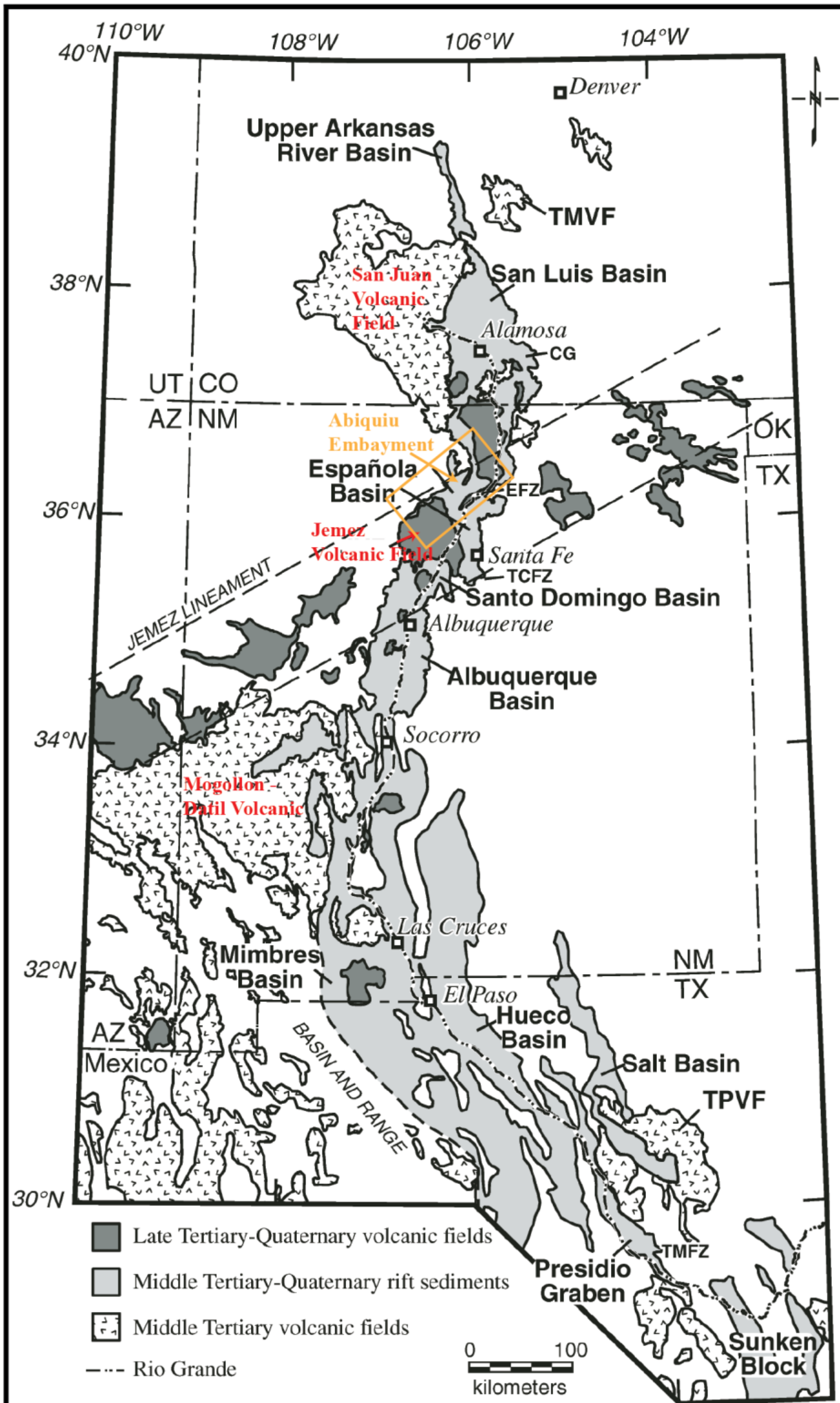


Figure 5: The Rio Grande Rift basins and surrounding volcanic centers from Hudson and Grauch (2013)

Initiation ages for the rift have been highly debated. Recent initiation ages within the study area have been estimated at 27 – 30 Ma by Kelley et al. (2013). Keller and Cather (1994) suggested that initial spreading began in the Late Oligocene to Early Miocene based on the age of the earliest rift-related sedimentary rocks. Ingersoll (2001) argues that sediment deposition during the formation of Rio Grande basins constrains the initiation of east-west extension to approximately 21-16 Ma. Rifting and sedimentation has been interpreted to have occurred most rapidly between 17 and 10 Ma (Ingersoll et al., 1990). The Rio Grande Rift also records changes in volcanism, beginning approximately 35 Ma and active until nearly 60 ka within the study region (Hudson and Grauch, 2013). Erosional denudation greatly attributed to the topography of the rift's landscape. This is evident by the wide-spread removal of Mesozoic and early Cenozoic strata through Quaternary incision.

The Rio Grande Rift is interpreted to have reactivated several structures built by the Laramide orogeny, thereby inverting the Laramide uplifts. A system of high-angle normal faults making up the  Picuris-Pecos system, east of the study area near Taos, bounding the San Louis Basin and the Sangre de Cristo Uplift, show approximately 6 km of offset (Ingersoll, 2001). The Picuris-Pecos Fault is interpreted to have been reactivated several times from the Precambrian through the Laramide orogeny. Reactivation along the southwestern side of the Nacimiento Mountains, along an eastward-dipping high-angle fault, has been attributed to extensional strain. Laramide structures reactivated due to extensional deformation are observed between the upper Nacimiento Uplift and the Abiquiu embayment where the NW-SE-trending Mesa Penabetal normal fault shows approximately 300 meters of structural relief attributing to the ~1 km of total structural relief between the two structures (Ingersoll, 2001).

### 2.1.4. Abiquiu Embayment

The Abiquiu Embayment encompasses the focus area of this paper. It is a shallow, early extensional basin of the Rio Grande Rift located in the northern portion of the Espanola Basin along the margin of the Colorado Plateau and the Rio Grande Rift (Maldonado, 2013). Cenozoic rocks within this embayment include the Eocene El Rito Formation, Oligocene Ritito Conglomerate, Oligocene–Miocene Abiquiu Formation, and Miocene Chama–El Rito and Ojo Caliente Sandstone Members of the Tesuque Formation (Santa Fe Group) (Figure 6). The El Rito Formation, Ritito Conglomerate, and Abiquiu Formation are the deposits of particular interest to this study. Volcanic rocks within the embayment include the Lobato Basalt (Miocene; ca. 15–8 Ma), El Alto Basalt (Pliocene; ca. 3 Ma), and dacite of the Tschicoma Formation (Pliocene; ca. 2 Ma). Quaternary deposition in the embayment is made up of axial and side-stream deposits of the ancestral Pleistocene Rio Chama as well as landslide, pediment, alluvium, colluvium, and Holocene channel and floodplain deposits of the modern Rio Chama (Maldonado et al., 2013).

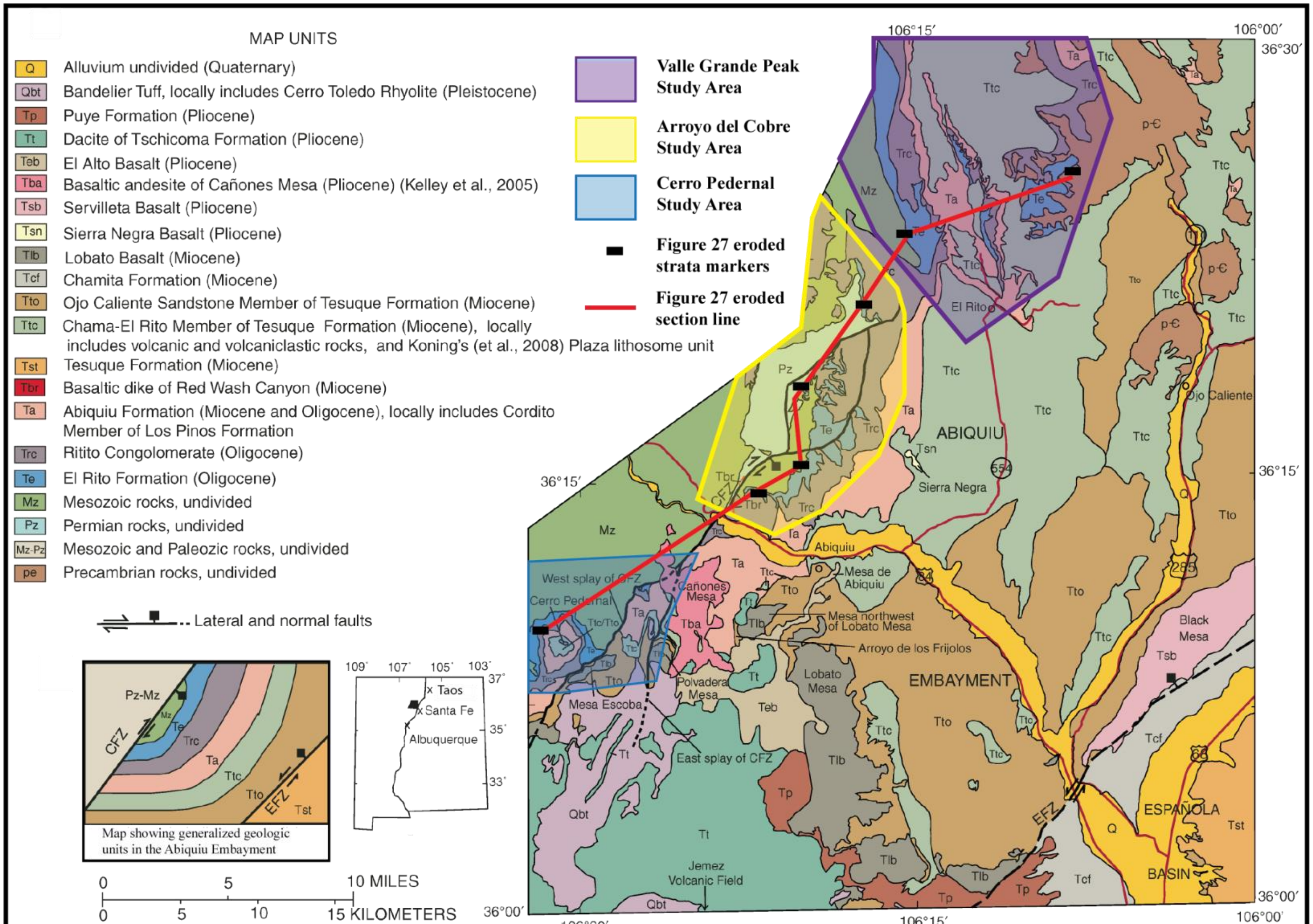


Figure 6: Geologic map modified from Maldonado et al. (2013) showing the Abiquiu Embayment and study areas.

The Abiquiu Embayment is an early Rio Grande Rift related feature that over prints the northern portion of the Paleogene-Eocene El Rito Basin (Maldonado et al., 2013). It is approximately 60 km northeast to southwest bound between the Tusas-Brazos Uplift in the northeast and the Nacimiento Uplift and Jemez Mountains to the southwest. The Cañones Fault zone in the north and Embudo Transfer zone to the south bound the ~ 28 km width of the embayment.

The Cañones Fault zone is the westernmost bounding fault of the Rio Grande Rift, and marks the boundary between the Espanola Basin and the Chama Basin. It displaces Mesozoic through Cenozoic strata along strike (Figure 6). The Early Permian-Late Triassic (~290-200 Mya) footwall strata are sub-horizontal and the Middle Jurassic-Oligocene hanging wall strata are folded into a west-verging shortening-related monocline (O'Keeffe, 2014). The Cañones Fault zone, on average, strikes N33°E with an average dip of 68°SE (O'Keeffe, 2014). The fault strike changes to an east-west direction in the north where it splays develop forming antithetically-dipping faults. Slickenlines have average rakes of 78°NE and 73°NE, suggesting a minor component of right-lateral strike-slip accompanying an otherwise primarily dip-slip sense of motion. Maldonado et al. (2013) measured vertical displacement of 335 m and right-lateral movement of ~2 km. Right-lateral slip rates have been estimated at 101 m/m.y. (Maldonado et al., 2013). The vertical offset is constrained by the 10-8 Ma Lobado Basalt flow showing ~550 m of offset and the younger ~3 Ma El Alto basalt flow that shows no offset. Vertical slip rates for the Cañones Fault zone decrease eastward from the Colorado Plateau to the western edge of the Abiquiu embayment and range from 16 m/m.y. to 42 m/m.y..

2.1.5. Pre-existing structures

The geometry and kinematics of ancient (Proterozoic) underpinning structures can be used to describe the geometrical similarity of temporally separated structures in north-central New Mexico. Many Paleozoic-Cenozoic overprinting structures are geometrically and kinematically similar to or affected by structures formed by earlier tectonism in north-central New Mexico (Chapin and Cather, 1994; Ingersoll, 2001; Karlstrom et al., 2004; Magnani et al., 2004). Cenozoic structural trends observed within the study area, and in other areas in the southwest, are similar to those active during the time of the Ancestral Rocky Mountains in the late Paleozoic (Karlstrom et al., 1999). Magnani et al. (2004) and Karlstrom and Daniel (1993) argue that the Jemez Lineament is the surface expression of a long-lived volcanic and tectonic boundary inherited from suturing of the Mazatzal accreted island arc terrain and the Yavapai proto-North American craton at 1.68-1.65 Ga (Figures 3 and 23). Volcanism began in the central portion of the Jemez lineament at 13.2 Ma, the southwest end around 9.8 Ma, and the northeast end about 8.2 Ma (Magnani et al., 2004). East of the Colorado Plateau, along the Jemez Lineament, sits the Jemez Volcanic Field where the Valles Caldera and the Toledo Caldera are found. The southwestern edge of the Embudo Transfer Fault terminates at the Jemez Volcanic Field and connects with the east-dipping Pajarito Fault zone (Maldonado et al., 2013). Structures associated with Laramide shortening south of the transfer are primarily west-vergent and east-dipping; structures north of the transfer are primarily east-vergant and west-dipping (Cather, 2004). This orientation is similar to structures associated with Rio

Grande Rift extension where dips south of the transfer are primarily to the east, and north of the transfer structures dip primarily to the west.

## 2.2. EOCENE PALEOGEOGRAPHIC INTERPRETATIONS

Eocene paleogeography throughout the western United States has been studied by many authors (Gorham and Ingersoll, 1979; Logsdon, 1981; Ingersoll and Cavazza, 1991; Baldridge et al., 1994; Cather, 2004; Galloway et al., 2011; Fan et al., 2011) to model the depositional and structural controls in the waning stages of the Laramide Orogeny. Many of these authors are also concerned with the unique climate variations during the epoch. The Laramide Orogeny was in its waning stages during the Eocene (Cather, 2004), during a period of unique change in climate. The early Eocene experienced a very wet environment during the Eocene Climate Optimum (Figure 7) that shifted to a dry and cold period toward the late Eocene (Zachos et al., 2001). This coincidence of climate change and structural compression has led to many differing ideas on the role of paleo-rivers and denudation, making interpretations of the paleogeography useful in understanding the links between kinematics, deposition, erosion, and climate.

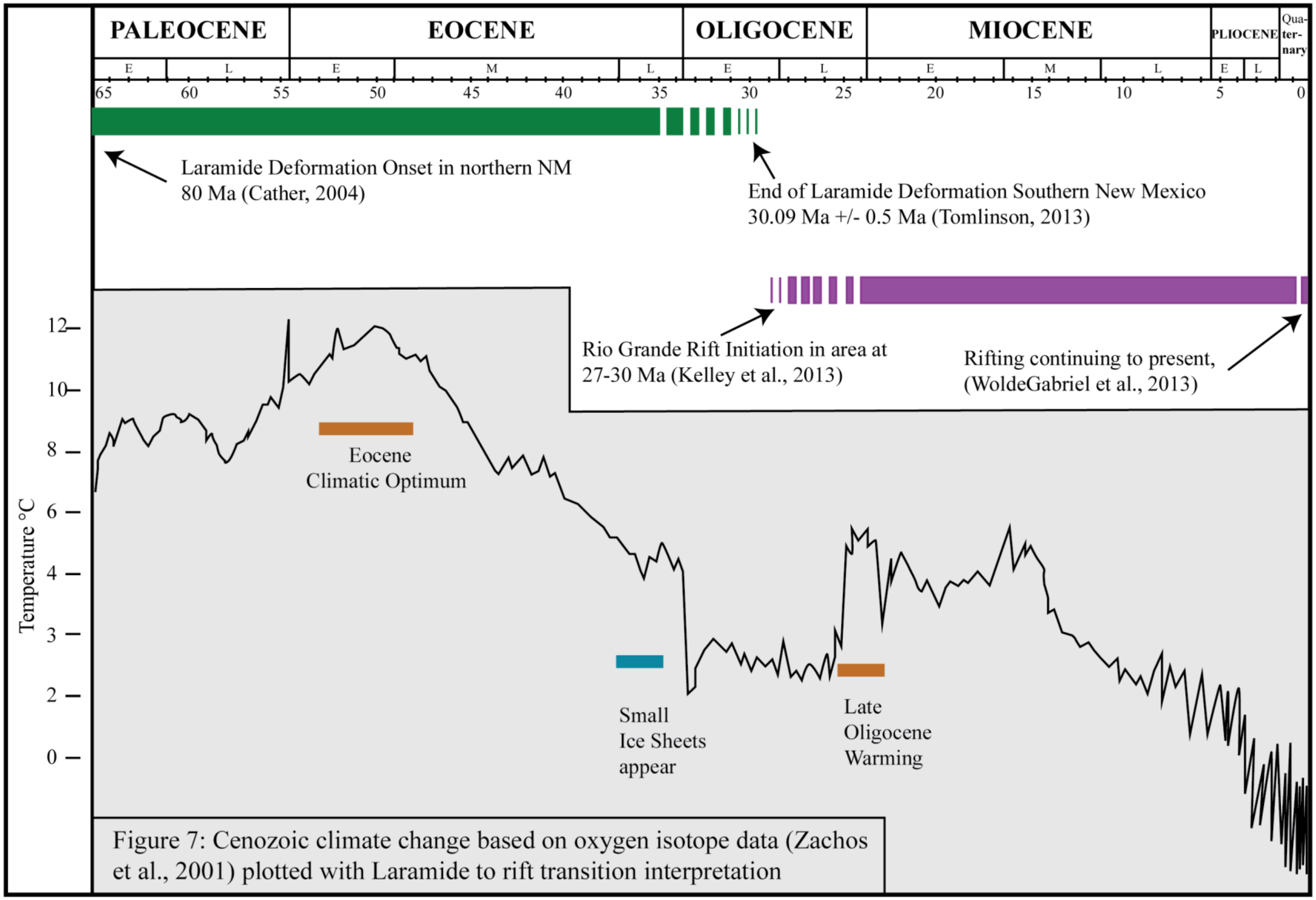


Figure 7: Cenozoic climate change based on oxygen isotope data (Zachos et al., 2001) plotted with Laramide to rift transition interpretation

### 2.2.1. Different interpretations of local and regional geography

Galloway et al. (2011) describes the paleo-drainage into the Gulf of Mexico to have been influenced by Paleocene through Eocene rivers traveling south-southwest across the Colorado Plateau and through the Laramide basins making up northern New Mexico. This broad regional view of an overall southwesterly drainage patterns during the late stages of Laramide uplift is commonly accepted. When the drainage patterns are interpreted at a more local level, variations in interpretation become apparent. In the Four Corners region, and more locally in the Abiquiu Embayment area, several authors have constructed interpretations addressing the paleogeography during the Eocene.

Logsdon (1981), Ingersoll et al., (1990), Cather (1992), , and Cather (2004) have published paleogeographic interpretations that illustrate conflicting ideas regarding the placement and magnitude of the paleo-Chama river system (Figures 8-11). Ingersoll et al. (1991) depicts a large braided river within an axial basin flanked by the Tusas-Brazos Uplift and the Nacimiento Uplift and restricted to the north by the Gallina-Archuleta Arch. Ingersoll et al. also report that the El Rito Basin may drain into an interior lake within the Galliesto Basin. Cather (2004) interprets the area from a more regional perspective, but pays close attention the El Rito Basin. He illustrates a system of small to medium size rivers feeding the axial basin El Rito Basin with no evidence for lacustrine deposition. Cather (1992) goes into greater detail and alludes to a northern source feeding the system from outside the Gallina-Archuleta Arch by the late Eocene providing for a change in magnitude of the river system. Logsdon (1981) shows the El Rito Basin with south-southeast drainage within an axial basin and also notes a lack of lacustrine deposition.

**Model 1: Ingersol et. al., 1990**

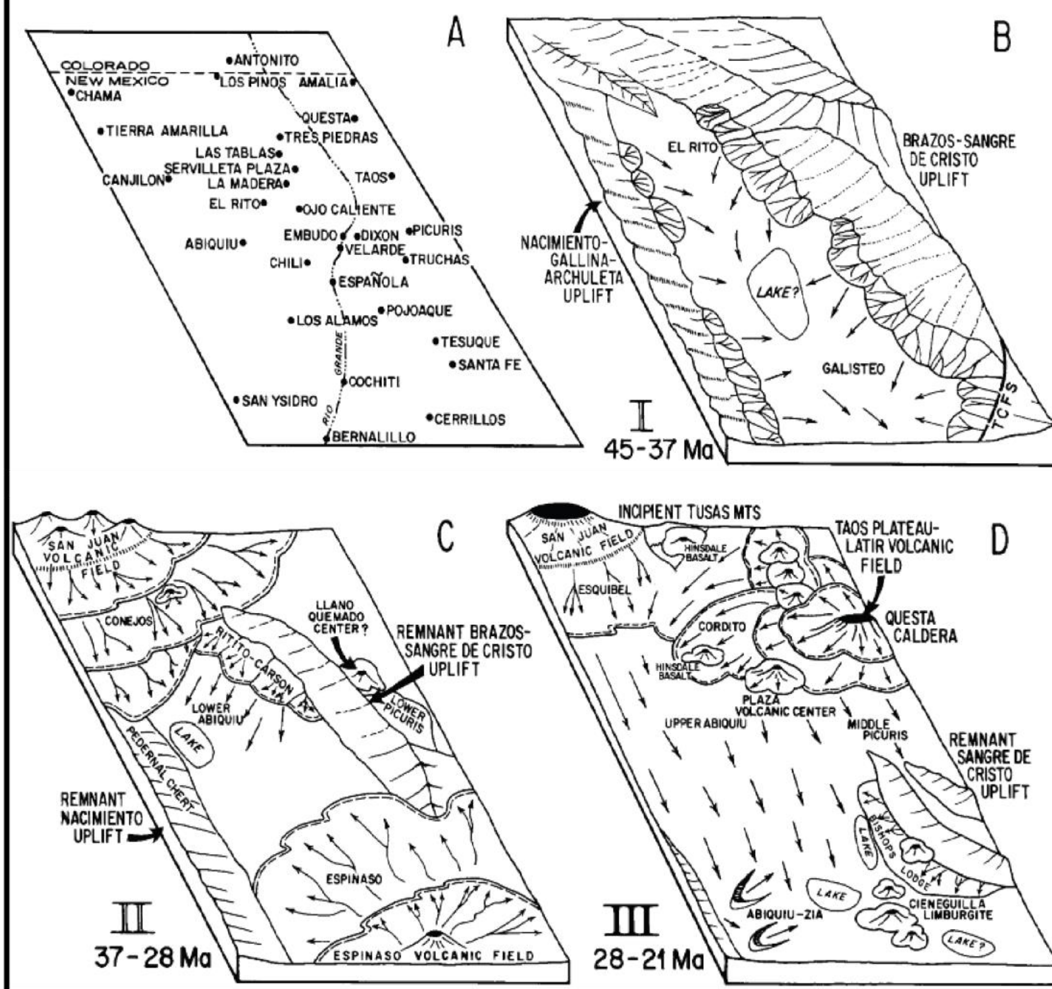


- Mainly southern drainage
- Axial basin
- Large braided river
- Lacustrine deposition

Figure 8: Paleogeographic interpretation from Ingersol et al., (1990)

**Model 2: Cather S.M., 2004**

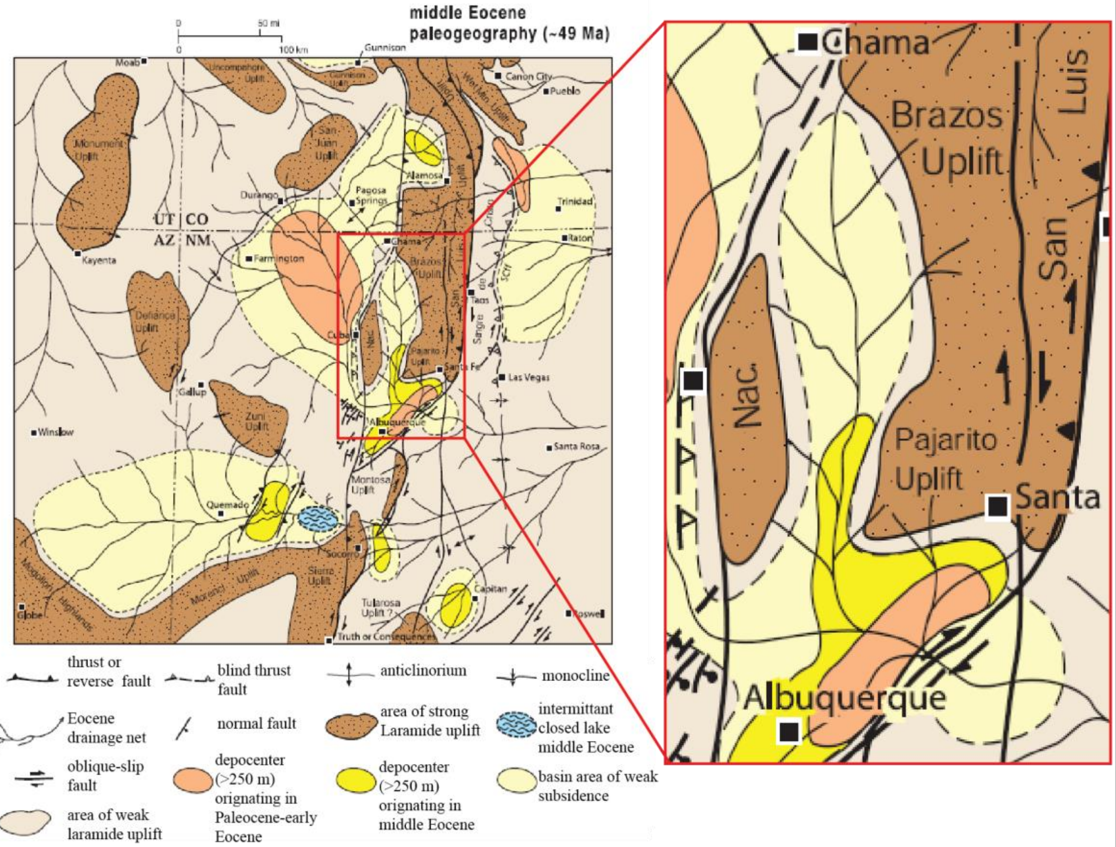


- Continous southern drainage
- Small to medium size rivers
- Axial basin
- No lacustrine deposition

Figure 9: Paleogeographic interpretation from Cather (2004)

**Model 3: Logsdon M.J., 1981**

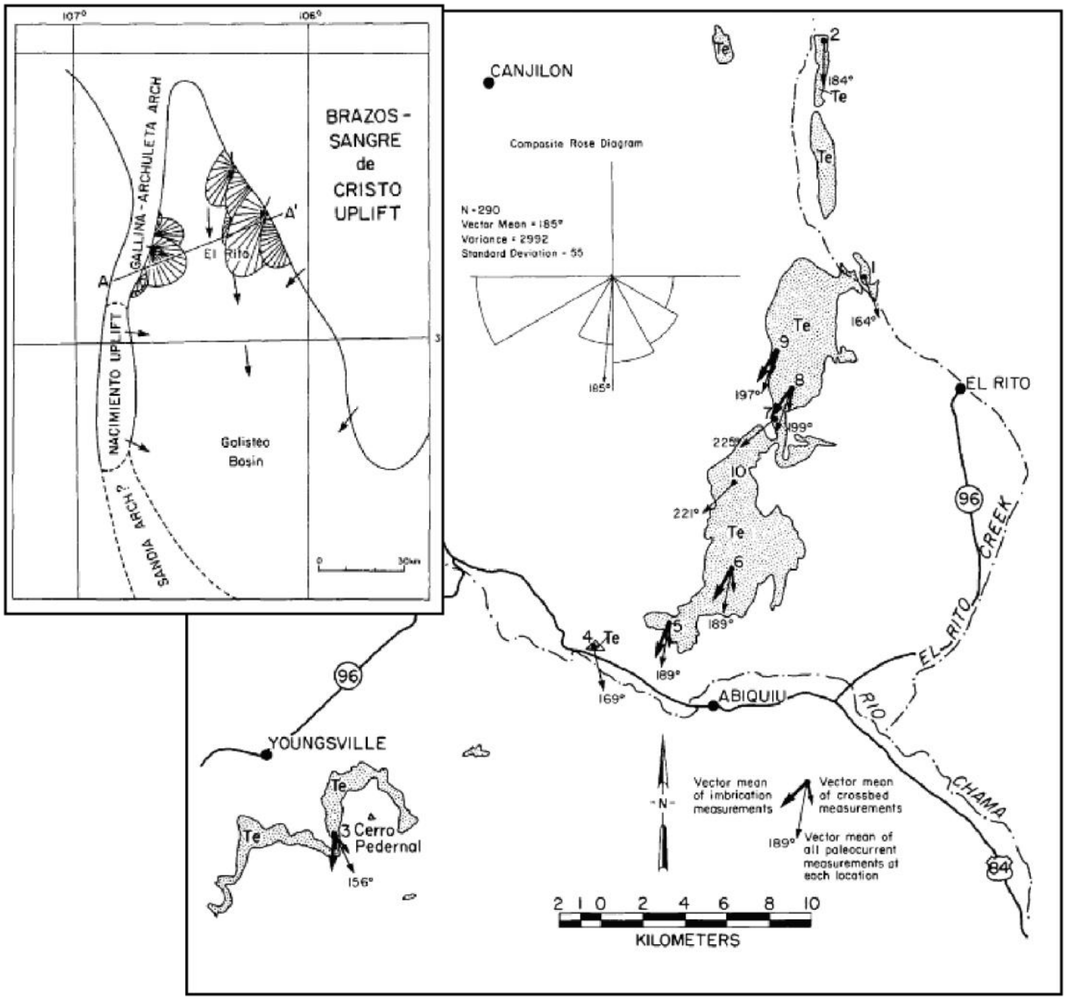


- South to southeast drainage
- No lacustrine deposition
- Axial basin

Figure 10: Paleogeographic interpretations from Logsdon (1981)

**Model 4: Cather, 1992**

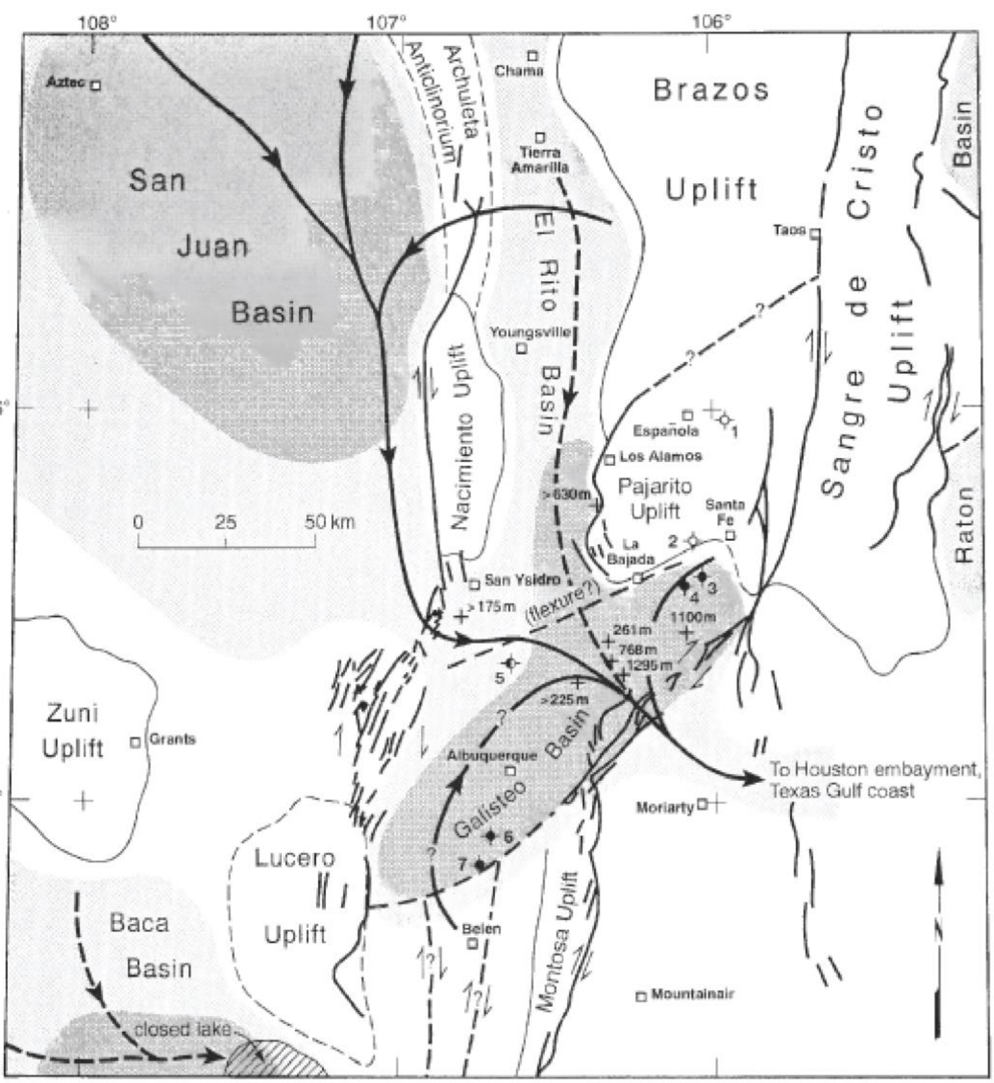


- Continous southern drainage
- Variations in magnitude of river
- Axial basin
- No lacustrine deposition

Figure 11: Paleogeographic interpretation from Cather (1992)

## 2.3. OLIGOCENE PALEOGEOGRAPHY

The Oligocene marks a drastic change in deposition throughout the area. The end of active uplift caused by Laramide deformation as well as a shift to a cooler climate and the presence of volcanism (Table 1) allow for subsidence and accumulation of volcaniclastic rocks (Smith et al, 2002). Kelley et al. (2013) present a paleogeographic interpretation of the area showing that deposition of the Ritito Conglomerate, which unconformably overlies the El Rito Formation, was restricted west of the remnant Tusas-Brazos Uplift. The Tusas-Brazos topographic high during this time is interpreted to have prevented the Ritito from receiving San Juan volcanic sediment. Kelley et al. (2013) documents the beginning of rift-related structures during this time frame, ~30-27 Ma. By 25 Ma the volcaniclastic rocks from the Latir Volcanic field make their way west and over the remnant Tusas-Brazos high to deposit the Abiquiu Formation.

| Volcanic Field | Rock Types | Age of Volcanism | References |
|---|---|---|---|
| Ortiz porphyry belt | Latite and quartz latite and related monzonite and quartz monzonite intrusions | **36-34 Ma** (calc-alkaline phase) **32-28Ma** (alkaline phase) | Stearns (1953), Disbrow and Stoll (1957), Sun and Baldwin (1958), Maynard et al. (1990), Erskine and Smith (1993), Sauer ( 1999) |
| San Juan (south-east caldera cluster) | Andacite and dacite lava (Canjoes Fm.). | **33-29.5 Ma** | Lipman (1975a), Lipman and Mehnert (1975), Lipman (1989), Lipman et al. (1996) |
| | Dacite, quartz latitic, and ryholitic ignimbrites (principally Treasure Mountain Group) and associated andesitic to rhyolite lava and tuff. | **31-28.4 Ma** | Lipman (1975a, 1989), Lipman and Mehnert (1975), Lipman et al. (1996) |
| | Slightly alkaline basalt and minor rhyolite lava and tuff | **26.8-22.0 Ma** | Lipman (1975a) |
| Latir | Andesitic and rhyodacitic lava; few rhyolitic ignimbrites. Includes San Luis Hills and volcanic rocks exposed along east side of San Luis basin Colorado | **28.5-26 Ma** | Lipman (1983), Lipman and Reed (1989), Johnson et al. (1989), Thompson et al. (1991),Wallace (1995) |
| | Peralkaline-rhyolite ignimbrites (e.g., Amalia Tuff), domes and related intrusions; formation of Questa caldera | **26-24 Ma** | Lipman and Reed (1989), Johnson et al. (1989), Czamanske et al. (1990) Lipman and Reed (1989), Johnson et al. ( 1989), Czamanske et al. (1990), |
| | Andesite, rhyodacite, and rhyolitic lava; intrusion of granite plutons; some volcanic products principally known as clasts in conglomerates | **22-18 Ma** | Ingersoll and Cavazza (1991), Smith et al. (2002) |
| Jemez Mountains | Tholetic basalt interspersed with and followed by andesite, dacite, quartz latite and locally important rhyolite lava and tuff | **14-2 Ma** | Smith et al. (1970), Gardner et al. (1986); Wolde-Gabriel et al. (2001) |
| | Rhyolitic ignimbrites (formation of Valles caldera), rhyolite lava domes | **1.87-0.06 Ma** | Smith et al. (1970), Goff et al. (1990) |

Table 1: **Volcanic Rocks of Northern New Mexico** modified from Smith et al. 2002.

# 3. Stratigraphy of Study Area

The geographical area considered in this study includes parts of the Nacimiento Mountains, the Chama River valley, and the Tusas-Brazos Mountains. Within this area there are Paleozoic through Cenozoic sedimentary and volcanic rocks, as well as numerous unconformities marking long and short periods of erosion and non-deposition. Figure 6 shows the study area broken up into specific field areas where the units of interest, the El Rito Formation and Ritito Conglomerate, can be found. The following sections detail the lithologic units found in the area, discuss the stratigraphy of the area, and provide a brief overview of the published geologic maps used in the study.

## 3.1. LITHOLOGIC UNITS

**Xv-Vadito Group Metavolcanic Schist**- This is a Proterozoic unit made up of white to light pink metarhyolite, consisting principally of fine-grained quartz, feldspar, and muscovite with possible quartz and feldspar porphyroblasts (Kempter et al., 2008). This unit is exposed along the uplifted eastern wall of Arroyo Seco canyon in the Tusas-Brazos Mountains, where it is overlain by the El Rito Formation conglomerate. Large blocks of the schist (up to 1 meter across) are incorporated into the basal El Rito conglomerate. This unit may correlate to the Cerro Colorado metarhyolite and the Arroyo Rancho metarhyolite found in the Ojo Caliente quadrangle. The Cerro Colorado metarhyolite has been dated at ~1.70 Ga based on zircons (Bishop, 1997) and has been interpreted to have originally been ash flow tuffs (Kempter et al., 2008).

**Xo-Ortega quartzite**- The Proterozoic Ortega quartzite is a massive gray to bluish gray quartzite that often preserves original bedding structures. It is medium to coarse-grained, vitreous cross-bedded quartzite consisting mostly of quartz with minor amounts of muscovite, kyanite, and layers of hematite (Kempter et al., 2008). The Ortega quartzite is locally brecciated near major faults and fold axes. Vein quartz is common in joints. The quartzite has been subjected to polyphase ductile deformation, multiple generations of folding and faulting, and lower greenschist to upper amphibolite grade metamorphism (Kempter et al., 2008). Williams et al. (1999) interpret the primary metamorphic age of the Ortega quartzite to be ~1.65 Ga. Maximum exposed thickness in the Valle Grande Peak quadrangle is ~200 meters, although this unit is interpreted to be over a kilometer in thickness (Koning et al, 2007).

**Pcu- Arroyo del Agua Formation**- This Early Permian unit is the upper part of the Cutler Group, which was divided into two distinct stratigraphic units, the Arroyo del Agua and the El Cobre Canyon Formations, by Lucas and Krainer (2005). This dominantly orange formation consists of many thick siltstone slope formers, interbedded with thin resistant beds of sandstone. The sandstones are generally arkosic and display trough-crossbedding (Kempter et al., 2007). It is easily differentiated from the underlying El Cobre Canyon Formation by its orange color and lack of thick cliff-forming sandstones. Only the Arroyo del Agua Formation is exposed at the study site and surrounding area. For mapping purposes Permian rocks are undifferentiated and named under a single moniker Pcu (Permian Cutler Formation).

**TRcp- Chinle Group-** Triassic Poleo Formation is the middle unit of the Chinle Group. It forms prominent cliffs of cross-bedded sandstone. It is brown to gray to yellow, medium- to fine-grained micaceous quartzose sandstone. The contact between the Poleo Formation and the underlying Permian rocks is sharp, where as a gradational contact exists between the Poleo and the overlying Upper Chinle Formation. The Poleo is 41 meters in the field area near Abiquiu Dam (Kelly et al., 2005).

**TRcu- Chinle Group-** This Triassic Upper Chinle stratigraphy includes two main formations which are not subdivided for the purposes of this study, but are lumped together as TRcl. These are the Rock Point Formation and the Petrified Forest Formation. The Rock Point Formation is reddish-brown to gray-red siltstone and fine-grained sandstone. It forms slopes and is up to 70 meters thick (Lucas et al., 2003). The Petrified Forest Formation is divided into two members: the basal Mesa Montosa Member that consists of red-brown laminated sandstone and the upper Painted Desert Member composed of red-brown mudstone. The formation as a whole is ~200 meters thick (Kelly et al., 2005).

**Je- Entrada Sandstone-** The Jurassic Entrada Sandstone is an eolian very fine-to medium-grained quartzose sandstone. It is well-sorted and moderately indurated. The Entrada Sandstone forms cliffs 60 to 67 meters thick that display a color scheme of red at the base, pink in the middle, and yellow at the top (Kelly et al., 2005). It is ~50-70 m thick throughout the area. Ripple-cross laminations as well as large scale trough crossbedding are present, along with deformation banding (Kempter et al., 2007).

**Jt- Todilto Formation**- The Jurassic Todilto Formation (Figure 2) is a non-marine or saline-paralic deposited limestone that is high in organic content and lacks bioturbation or wave-formed features (Berglof, 2003). It is thinly laminated at the base and locally microfolded and contorted, and massive near the top. Its age is middle Callovian based on fossil evidence collected by Lucas (1985). In the study area the Todilto is up to 5 meters thick. The Todilto is bound by unconformities at its top and base. It overlies the Entrada Sandstone and is just below the Jurassic Morrison Formation (Kempter et al., 2007).

**Jm- Morrison Formation**- The Morrison Formation is divided onto the Jackpile Sandstone and the Brushy Basin Member (Kelly et al., 2005). Only the Brushy Basin Member of the Morrison Formation is present in the field area. The 8 meter thick base of the unit contains individual packages of interbedded mudstone and trough-crossbedded sandstone. Toward the top it is a variegated green to reddish orange and in some places dark reddish brown siltstone and mudstone with significant bentonite content (Kelly et al., 2005). This unit is on the order of 40 to 70 meters thick (Kempter et al., 2007).

**Ter- El Rito Formation**- The Eocene El Rito Formation underlies the Ritito Conglomerate and unconformably lies atop of Proterozoic to Cretaceous rocks. It consists of Proterozoic granite and quartzite pebbles to cobbles in an orange-red to brick-red, hematitic, micaceous mudstone and siltstone, and lenses of fine- to medium-grained arkosic sandstone matrix. Locally, the 2 to 10 meter-thick basal conglomerate section is made up of very well-rounded hematitic Proterozoic Ortega quartzite, as well as Proterozoic schist and gneiss cobbles and boulders (up to 1 m) in a weakly to well-indurated matrix of coarse-grained ferruginous sandstone (Kelly et al., 2005). In the Arroyo del Cobre area the upper portion of the formation is dominated by massive medium-to coarse-grained crossbedded channel sandstone lenses interfingered with siltstone to fine-grained sandstone. A possible ~1 m thick paleosol (this study) sits at the top of the formation, at the base of the angular unconformity with the Ritito Conglomerate. The formation is ~50 m to 150 m-thick.

**Tr - Ritito Conglomerate**- The Ritito Conglomerate was originally included in the Abiquiu Formation as the lower member (Smith, 1938; Church and Hack, 1939), but based on major differences in lithology and provenance, has since been designated a separate formation (Maldonado and Kelley, 2009). It is made up primarily of conglomerate containing subrounded to subangular pebble-to cobble-sized clasts in a gray to pinkish sandy matrix. It is poorly sorted, weakly to moderately indurated, and calcareous. Conglomerate clasts are typically Proterozoic granites and quartzites that vary in size up to 1 meter. Thickness of this unit varies up to 60 meters (Kempter et al., 2007). K-Ar ages on a basalt near its base and $^{40}Ar/^{39}Ar$ ages on the Amalia Tuff in the Upper Abiquiu Formation bracket the age of the Lower Abiquiu Formation between 25.1 and 27 Ma (Moore, 2000; Smith et al., 2002).The unit is exposed in several localities between the Tusas Mountains and the Nacimiento Mountains. Due to the age of this unit, the location of outcrops at high structural positions, and that it unconformably overlies the synorogenic El Rito Formation, the Ritito has been proposed have been deposited in a syn-rift alluvial fan environment (Kelley et al., 2013).

The clast content and paleoflow data are similar to that of the underlying El Rito Formation (Hamilton, 2009). This suggests that the same basins active during late Laramide, that were filling with El Rito sediments, were also the first basins to record syn-rift activity. The Ritito Formation is preserved at high elevations, suggesting that these former basins were inverted and not down dropped further during rifting.

**Tap- Pedernal Chert member.** The Pedernal Chert is a varicolored, white, blue-gray, black, red and yellow cryptocrystalline, massive chert, limey chert, and limestone containing nodular chert. It is a conspicuous ledge former found primarily west of the Chama River. It has been interpreted to be diagenetically altered from paleosols and floodplain deposits through silica replacement of calcium carbonate during burial (Vazzana and Ingersoll, 1981). The chert is locally interlayered with thin beds of arkosic sandstone and conglomerate and is typically more limey at its base. It occurs in lenses that are 2 to 10 m thick.

**Ta- Abiquiu Formation**- The Abiquiu Formation consists of beige to white to gray interbedded shales, sandstones, conglomerates, and tuffs. It ranges in age from late Oligocene to early Miocene. The proportion of volcanic lithic fragments increases toward the top of the formation. In the study area south of the Chama River this unit reaches a maximum thickness of 350 meters (Kempter et al., 2007).

**Tb- Lobato Formation-** The Lobato Formation consists of two separate volcanic members: the Pliocene Lobato Andesite and Lobato Basalt. K-Ar dating has determined an age of 7 Ma for both the basalt and andesite. It is thought to be sourced from many separate volcanic vents and is widely distributed around the northeast margin of the Jemez Mountains (Manley and Mehnert, 1981). The Lobado Basalt ranges in thickness up to 200 meters in some areas (Aldrich and Dethier, 1990). In the local study area however, it is considerably thinner. For the purposes of this study it is confined to the southwestern corner of the mapped area (mapped by Hicks, 2008). It is of particular importance in this study as it is dated at 7 Ma and is offset by the Cañones Fault.

**Teb- El Alto Basalt-** The El Alto Basalt is not located in the immediate study area, but is relevant to the study because it crosses the Cañones Fault and shows no offset (Gonzalez and Deither, 1991). It is dark brown to black vesicular basalt and contains plagioclase, pyroxene and olivine phyenocrysts. It overlies basaltic andesite of Cañones Mesa and reaches thickness of up to 120 meters (Kelly et al., 2005). K-Ar dating reveals an age of 3 Ma (Manley and Mehnert, 1981).

**Qal- Quaternary Alluvium-** For the purposes of this study, all Quaternary units in the mapped area are included under the nomenclature Qal. This unit includes both slightly lithified sedimentary rocks and loose unconsolidated sediments with extreme variation in clast size ranging from silt to boulder.

This unit is primarily confined to stream beds and nearby floodplains. Thicknesses vary up to a maximum of 8 meters (Kempter et al., 2007).

## 3.2. STRATIGRAPHY

Figure 12 below illustrates the stratigraphy, age, and thickness of the units in the area. A quick guide to the general thickness of each unit and the mode of deposition is also listed.

| AGE | UNIT | Depositon | Thickness |
|---|---|---|---|
| Pleistocene | Quaternary: Qal | Alluvial fan, river | ~0.5m-8m |
| Pliocene | Jemez Volcanic Field Lava Flows: Tb, Teb | Volcanic eruptions | ~7m-80m |
| Miocene | Santa Fe Group | River, alluvial fan, and dune fields | ~185m |
| | Abiquiu Formation: Ta | Braided stream, alluvial fan | 150m-350m |
| Oligocene | Pedernal Chert: Tap | Silica-rich groundwater | 2m-35m |
| | Ritito Conglomerate: Tr | Braided stream, alluvial fan | 60m-100m |
| Eocene | El Rito Formation: Ter | River, floodplain, and alluvial fan | 50m-150m |
| Cretaceous | Mancos Shale | Marine | ~70m-200m |
| | Dakota Sandstone | Marine to marginal | |
| | Burro Canyon Formation | River | |
| Jurassic | Morrison Formation: Jm | River and floodplain | ~125m-230m |
| | Bluff sandstone | Dune field | |
| | Summerville Formation | Alluvial fan | |
| | Toldito Formation: Jt | Saline | |
| | Entrada Sandstone: Je | Dune field | |
| Triassic | Chinle Group: TRcp, TRcu | River | ~170m |
| Permian | Yeso Formation<br>Cutler Group: Pcu | Dune field<br>River | 240m-510m |
| Pennsylvanian | Madera Group | Marine | minimal exposure in Nacimiento |
| Precambrian | Igneous and Metamorphic Rocks: Xv, Xo | Island arc within orogeny | ~200m-1km interpreted |

Figure 12:Stratigraphic chart of the study area. Modified from Hunt and Kelley, 2010

## 3.3. GEOLOGIC MAPS

A multitude of geologic maps were used in this study to identify the regional extent of the unconformities bounding the El Rito Formation. Local maps compiled and created from field studies from other students were used (Hamilton, 2009; O'Keeffe, 2014) to directly correlate the units within the Arroyo del Cobre area (Figures 13 and 14). 7.5 minute quadrangle maps created for the New Mexico Bureau of Geology and USGS were used both to reconstruct their cross sections and to make a large digital compilation of the study area (Figure 15). Maps from the Valle Grande Peak (Kempter et al., 2008), El Rito (Koning et al., 2008), Cañjilon SE (Kempter et al., 2007), Abiquiu (Maldonado, 2008), Cañones (Kelley et al., 2005b), Youngsville (Kelley et al., 2005a), and Cerro del Grant (Lawrence et al., 2004) quadrangles were compiled to make the digital map.

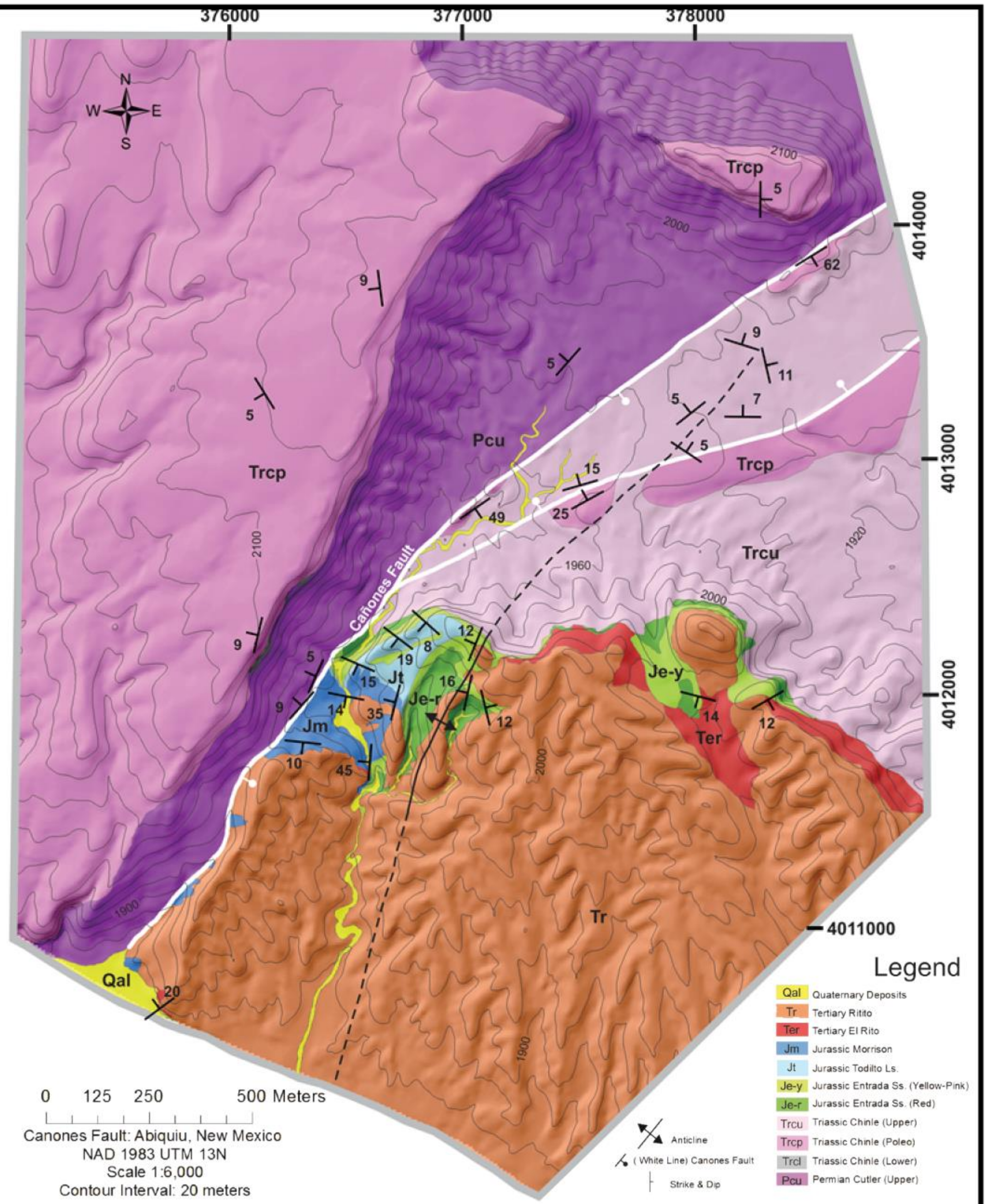


Figure 13: Geologic map of the Canones Fault west of Arroyo del Cobre (O'Keeffe, 2014)

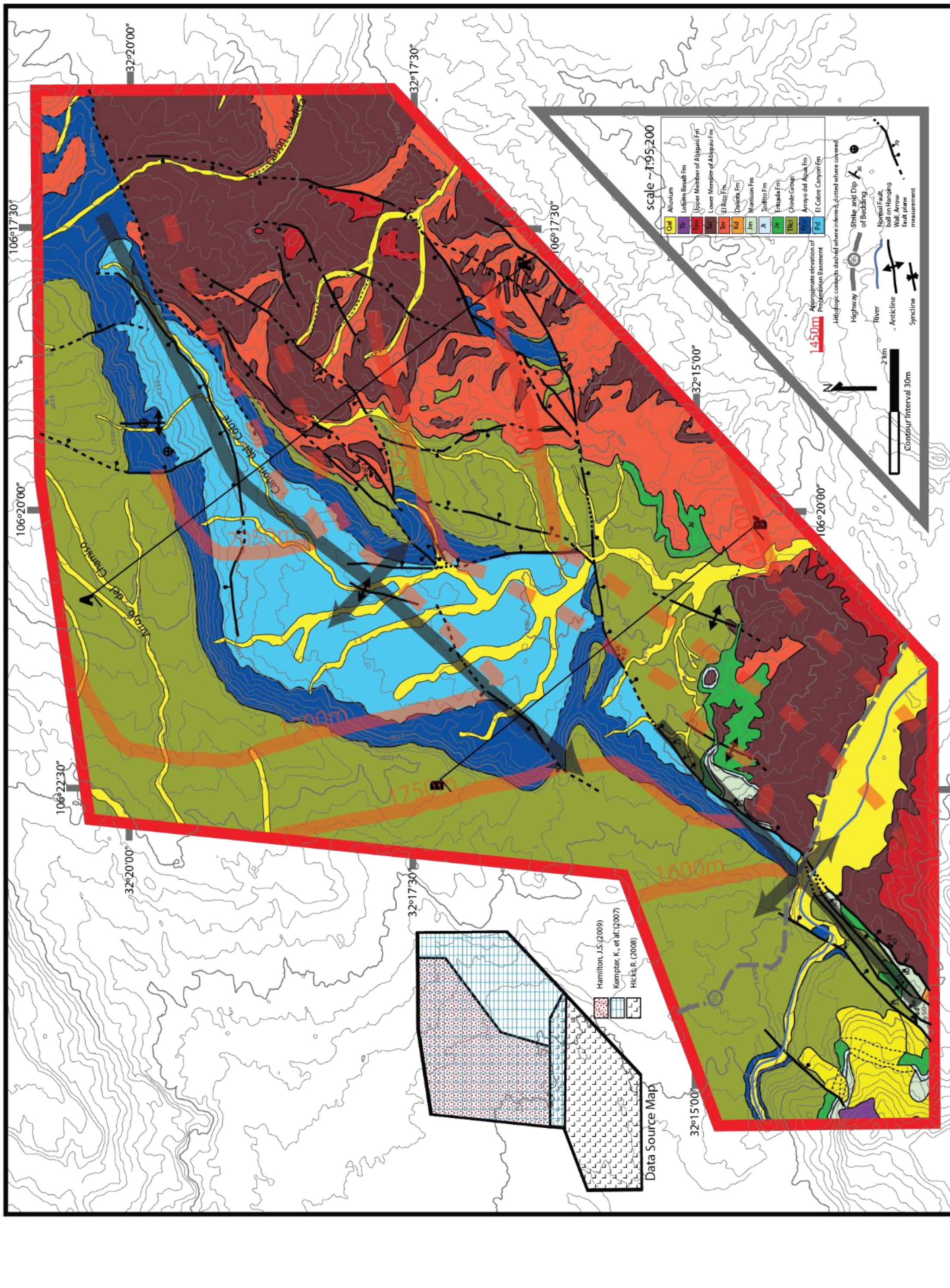


Figure 14: Geologic map of the Arroyo del Cobre area (Hamilton, 2009)

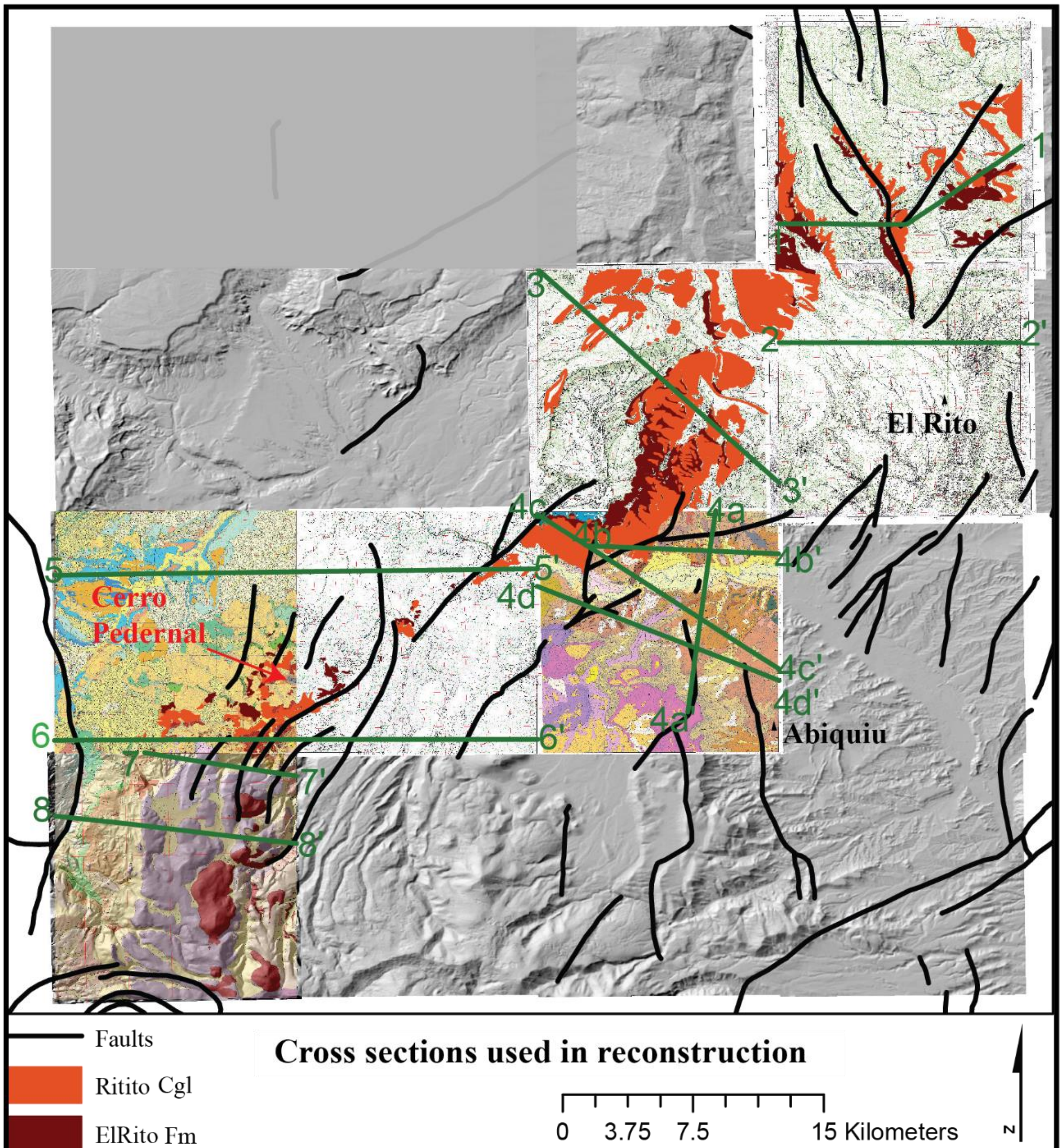


**Figure 15: Compilation of geologic maps used to digitally reference the unconformities above and below the El Rito Formation. Major faults shown in black. Green lines denote cross section lines from individual maps that are used to reconstruct the Eocene unconformity.**

# 4. Sedimentology

The study area is divided into three regions covering the exposed outcrops of the El Rito Formation and Ritito Conglomerate. The three areas cover the outcrops that can be found at high altitudes in the Nacimiento Mountains and Tusas-Brazos Mountains as well as the outcrops that are found at lower elevations near the present-day Chama River. The main focus of the study is within Arroyo del Cobre north of the town of Abiquiu and in the Tusas-Brazos Mountains north of the town El Rito. These two areas have the best outcrops of the base of the El Rito formation. The Arroyo del Cobre features a complete section of the El Rito Formation from the base of the unit where it sits between the angular unconformity above the Triassic Chinle formation and the angular unconformity below the Ritito Conglomerate. A detailed measured section of the E Rito Formation was gathered using a Jacob staff and Brunton compass. The section was measured to be 57 m (Figure 16). Paleoflow measurements from imbricated clasts and clast counts to assess provenance were made in Arroyo del Cobre and also in the Tusas-Brazos Mountains. Samples were collected from key areas within the measured section and petrographic thin sections were made to help quantify the provenance and tectonic regimes affecting the area during deposition.

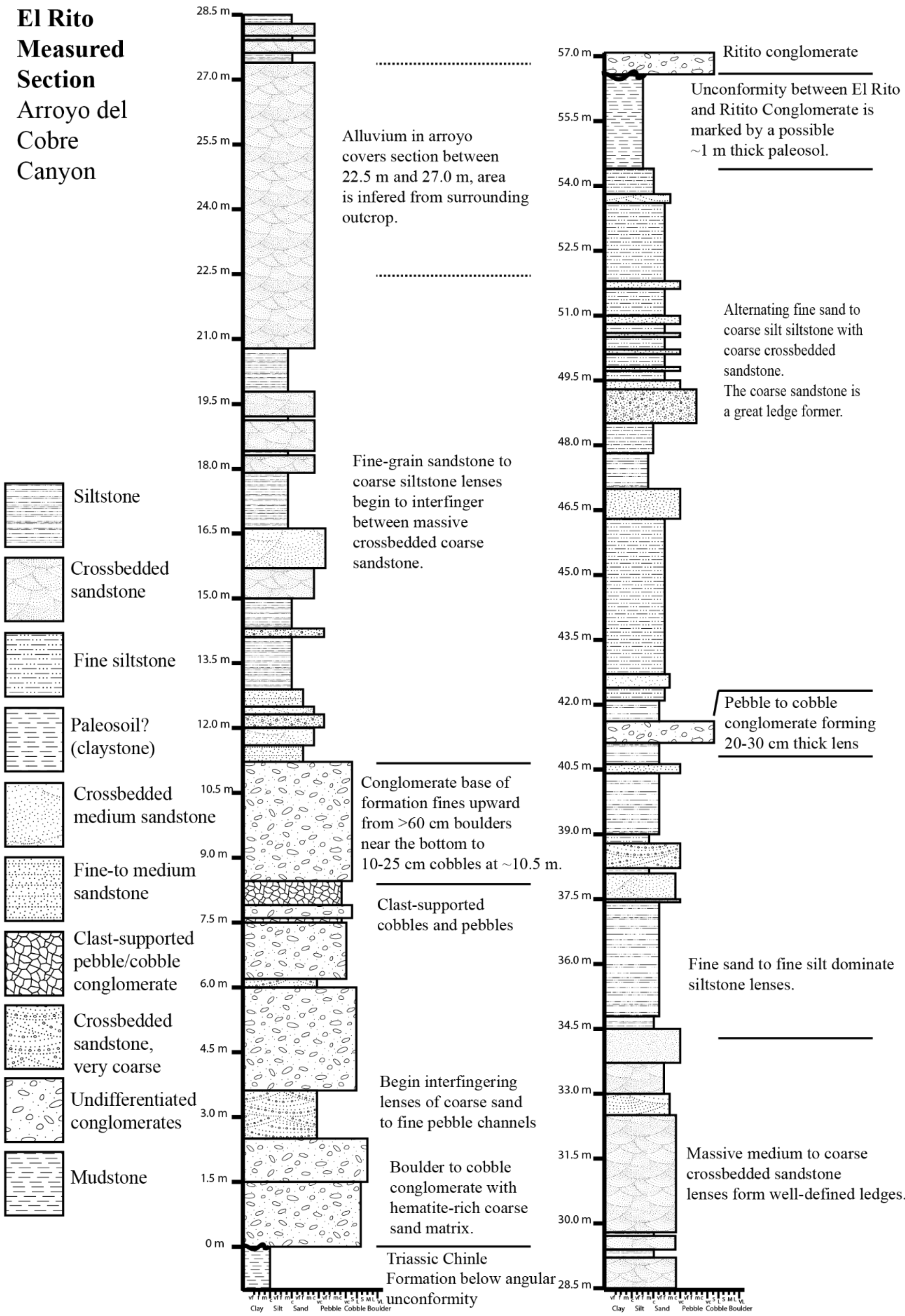


Figure 16: Measured section of the El Rito Formation in Arroyo del Cobre

## 4.1. PALEOFLOW

The El Rito Formation and Ritito Conglomerate are ideal units for measuring paleoflow from imbricated clasts. The El Rito Formation has a basal unit that is 2-10 m of cobble to boulder conglomerate, and additional 0.25-1 m pebble to cobble sized lenses are found just above the basal conglomerate, where clast on clast measurements area easily attainable. The pebble-to boulder-sized clasts are sub-rounded to well-rounded, and many of the clasts are elongate, providing an exceptional surface for acquiring attitude measurements. An approximate 1 m by 1 m sample area was established and photographed at each location where paleoflow measurements were acquired. Within each sample area 20 individual imbricated clast measurements were obtained, although a few areas in Arroyo del Cobre had less than 20 samples when the sample area had more matrix-supported conglomerates, hindering the clast on clast possibilities. Rose diagrams are used to display the paleoflow measurements. Common errors found in rose diagrams described by Wells (2000) are mitigated by the small sample size, that plot more accurately than larger sample sizes, and conformable radi of the plots.

### 4.1.1. Arroyo del Cobre

The paleoflow measurements in Arroyo del Cobre were obtained along the transect of the measure section, west of the arroyo near the Cañones Fault, and east of the arroyo along one of the arroyos' drainages. Figure 17 overlays the paleoflow rose diagrams against their locations within the Arroyo del Cobre area. The imbricated clast measurements ae focused on the lower 15 m of the El Rito Formation where clast on clast measurements are easily attained. This lower section is also of particular interest because it records the earliest deposition of the El Rito Formation making it a key indicator of the structure and depositional environment following the unconformity.

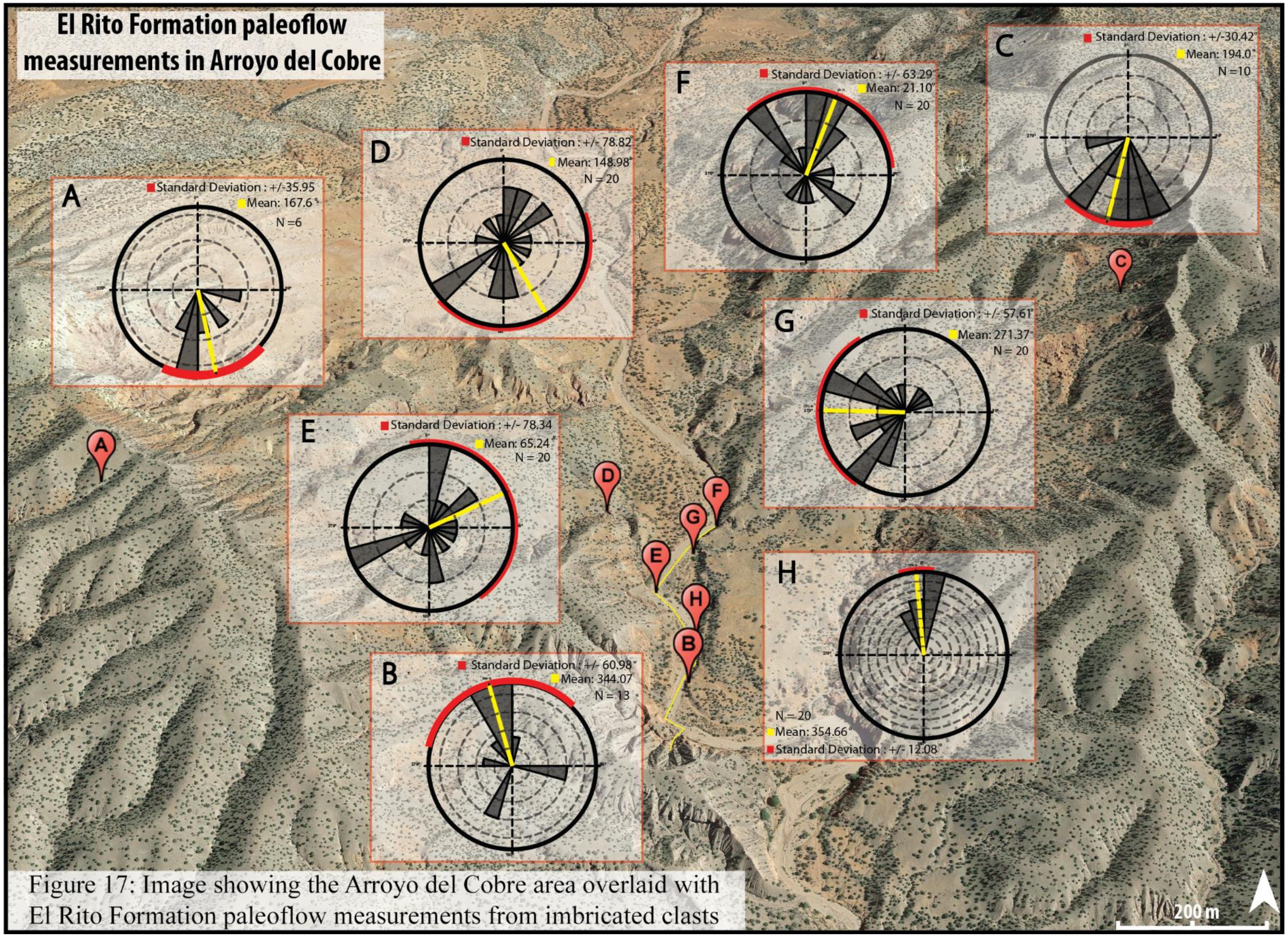


Figure 17: Image showing the Arroyo del Cobre area overlaid with El Rito Formation paleoflow measurements from imbricated clasts

### 4.1.2. Valle Grande Peak

The Valle Grande Peak area was studied from separate two locations. The first at the campground along County Road 110 northwest of El Rito, and the second along County Road 247 near Valle Grande Peak. In both of these areas the El Rito Formation is deposited on Proterozoic rocks of the Vadito Group and Ortega Quartzite. The basal conglomerate in the campground is made up of well-sorted, rounded to well-rounded, clast-supported cobbles to boulders and is prone to form cliffs and pinnacles. Figure 18 combines measurements from five sample sites near the campground and one sample site on the Valle Grande Peak, illustrated on the right side of the diagram.

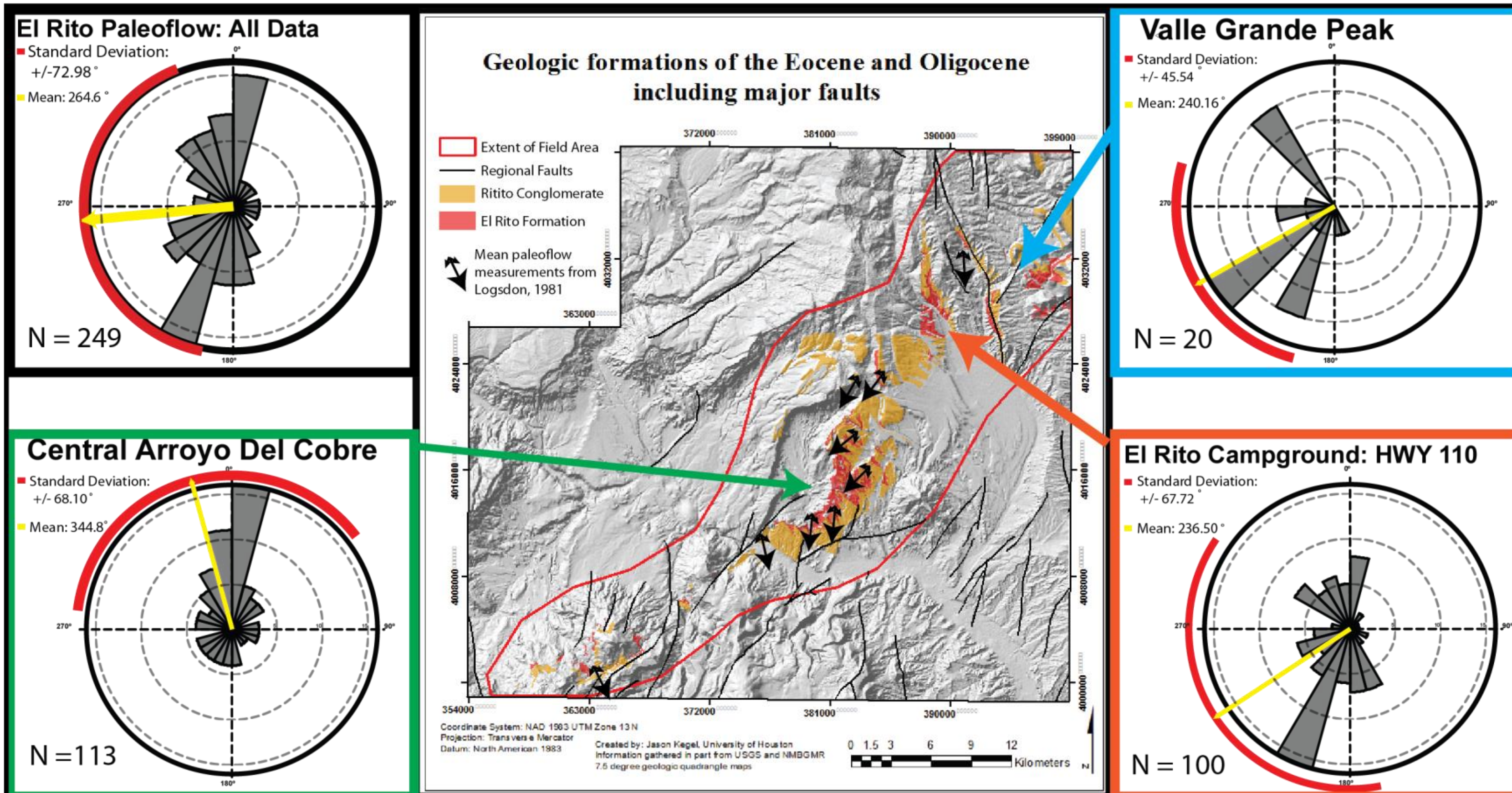


Figure 18: Compiled paleoflow measurements of the El Rito Formation. Rose diagrams are compiled from individual measurements from the Valle Grande Peak, El Rito campground, and Arroyo del Cobre study areas. Individual measurements from figure 17 were compiled to make the Central Arroyo del Cobre diagram. Mean paleoflow indicators from the upper El Rito Formation, by Logsdon (1981), are overlaid on the central map.

### 4.1.3. Local and regional patterns

Following compilation of the data, local patterns emerged showing a variation of southwest-directed flow in the northeast Valle Grande Peak area and a northerly flow in the Arroyo del Cobre area (Figure 18). The merged datasets, in the "El Rito Paleoflow: All Data" rose diagram in figure 18, show a bimodal north and south flow direction distribution. Significant variations in paleoflow direction are found in the Arroyo del Cobre area where the majority of the samples are taken. These variations tend to show paleoflow measurements toward the south on the east and west margins of the Arroyo del Cobre area with northerly, southerly, and westerly flow directions within the center of the arroyo. The overall direction of current for the lower 20 meters of the El Rito formation, based on 249 imbricate clast measurements, is illustrated in the rose diagrams to be bimodal (Figure 18). My measurements differ from the measurements made by Logsdon (1981), because I focused on paleoflow in the basal conglomerate, whereas Logsdon (1981) included the remaining trough-cross stratified upper ~30 m of the El Rito Formation.

## 4.2. SAMPLE IDENTIFICATION

Petrographic samples were collected from the El Rito Formation in the Arroyo del Cobre area. Seven samples from four different locations were used for thin-section analysis. The samples were obtained from the western and eastern boundaries of Arroyo del Cobre and along the measured section transect. Sample ERS1 was taken from the west of Arroyo del Cobre near the Cañones Fault, sample ERS34 was taken from the eastern part of the arroyo along one of the northern drainages, Sample ERE1 was taken along the measured section transect just above the basal conglomerate, and samples ERE5a-d were taken from the upper quarter of the measured section transect in an area of fining upward sand to silt. The samples were analyzed in thin section using point counting methods described by (Dickinson, 1970 and Ingersoll et al., 1984) to determine the relative amounts of quartz, feldspars, and lithics. The results were plotted using Excel ternary diagrams published by Zahid and Barbeau (2011) to determine the sandstone classification (Folk, 1990) and provenance classifications (Weltje, 2006) for the El Rito Formation.

#### 4.2.1. Petrographic analysis of El Rito samples

The thin sections show on average poor to moderately sorted with sub-angular to rounded grains within a matrix of red hematite cement and clay. The samples higher in the section have a higher clay content. The grain size in the thin sections varies from 2 um to ~ 0.20 mm and can change rapidly across the thin section. Figure 19 shows thin-section images from sample ERS1 and ERE1 as well as a sandstone classification diagram and two provenance ternary diagrams. The Folk classification ternary diagram shows the four samples are feldspathic litharenites. The two provenance ternary diagrams from Weltje (2006) show that the samples plot in the recycled orogen provenance.

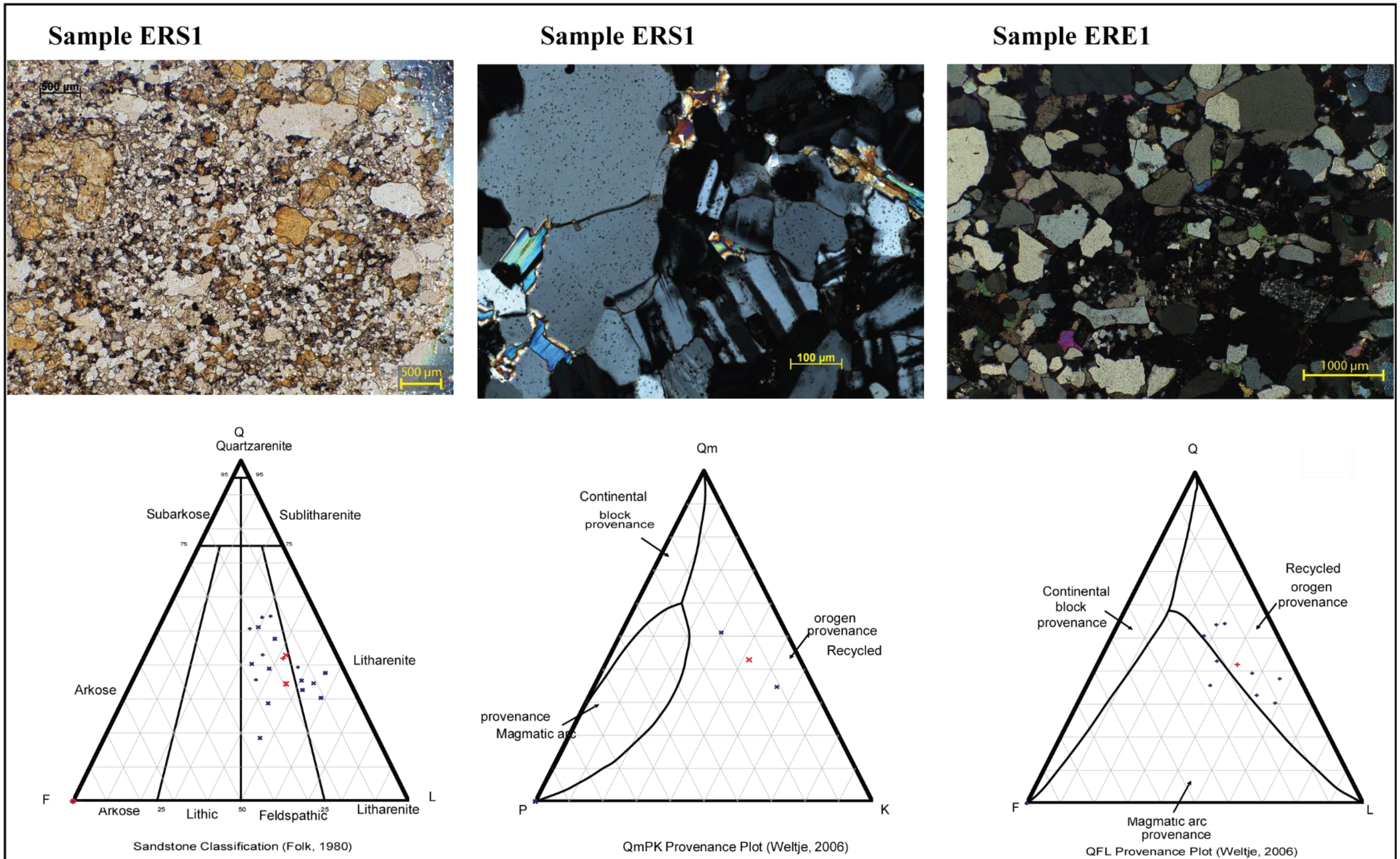


Figure 19: Thin-section petrographic analysis

## 4.3. PROVENANCE

Provenance is classified from clast counts taken from the same locations as paleoflow data. The clast counts were made by identifying ~100 clasts within the 1 m by 1 m sample area. The clasts were distributed throughout the sample area and an attempt was made to pick them as randomly as possible. Pictures were taken of the sample areas and chalk marks can be seen on the identified clasts. Figure 20 shows a geologic map of the Abiquiu Embayment along with two cross sections from Smith (2004). This geologic map is overlaid with stars indicating the location of provenance clast data. The cross sections can be used to highlight the current structure of the basin.

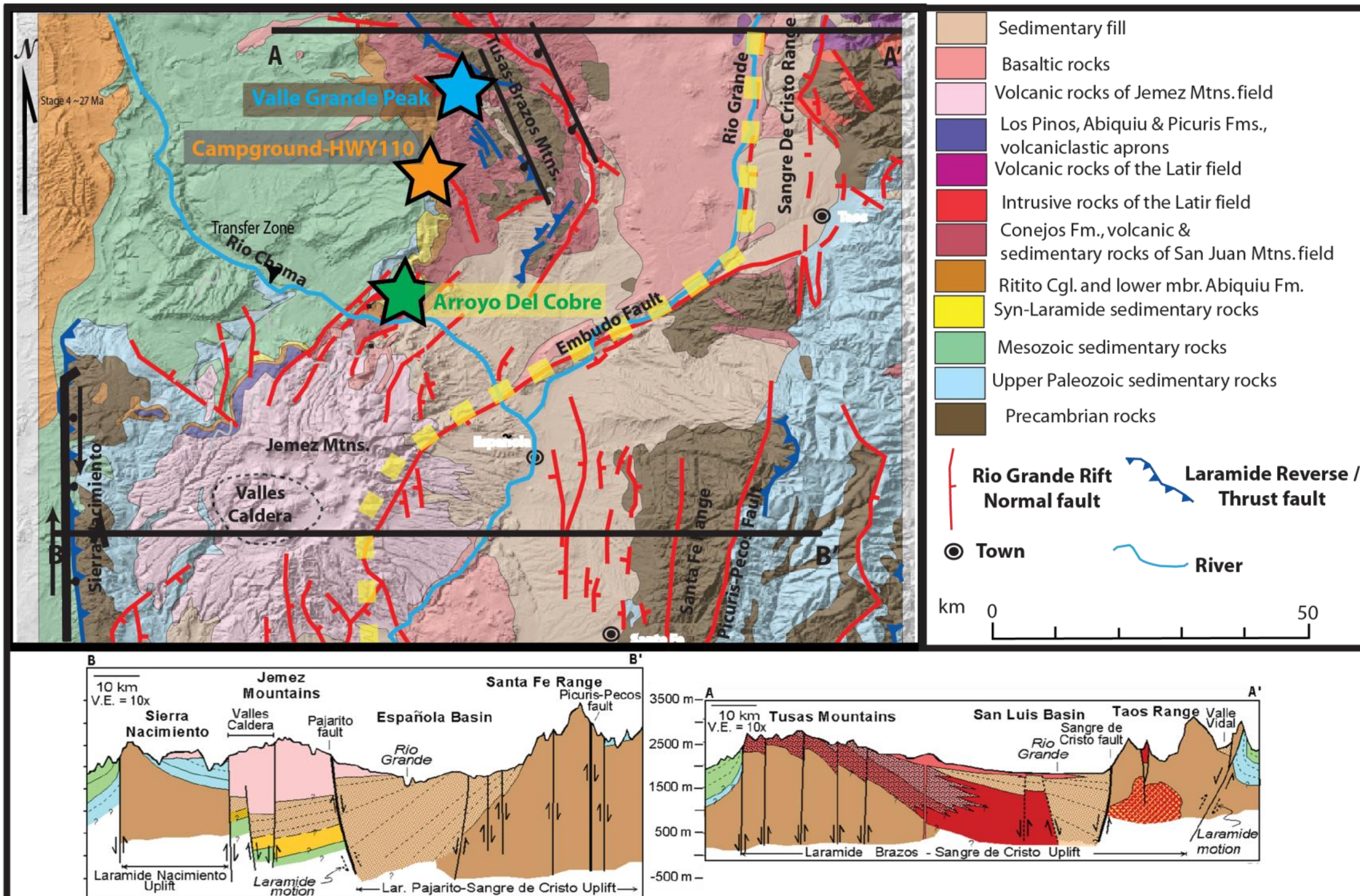


Figure 20: Geologic map and cross sections showing location of province clast counts, modified after Smith (2004).

4.3.1. Arroyo del Cobre clasts

The clasts studied to infer provenance in the Arroyo del Cobre area show the largest amount of granite within the sample location in located centrally in the arroyo. The central portion of the arroyo also has very little sandstone and schist/mylonite when compared to the samples located to the east and west. To the west and east little to no granite is recorded although greater amounts of sandstone are quantified. Figure 21 shows illustrates Arroyo del Cobre study area denoted by a green star on Figure 20. Pie charts illustrate the percentage of clasts found in the sample area.

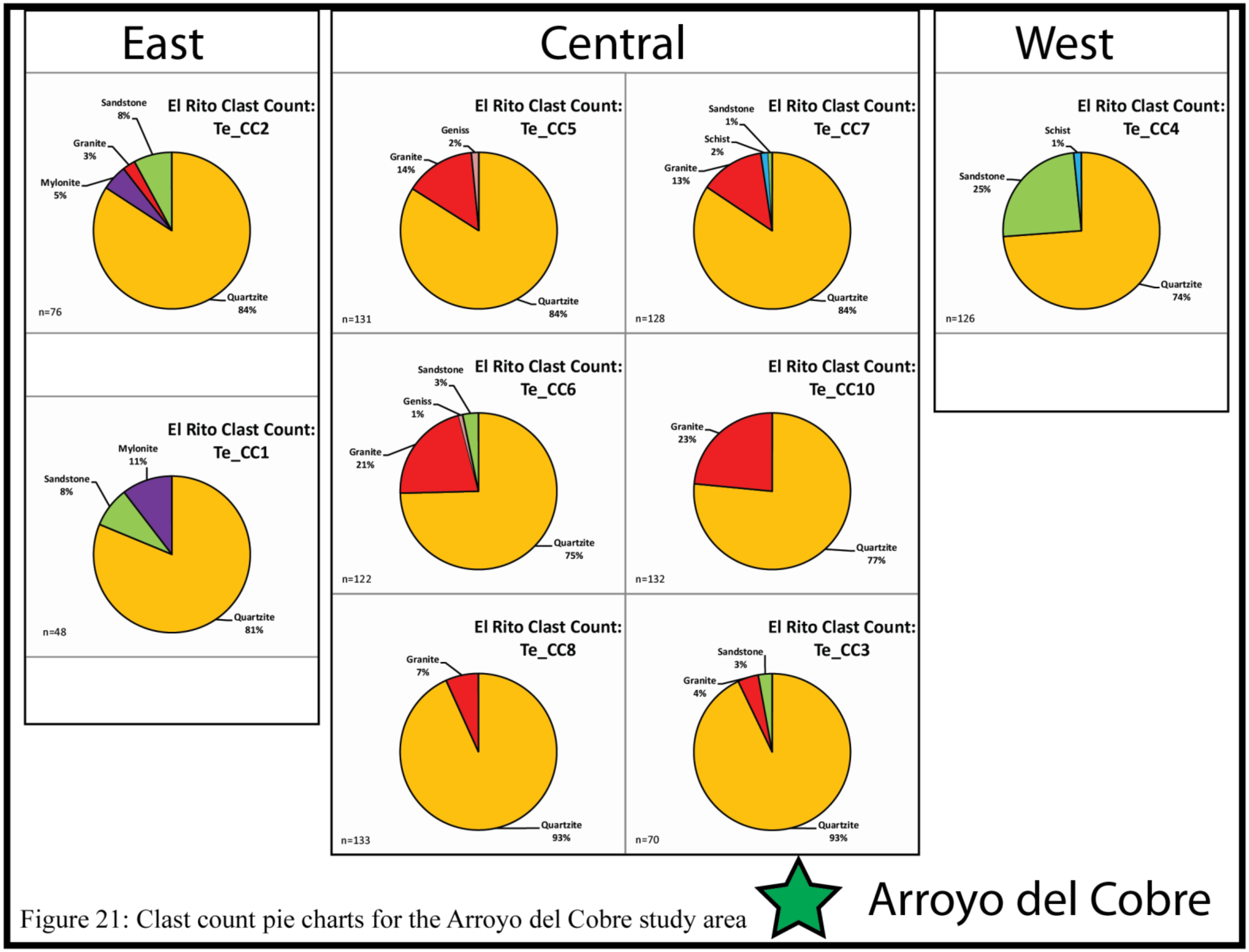


Figure 21: Clast count pie charts for the Arroyo del Cobre study area

### 4.3.2. Valle Grande Peak clasts

The clasts counted in the Valle Grande Peak area consist of two data sets. One form the campground area near HWY 110 and the other a single data sample from the Valle Grande Peak area. The composition of these clasts is mainly quartzite with small amounts of schist. Two of the samples recorded less than 2% composition of gneiss and sandstone. Figure 22 illustrates the pie charts for the Valle Grande peak areas marked by the orange and blue stars found on figure 20.

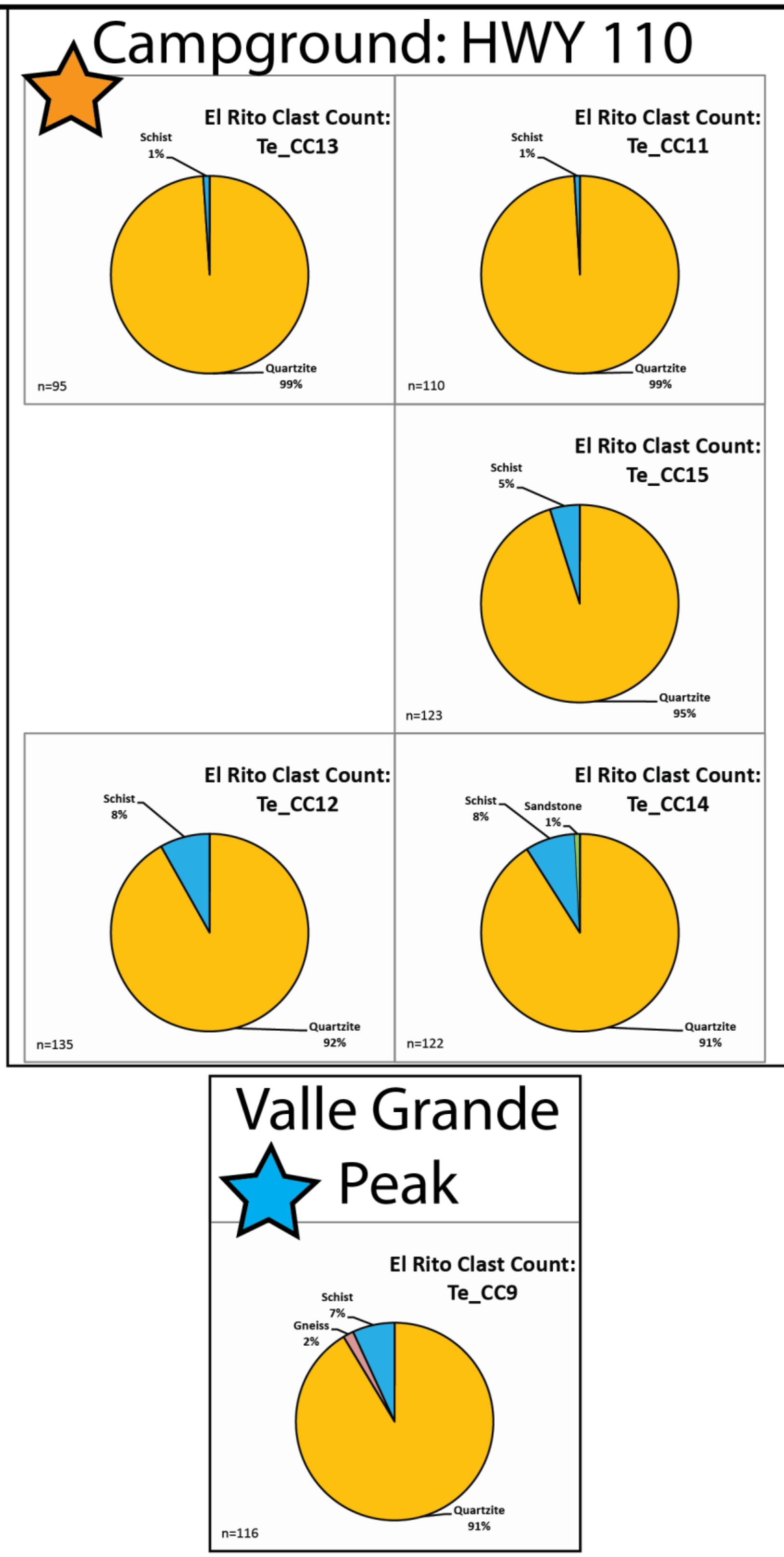


Figure 22: Clast count pie charts for the Valle Grande Peak study area

4.3.3. Regional influence

This provenance data quantifies the abundance of Proterozoic clasts found in the El Rito Formation. The majority of clasts consist of quartzite, likely derived from the Ortega unit in the Tusas-Brazos basement-cored Laramide uplift. Minor amounts of sandstone, likely derived from the Mesozoic, schist and mylonite derived from the Vadito unit of the Tusas-Brazos Uplift, and granite likely derived from the basement core of the westerly Nacimiento Uplift are all present. Figure 23 is a modified portion of a map from Karlstrom et al. (2004) showing the Proterozoic basement rocks found in the region.

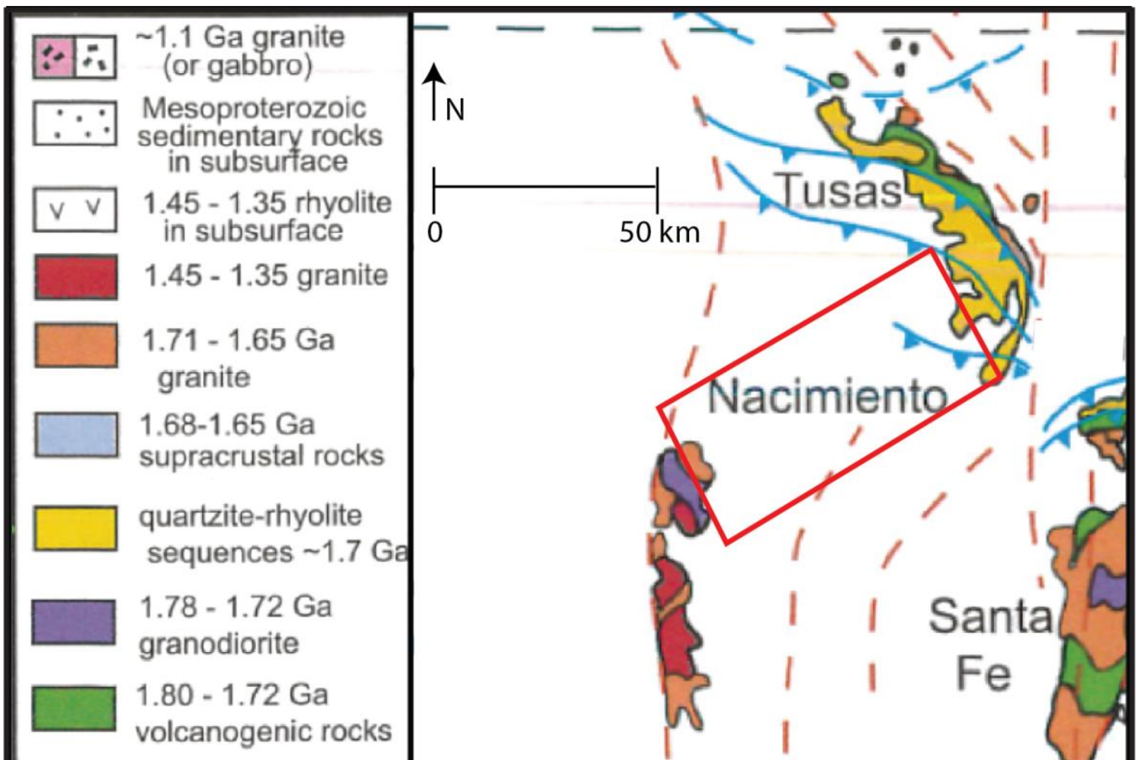


Figure 23: Proterozoic basement rocks found in the Chama-Espanola basin modified from Karlstrom et al., 2004. Study area in outlined in red box.

# 5. Structure

The structural changes influencing the Abiquiu Embayment during the transition from Laramide related uplift to Rio Grande Rift extension can be inferred from the two unconformable surfaces bounding the El Rito Formation (Maldonado et al., 2013).

## 5.1. RECONSTRUCTING THE EOCENE UNCONFORMITY

The geologic trace of the outcrop of these surfaces have been identified throughout seven 7.5 minute quadrangle geologic maps (figure 15) and digitized in ArcGIS where the regional strike and dip of the Eocene surface was calculated using a triple point TIN (triangular integrated network). The calculated surface shows the interpreted subsurface gradient of the Eocene unconformity (Figure 24). Elevation profiles along the surface were calculated and the results show, unsurprisingly, that the modern Eocene unconformity follows a similar trend as the modern topography. The modern topography of the basin shows highs to the east and west in the Tusas-Brazos Mountains and Nacimiento Mountains with a low along the valley floor near the Chama River. This modern topography is a result of Rio Grande Rift extension. To better understand what the surface of the base El Rito Formation looked like it is necessary to reconstruct the Eocene Unconformity.

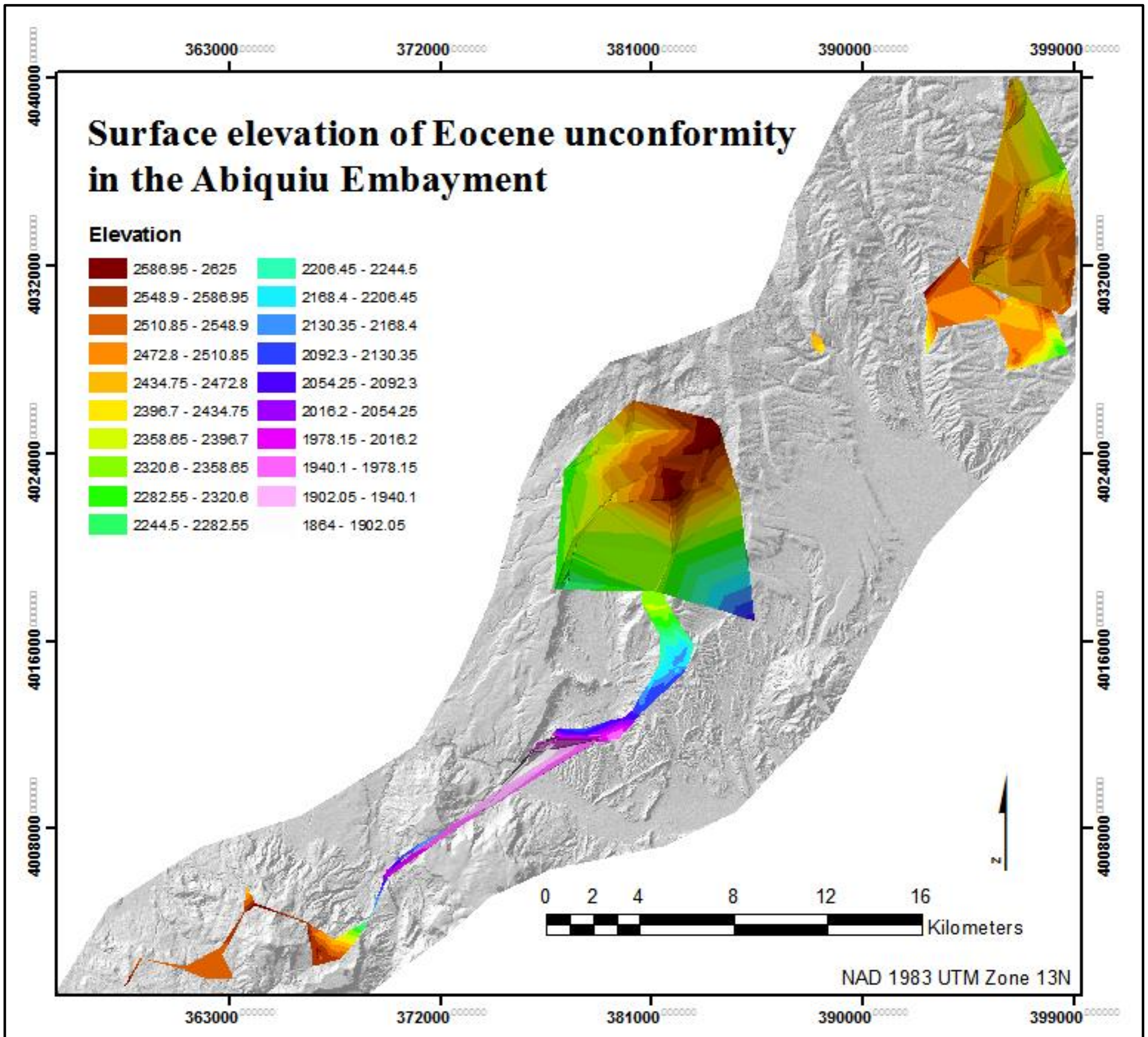


Figure 24: Modern Eocene unconformable surface calculated using a TIN (triangular integrated network) approach in ArcGIS

5.1.1. Cross sections

Eleven cross sections from the seven 7.5 minute geologic quadrangle maps (figure 16) were digitized and the Eocene surface was restored to along the fault trace. This restoration was done by hand using Adobe Illustrator and the resulting current elevation, as it relates to the vertical scale for each individual maps cross section, was recorded along the interpreted restored surface. The unconformity at the base of the El Rito was used as the datum for restoration of the surface. A few notes on the creation of this surface. First, the restoration stayed true to the individual authors' interpretation of the thickness of the El Rito Formation. Doing so introduces some error into the overall restoration because the authors would not always have a similar or consistent thickness denoted. Second, the El Rito formation is eroded to the north of the Cañones Fault zone and this restoration did not interpolate the missing strata. Computer generated kriging algorithms were used to extrapolate the shape of the base El Rito to expand the boundary of interpolated data. The data points along the cross section transects containing the interpreted elevation of the base El Rito were loaded into ArcGIS where gridding algorithms could model the surface.

### 5.1.2. Using ArcGIS to create surface

To create the points in ArcGIS the points interpreted in Adobe Illustrator needed to be digitized and georeferenced. The interpreted elevations of the base El Rito were documented along a line matching the exact length of the cross section transect. These lines with elevation points written on them were exported as a tiff image and brought into ArcGIS to be georeferenced. Once the tiff image was georeferenced to the same line from the 7.5 minute quadrangle maps points were placed at the exact location as the elevation data points. The attribute table for the point shapefile was then populated with the corresponding elevation data point providing the point with a Z value that could be used to create new grids.

Spatial Analyst and 3D Analyst were used to transform the point data into gridded surfaces in ArcGIS. Figure 25 shows the interpolated base Eocene unconformable surface above a current digital elevation model for the area. This surface was created using a natural neighbor gridding method holding the data to the exact extend of the input data. Figure 26 uses the extrapolated fault reconstruction measurements and grids the point data using an inverse distance method. The grid is interpreted outside of the input data within a defined boundary and overlaid on a current digital elevation model. The grids show a surface with a low in the middle and highs to the north and south. An additional low is observed along the north east side of figure 26.

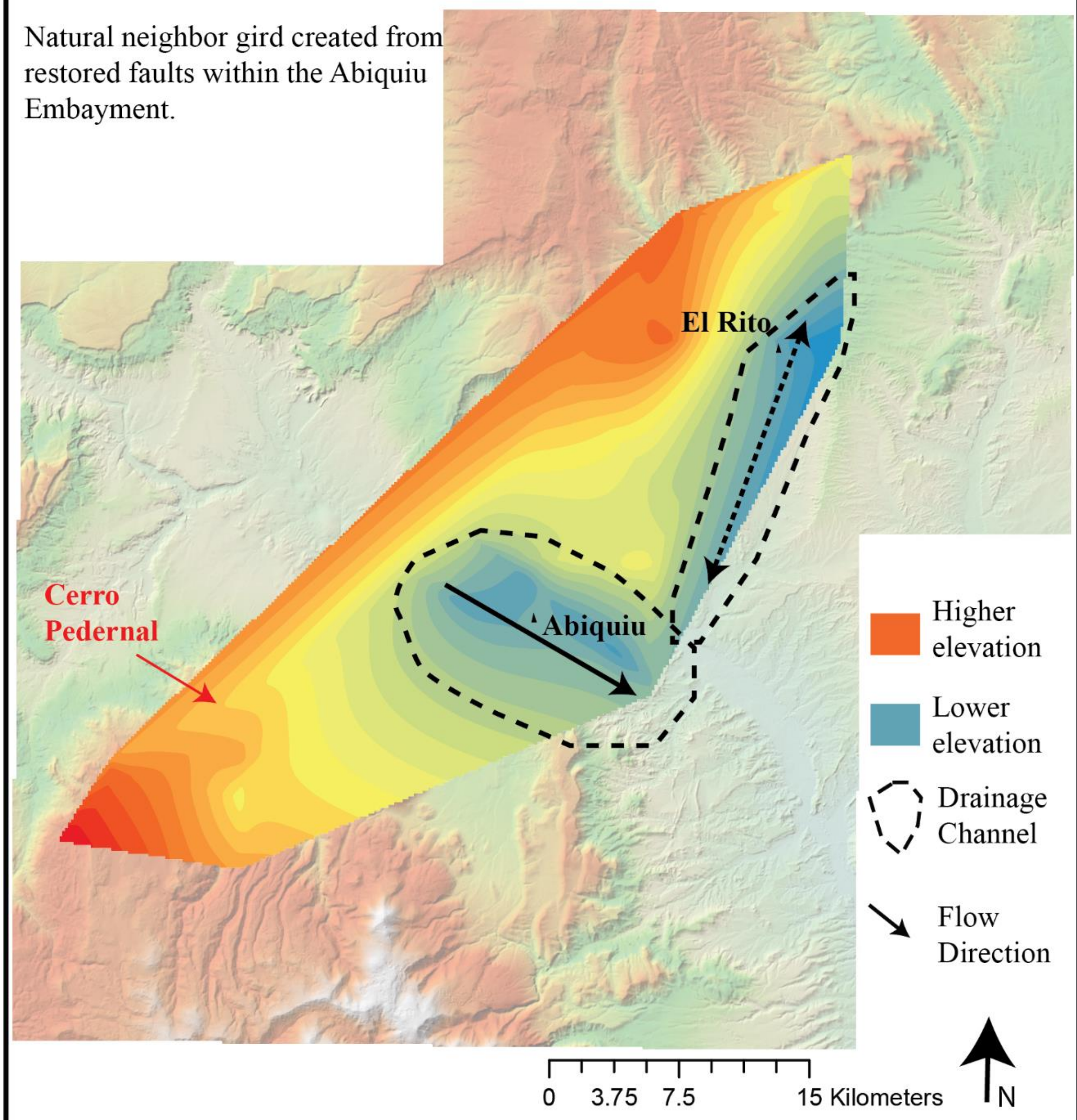


Figure 25: **Interpreted Eocene unconformity** Extrapolated from fault reconstruction measurements and modeling a surface grid using a natural neighbor method with a boundary defined by the exact extent of the area containing data. Paleocurrent directions are interpreted from topographic changes in the surface and from data collected within this study.

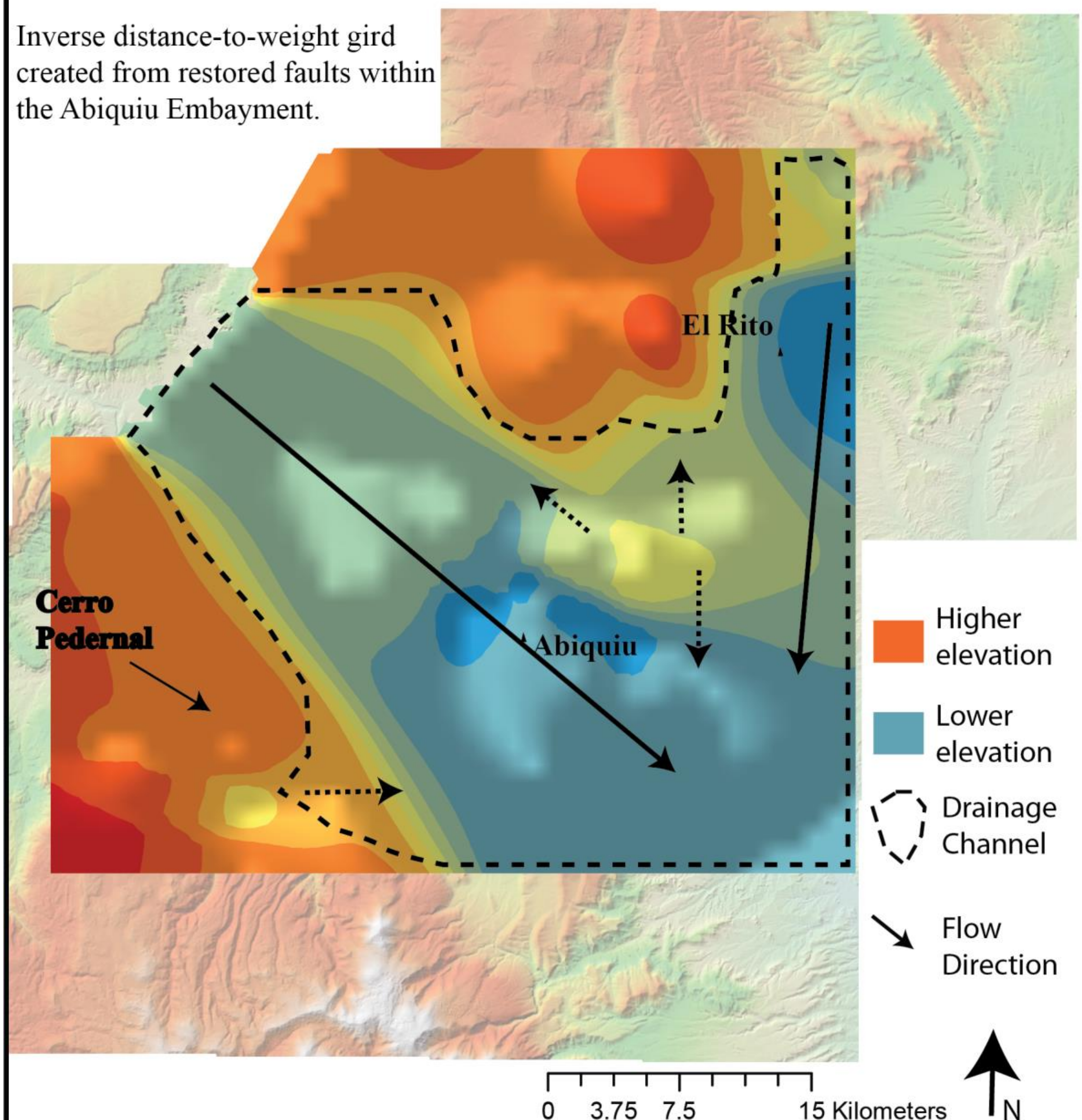


Figure 26: **Interpreted Eocene unconformity** Extrapolated from fault reconstruction measurements and modeling a surface grid using a inverse distance-to-weight method with a boundary defined by the exact extent of the area containing data. Paleocurrent directions are interpreted from topographic changes in the surface and from data collected within this study.

# 6. Interpretation and Discussion

## 6.1. PROVENANCE AND PALEOFLOW

The clast-count data and the point-count results indicate that the majority of sediment accumulated in the Eocene El Rito Basin was derived from the Tusas-Brazos Uplift. This is shown through the large amount of quartzite recorded within the sample areas that most likely is derived from the Proterozoic Ortega quartzite. The point-count data, recorded from samples higher in section than the clast counts, record a large amount of polymorphic quartzite and schist, suggesting a continued influence from the Tusas-Brazos Uplift, and increasing influence from Proterozoic Vadito group metavolcanic schist as Eocene time progressed. The Vadito group may have had more influence in the lower section as well; however the metavolcanic schist is prone to erosion at a much quicker rate than the quartzite.

The paleoflow measurements were limited to the base of the El Rito due to the abundance of clast on clast imbrication in the basal conglomerate. Imbricated clast measurements can be difficult in the best of circumstances, and the sub- to well-rounded cobble to boulders of the El Rito Formation do not form ideal imbrication. This simple field truth made it particularly important to gather the best clast-on-clast measurements possible, and to gather as many of them as were available in the 1m by 1m sample area. This leads me to have more faith in the sample locations where the full twenty measurements were taken over the locations with fewer. The larger sample sizes provides more evidence suggesting the bimodal flow indicated in the consolidated measurements, that show a north-south distribution of paleoflow (Figure 18), to be more representative of the drainage patterns than the individual smaller sample size areas. The overall bimodal, north-south distribution, along with the well indurated large clasts and provenance interpretation show that this particular study area was in close proximity to the flanks of the Tusas-Brazos Uplift. Suggesting that the base El Rito Formation was deposited in a high energy alluvial fan that accommodated the sediments shed longitudinally from the Tusas-Brazos Uplift.

#### 6.1.1. Local and regional topographic highs

The Laramide basement-cored structures flanking the El Rito Formation during the Eocene are similar, if not near identical to the basement-cored uplifts flanking the Abiquiu embayment today. This makes it particularly exciting when tracking down provincial detritus. There are three possibilities for sourcing the granite found in Arroyo del Cobre, all three of which have potential implications to the paleogeography. First, the clasts could be derived from the granite in the Nacimiento Uplift; because of the slight offset between the Tusas-Brazos and Nacimiento Uplifts this may require an easterly or northeasterly Nacimiento drainage pattern. Second, the granite could be derived from the granite found on the eastern edge of the modern Tusas-Brazos Uplift. This would require the granite to pass over a long distance, but because the Tusas-Brazos used to be connected to the now inverted San Luis Uplift, this distal westerly drainage pattern might be possible, were it not for the complete lack of granite in the El Rito Formation near the Tusas-Brazos study area. The third option requires the granite to be sourced from the Pajarito Uplift which is now inverted south and east of the Embudo transfer zone. This possibility would leave open the opportunity for north-directed drainage during deposition of the early El Rito Formation. The direct influence of deposition related to the regionally high Gallina-Archuleta is lacking in the study area. Cather (1992) suggests that northerly drainage existed in this basin in the Late Cretaceous, but was switched to south directed flow when the Gallina-Archuleta Arch redirected the river system. More research will need to be conducted to better understand the role the Gallina-Archuleta Arch had on the Eocene deposition.

## 6.2. EOCENE UNCONFORMABLE SURFACE

.

The angular unconformity at the base of the El Rito Formation marks a period of erosion and non-deposition that coincides with the large magnitude of uplift in the area during Laramide compression. The uplift can be constrained by apatite fission track data analyzed and collected by Kelley et al. (1992) and Ricketts (2014). The data indicate an 88 +\- 1 Ma AFT age for the northern Nacimiento Mountains and a younger 65.9 +\- 3.9 to 46 +\- 5 AFT age for the southern Nacimiento Mountains. To the east of the San Luis Basin, AFT ages indicate a ~46-35 Ma for the Sangre de Cristo Mountains. Although, there are younger data that show a double dating trend in this area caused by Cenozoic rifting. The AFT data show that the area to the west in the Nacimiento began to uplift in the Late Cretaceous and continued through the Paleogene, and since then that area has been relatively stable. This is in direct contrast to the easterly Sangre de Cristo Mountains, that have undergone reactivation and inversion due to Rio Grande rifting. The Tusas-Brazos Mountains, between the Nacimiento and Sangre de Cristo Ranges, are likely to have had an early uplift history similar to the Sangre de Cristos; however the Cenozoic history is more likely similar to the Nacimiento Range due to the lack of rift-related inversion within the westerly Tusas-Brazos front.

The uplift of these adjacent mountain ranges play a direct role in the erosional surface described here as the Eocene unconformity. To better understand the magnitude of this period of depositional hiatus the strata interpreted to overlie the unconformity has been calculated. The stratal thickness was interpreted in relation to seven outcrop locations where the El Rito Formation is found deposited unconformably above Paleozoic to Cretaceous strata. The thickness of the missing material is determined from an average recorded unit thicknesses within the region as indicated on the 7.5 minute quadrangle maps used in the ArcGIS portion of the study. The strata above the youngest Cretaceous rocks in the area was interpreted from a well log utilized in Cather (2004), this well log captures the stratal accumulations of the late Cretaceous prior to uplift that likely covered the study area. Figure 27 shows the thickness of strata removed prior to deposition of the El Rito Formation.

This pattern seen in the denudation history illustrated in figure 27 highlight the larger magnitude of erosion found toward Valle Grande Peak within the Tusas-Brazos Mountains. The erosion of the Ortega quartzite had to have begun prior to the deposition of the El Rito formation due to the abundance of quartzite cobbles and boulders in the lower El Rito sections. The larger magnitude of erosion toward the west may also indicate the proximity of the study area to the mountain range, both today and during the Eocene. This proximity to the Tusas-Brazos Uplift during the Eocene is likely driving the alluvial fan sedimentation observed in the stratigraphic measured section and the paleoflow study.

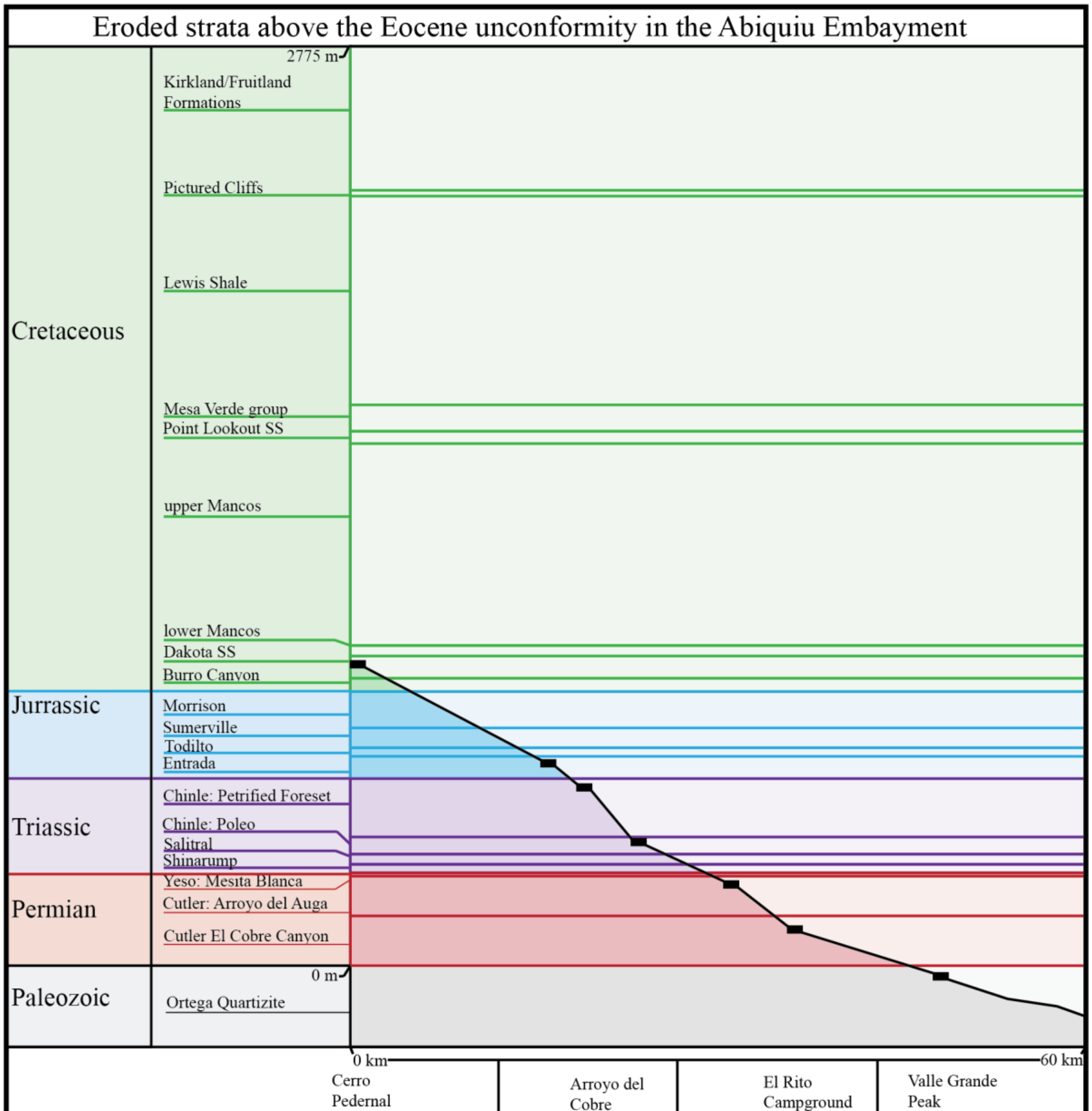


Figure 27: Plot illustrating the amount of strata eroded above the Eocene unconformity. Stratal thicknesses estimated from regional 7.5 minute geologic quadrangle maps. Line of section displayed in figure 6.

### 6.2.1. Basin geometry

Regardless of the quality and possible error of the surface the workflow was able to produce a model for the base of the El Rito Formation. This surface should show the orientation and topography for the basin near the time of initial deposition. The gridded surface depicts an axial basin with a floodplain width of 15 km that quickly rises up to the northeast and southwest into the respective Tusas-Brazos and Nacimiento Uplifts. As a comparison, the present Chama River valley has an average width of 6 km.

## 6.3. EOCENE PALEO-CHAMA RIVER

The digital-derived surface models, along with field measurements provide qualitative evidence for a possible Eocene paleo-Chama River. From the paleoflow measurements and provenance data the axis of the early paleo-Chama River drainage system may be further to the east, with the alluvial fan system feeding the system from the east. The inferred axial paleo-Chama river is interpreted as having begun as a north-draining intermontain basin, similar to the model proposed by Cather (1992). The timing and duration of the northerly flow is poorly constrained, although it is likely to have ended before the final deposition of the basal conglomerate in the Arroyo del Cobre area. This is inferred from the introduction of sand and silt lenses showing a change in flow direction and in detritus. The likely cause of a change in the river direction could be the continued rise of the Colorado Plateau, shifting the drainage north of the Nacimiento through the gap created in the Gallina-Archuleta Arch and then due south through the El Rito Basin and on into the Galisteo Basin, or the subsequent subsidence of the Pajarito Uplift in the south. The Galisteo Basin does see evidence for an added influx of sediment in the middle Eocene that may correspond to added load from a paleo-Chama river system joining with the current load from west of the Nacimiento Mountains.

## 6.4. PALEOGEOGRAPHIC INTERPRETATION

This study supports the Eocene paleogeography of Cather (1992). In this interpretation he shows the evolving importance of the paleo-Chama as a sediment source in the El Rito and Galiesto Basins. Figure 11 shows the interpretation and illustrates how early on the flow was north directed before the river system began to source from the Colorado Plateau, and as seen in this study began receiving a majority of its sediment from inundation of the Tusas-Brazos Uplift. The drainage was most likely axial with a larger input coming from the larger catchment toward the west (Figure 28), although the Tusas-Brazos did act as a barrier hindering the San Juan volcanism from leaking into the basin. The basin shows that toward the end of deposition a combination of a drier climate and eroded nearby uplifts made it possible to create a wide floodplain valley, as evidence by the likely paleosol deposited before the angular unconformity below the Rititio Conglomerate.

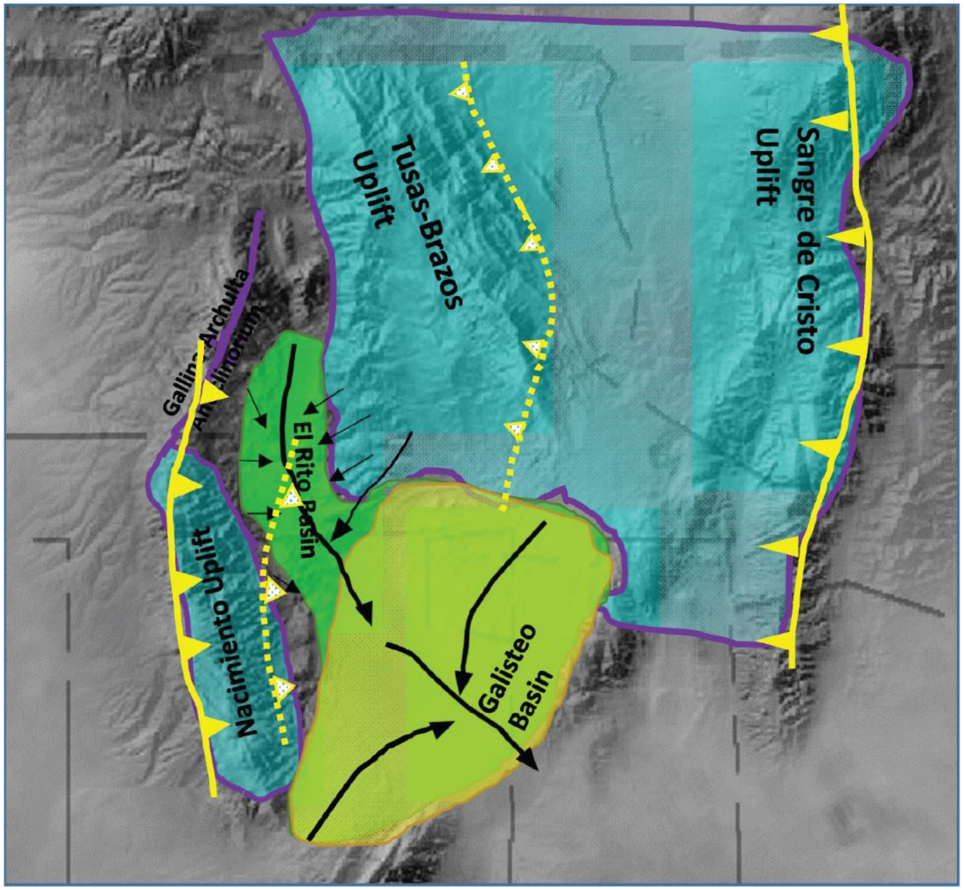


- Paleogeographic illustration of the middle-to late Eocene
- West vergent flow at southern end of El Rito Basin
- Present day geography in study area is similar to Eocene, despite a drastic change in structural styles

Basement-cored uplifts

El Rito piggy-back Basin

Galisteo Basin

Figure 28: Paleogeographic reconstruction of the middle to late Eocene. Created using data gathered in this study and modified from Cather 1992 and Cather 2004

# 7. Conclusions

Reactivation of Late Cretaceous to Paleogene thrust faults in the Cenozoic due to rift-related extension resulted in a landscape very similar to that which existed during the Eocene. The basement-cored Tusas-Brazos and Nacimiento Uplifts flank the Eocene El Rito Basin. These uplifts are initially driven by opposing polarity reverse faults, bounding the EL Rito Basin in a piggy-back style structure. In the Cenozoic, as a consequence of Rio Grande Rift extension, the eastern portion of the Tusas-Brazos Uplift, the San Luis Uplift, becomes inverted and causes the Tusas-Brazos to become a significant uplift again. The relative elevation of the area remained topographically high, even after Laramide compression waned. This was helped by a very short-lived transition between the regional final stages of Laramide compression (30.09 +/- 0.5 Ma Tomlinson, 2013) and the initial stages of Rio Grande rifting in the area (27-30 Ma Kelley et al., 2013). The paleo-Chama River system followed a very similar path as it does today during the middle to late Eocene and can be interpreted through field measurements and through the palinspastic reconstruction of local faults using the angular unconformity below the El Rito Formation as a datum.

# 8. Appendices

## APPENDIX 8.1. PALEOFLOW DATA

| | | | | | | | |
|---|---|---|---|---|---|---|---|
| **Appendix 8.1. Paleoflow data** | | | | | | | |
| The data indicate the field measurement and the compass direction of flow. Data were gathered at three | | | | | | | |
| different areas: Arroyo del Cobre (ADC), Valle Grande Peak (VGP), and El Rito Camp Ground (ERC) | | | | | | | |
| | | | | | | | |
| **Location** | **Type** | **ID/Unit** | **Strike** | **Dip** | **Azimuth° (RRR)** | **Flow direction** | **Area** |
| 0378360E 4011694N | Imbrication | Te_PF1 | N82W | 24NE | 278 | 188 | ADC-Eggs |
| | | | N62W | 31NE | 298 | 208 | |
| | | | S80W | 40NW | 260 | 170 | |
| | | | N02E | 50NW | 182 | 92 | |
| | | | S55W | 34NW | 235 | 145 | |
| | | | | | | | |
| 0380440E 4012218N | Imbrication | Te_PF2 | S55E | 33NE | 305 | 215 | East ADC |
| | | | west | 29N | 270 | 180 | |
| | | | N70W | 56NE | 290 | 200 | |
| | | | S85W | 9NW | 265 | 175 | |
| | | | N81W | 52NE | 279 | 189 | |
| | | | NORTH | 44E | 0 | 270 | |
| | | | S75W | 34NW | 255 | 165 | |
| | | | N45W | 65NE | 315 | 225 | |
| | | | S67W | 32NW | 247 | 157 | |
| | | | N88W | 34NE | 272 | 182 | |
| | | | | | | | |
| 0379462E 4011298N | Imbrication | Te_PF3 | 90W | 27S | 90 | 360 | ADC-Central |
| | | | S64W | 43SE | 64 | 334 | |
| | | | S78W | 29SE | 78 | 348 | |
| | | | S84W | 30SE | 84 | 354 | |
| | | | S71W | 39SE | 71 | 341 | |
| | | | S70W | 41SE | 70 | 340 | |
| | | | N51E | 57SE | 51 | 321 | |
| | | | N10E | 49NW | 190 | 100 | |
| | | | N12E | 55NW | 192 | 102 | |
| | | | S11W | 40SE | 11 | 281 | |
| | | | N85W | 24SW | 95 | 365 | |
| | | | S74E | 29SW | 286 | 196 | |
| | | | N73W | 44NE | 287 | 197 | |
| | | | | | | | |
| 378487E 4011636N | Cross-set Pair | Te_PF4_xs | N75W | 25SW | 105 | 186 | ADC-Eggs |
| | | | N40E | 24SE | 40 | 186 | |
| | | | | | | | |

Appendix 8.1. Continued

| Location | Type | ID/Unit | Strike | Dip | Azimuth° (RRR) | Flow direction | Area |
|---|---|---|---|---|---|---|---|
| 0379306E 4011700N | Imbrication | Te_PF5 | S49E | 42SW | 137 | 47 | ADC-Central |
| | | | S68E | 7SW | 118 | 28 | |
| | | | S72E | 1NE | 294 | 204 | |
| | | | S45E | 32NE | 321 | 231 | |
| | | | N5W | 39NE | 1 | 271 | |
| | | | N72W | 9SW | 114 | 24 | |
| | | | S84W | 5NW | 270 | 180 | |
| | | | S11E | 31SW | 175 | 85 | |
| | | | N85E | 12NW | 271 | 181 | |
| | | | N42W | 36NE | 324 | 234 | |
| | | | S72W | 8SE | 78 | 348 | |
| | | | N89E | 22SE | 95 | 5 | |
| | | | N49E | 2SE | 55 | 325 | |
| | | | N50E | 31NW | 236 | 146 | |
| | | | N48W | 16NE | 318 | 228 | |
| | | | N15E | 45NW | 201 | 111 | |
| | | | S75E | 16NW | 261 | 171 | |
| | | | N49W | 36SW | 137 | 47 | |
| | | | S81E | 4SW | 105 | 15 | |
| | | | N82W | 12NE | 284 | 194 | |
| | | | | | | | |
| 0379399E 4011522N | Imbrication | Te_PF6 | S88W | 2NW | 274 | 184 | ADC-Central |
| | | | S21W | 31SE | 27 | 297 | |
| | | | N86E | 36SE | 92 | 2 | |
| | | | N4W | 40NE | 2 | 272 | |
| | | | N64W | 41SW | 122 | 32 | |
| | | | N39W | 56SW | 147 | 57 | |
| | | | N75E | 15NW | 261 | 171 | |
| | | | 90E | 20S | 96 | 6 | |
| | | | N70E | 4NW | 256 | 166 | |
| | | | 180S | 41W | 186 | 96 | |
| | | | S39E | 11NE | 327 | 237 | |
| | | | N44W | 8SW | 142 | 52 | |
| | | | N25W | 14NE | 341 | 251 | |
| | | | N35W | 21NE | 331 | 241 | |
| | | | N68W | 27SW | 118 | 28 | |
| | | | S50W | 69NW | 236 | 146 | |
| | | | N16W | 20SW | 170 | 80 | |
| | | | N25W | 20NE | 341 | 251 | |
| | | | S19W | 50NW | 205 | 115 | |
| | | | N88W | 60SW | 98 | 8 | |

Appendix 8.1. Continued

| Location | Type | ID/Unit | Strike | Dip | Azimuth° (RRR) | Flow direction | Area |
|---|---|---|---|---|---|---|---|
| 0379471E 4011668N | Imbrication | Te_PF7 | S75E | 16SW | 105 | 15 | ADC-Central |
| | | | S55E | 21SW | 125 | 35 | |
| | | | S51W | 12SE | 51 | 321 | |
| | | | 270W | 16N | 270 | 180 | |
| | | | N79W | 23NE | 281 | 191 | |
| | | | S89W | 42SE | 89 | 359 | |
| | | | N42E | 31SE | 42 | 312 | |
| | | | S54W | 38SE | 54 | 324 | |
| | | | S59E | 37SW | 121 | 31 | |
| | | | N32E | 3NW | 212 | 122 | |
| | | | N27E | 72NW | 207 | 117 | |
| | | | N73W | 27SW | 107 | 17 | |
| | | | S48W | 5SE | 48 | 318 | |
| | | | N14W | 24SW | 166 | 76 | |
| | | | N80W | 28SW | 100 | 10 | |
| | | | S35W | 42NW | 215 | 125 | |
| | | | N59W | 51NE | 301 | 211 | |
| | | | S86E | 39SW | 94 | 4 | |
| | | | N71W | 54SW | 109 | 19 | |
| | | | N65W | 25SW | 115 | 25 | |
| | | | | | | | |
| 0379487E 4011637N | Imbrication | Te_PF8 | N74W | 22NE | 286 | 196 | ADC-Central |
| | | | N39E | 56SE | 39 | 309 | |
| | | | S45E | 40SW | 135 | 45 | |
| | | | N55W | 35NE | 305 | 215 | |
| | | | N25W | 31NE | 335 | 245 | |
| | | | N14E | 36SE | 14 | 284 | |
| | | | N80E | 21SE | 80 | 350 | |
| | | | S26E | 1SW | 154 | 64 | |
| | | | S18W | 37SE | 18 | 288 | |
| | | | N41W | 42SW | 139 | 49 | |
| | | | N32W | 44NE | 328 | 238 | |
| | | | S46E | 56NE | 314 | 224 | |
| | | | N58W | 55NE | 302 | 212 | |
| | | | N39E | 21SE | 39 | 309 | |
| | | | S55W | 41SE | 55 | 325 | |
| | | | S23W | 29SE | 23 | 293 | |
| | | | S18W | 29SE | 18 | 288 | |
| | | | S28E | 29NE | 332 | 242 | |
| | | | N62W | 20NE | 298 | 208 | |
| | | | N13W | 43NE | 347 | 257 | |

Appendix 8.1. Continued

| Location | Type | ID/Unit | Strike | Dip | Azimuth° (RRR) | Flow direction | Area |
|---|---|---|---|---|---|---|---|
| 0396218E 4030479N | Imbrication | Te_PF9 | S32E | 30NE | 328 | 238 | VGP |
| | | | S10W | 53SE | 10 | 280 | |
| | | | N53E | 39SE | 53 | 323 | |
| | | | N52E | 41SE | 52 | 322 | |
| | | | N52W | 28NE | 308 | 218 | |
| | | | N32W | 43NE | 328 | 238 | |
| | | | N72W | 44NE | 288 | 198 | |
| | | | S41E | 41NE | 319 | 229 | |
| | | | N11W | 70NE | 349 | 259 | |
| | | | N70W | 22NE | 290 | 200 | |
| | | | N40W | 30NE | 320 | 230 | |
| | | | N60E | 41SE | 60 | 330 | |
| | | | S49W | 49SE | 49 | 319 | |
| | | | S26E | 74NE | 334 | 244 | |
| | | | S62E | 35NE | 298 | 208 | |
| | | | S87W | 53NW | 267 | 177 | |
| | | | N72W | 32NE | 288 | 198 | |
| | | | N10W | 22NE | 350 | 260 | |
| | | | S36E | 61NE | 324 | 234 | |
| | | | S68E | 41NW | 248 | 158 | |
| | | | | | | | |
| 0379470E 4011426N | Imbrication | Te_PF10 | N85W | 31SW | 95 | 5 | ADC-Central |
| | | | N86W | 62SW | 94 | 4 | |
| | | | S75W | 48SE | 75 | 345 | |
| | | | N76W | 46SW | 104 | 14 | |
| | | | 270W | 65S | 90 | 0 | |
| | | | N88W | 66SW | 92 | 2 | |
| | | | N84W | 32SW | 96 | 6 | |
| | | | S71W | 85SE | 71 | 341 | |
| | | | S64W | 73SE | 64 | 334 | |
| | | | N67E | 46SE | 67 | 337 | |
| | | | N75W | 35SW | 105 | 15 | |
| | | | S85E | 38SW | 95 | 5 | |
| | | | N78E | 33SE | 78 | 348 | |
| | | | N82E | 37SE | 82 | 352 | |
| | | | N85E | 59SE | 85 | 355 | |
| | | | N78E | 61SE | 78 | 348 | |
| | | | N82E | 24SE | 82 | 352 | |
| | | | N86W | 59SW | 94 | 4 | |
| | | | S82W | 27SE | 82 | 352 | |
| | | | S64W | 40SE | 64 | 334 | |

Appendix 8.1. Continued

| Location | Type | ID/Unit | Strike | Dip | Azimuth° (RRR) | Flow direction | Area |
|---|---|---|---|---|---|---|---|
| 0388773E 4028522N | Imbrication | Te_PF11 | S54E | 84SW | 126 | 36 | ERC |
| | | | S76E | 84SW | 104 | 14 | |
| | | | N10E | 42SE | 10 | 280 | |
| | | | 0N | 55E | 0 | 270 | |
| | | | S7E | 67NE | 353 | 263 | |
| | | | S42E | 33NE | 318 | 228 | |
| | | | N8E | 32SE | 8 | 278 | |
| | | | S76E | 52SW | 104 | 14 | |
| | | | S43W | 41SE | 43 | 313 | |
| | | | S57W | 49SE | 57 | 327 | |
| | | | N61W | 59NE | 299 | 209 | |
| | | | S14E | 47NE | 346 | 256 | |
| | | | S52E | 42NE | 308 | 218 | |
| | | | N65E | 76NW | 245 | 155 | |
| | | | N22W | 49NE | 338 | 248 | |
| | | | S50E | 54NE | 310 | 220 | |
| | | | S42E | 59NE | 318 | 228 | |
| | | | S75E | 50NE | 285 | 195 | |
| | | | S73E | 24NE | 287 | 197 | |
| | | | S38W | 20SE | 38 | 308 | |
| | | | | | | | |
| 0389008E 4028262N | Imbrication | Te_PF12 | N80E | 57SE | 80 | 350 | ERC |
| | | | S18W | 20NW | 198 | 108 | |
| | | | 270W | 36S | 90 | 0 | |
| | | | N57E | 33SE | 57 | 327 | |
| | | | S60E | 20NE | 300 | 210 | |
| | | | N75E | 31NW | 255 | 165 | |
| | | | S42W | 28SE | 42 | 312 | |
| | | | S77W | 68NW | 257 | 167 | |
| | | | S75E | 35NE | 285 | 195 | |
| | | | N85E | 50SE | 85 | 355 | |
| | | | N65E | 58SE | 65 | 335 | |
| | | | S81E | 30NE | 279 | 189 | |
| | | | S70E | 52NE | 280 | 190 | |
| | | | N75W | 43SW | 105 | 15 | |
| | | | S71E | 31NE | 289 | 199 | |
| | | | S64E | 71NE | 296 | 206 | |
| | | | S40E | 59NE | 320 | 230 | |
| | | | S30E | 54NE | 330 | 240 | |
| | | | S56E | 64NE | 304 | 214 | |
| | | | N66W | 57NE | 294 | 204 | |

Appendix 8.1. Continued

| Location | Type | ID/Unit | Strike | Dip | Azimuth° (RRR) | Flow direction | Area |
|---|---|---|---|---|---|---|---|
| 0388997E 4028268N | Imbrication | Te_PF13 | S65E | 54NE | 295 | 205 | ERC |
| | | | S54W | 13SE | 54 | 324 | |
| | | | S85E | 39SW | 95 | 365 | |
| | | | S19E | 23NE | 341 | 251 | |
| | | | N75E | 28NW | 255 | 165 | |
| | | | N60W | 23NE | 300 | 210 | |
| | | | N28E | 23NW | 332 | 242 | |
| | | | N70W | 45NE | 290 | 200 | |
| | | | S20E | 54NE | 340 | 250 | |
| | | | N80E | 28NW | 260 | 170 | |
| | | | S30W | 75NW | 210 | 120 | |
| | | | N48W | 48SW | 132 | 42 | |
| | | | S18E | 35SW | 162 | 72 | |
| | | | S8E | 50SW | 172 | 82 | |
| | | | S30E | 45SW | 150 | 60 | |
| | | | S50W | 52NW | 230 | 140 | |
| | | | N28E | 42SE | 28 | 298 | |
| | | | N85E | 49NW | 265 | 175 | |
| | | | S85E | 63SW | 95 | 365 | |
| | | | N45W | 38NE | 315 | 225 | |
| | | | | | | | |
| 0389014E 4028250N | Imbrication | Te_PF14 | S70W | 62SE | 70 | 340 | ERC |
| | | | S72E | 32NE | 288 | 198 | |
| | | | N83E | 40NW | 263 | 173 | |
| | | | S61E | 23NE | 299 | 209 | |
| | | | S26E | 50NE | 334 | 244 | |
| | | | S55E | 13NE | 305 | 215 | |
| | | | N72W | 36NE | 288 | 198 | |
| | | | S84E | 22NE | 276 | 186 | |
| | | | S48E | 32NE | 312 | 222 | |
| | | | S61E | 24NE | 299 | 209 | |
| | | | S5E | 25NE | 355 | 265 | |
| | | | N70E | 41SE | 70 | 340 | |
| | | | S71W | 27SE | 71 | 341 | |
| | | | S45W | 30NW | 225 | 135 | |
| | | | N54E | 37NW | 234 | 144 | |
| | | | S70W | 45NW | 250 | 160 | |
| | | | S78W | 30NW | 258 | 168 | |
| | | | N80E | 71NW | 260 | 170 | |
| | | | S75W | 70NW | 255 | 165 | |
| | | | N66W | 19NE | 294 | 204 | |

Appendix 8.1. Continued

| Location | Type | ID/Unit | Strike | Dip | Azimuth° (RRR) | Flow direction | Area |
|---|---|---|---|---|---|---|---|
| 0389088E 4028207N | Imbrication | Te_PF15 | N43E | 39SE | 43 | 313 | ERC |
| | | | S38W | 33SE | 38 | 308 | |
| | | | N65E | 61NW | 245 | 155 | |
| | | | S71W | 38NW | 251 | 161 | |
| | | | N57E | 63SE | 57 | 327 | |
| | | | N67E | 76SE | 67 | 337 | |
| | | | 90E | 34N | 270 | 180 | |
| | | | N44E | 63SE | 44 | 314 | |
| | | | N87E | 35SE | 87 | 357 | |
| | | | N66W | 40NE | 294 | 204 | |
| | | | S78E | 37SW | 102 | 12 | |
| | | | S61W | 33SE | 61 | 331 | |
| | | | S66E | 31NE | 294 | 204 | |
| | | | S25E | 34NE | 335 | 245 | |
| | | | S88E | 57NE | 272 | 182 | |
| | | | N86E | 35SE | 86 | 356 | |
| | | | N78W | 36SW | 102 | 12 | |
| | | | S84W | 43SE | 84 | 354 | |
| | | | S39W | 41SE | 39 | 309 | |
| | | | S55W | 26SE | 55 | 325 | |

# APPENDIX 8.2. CLAST DATA

| **Appendix 8.2. Clast Data** | | | | | | | | | | |
|---|---|---|---|---|---|---|---|---|---|---|
| Site # | Field Page | X-Coordinate | Y-Coordinate | Elevation(ft) | picture # | Formation | Rock Type | Count | Relative% | n |
| Te_CC1 | 25 | 0378360E | 4011694N | 6586 | | El Rito | white quartzite w/black seams | 8 | 16.666667 | 48 |
| | | | | | | | grey quartzite | 11 | 22.916667 | 48 |
| | | | | | | | grey & white banded quartzite | 8 | 16.666667 | 48 |
| | | | | | | | yellow-green quartzite | 5 | 10.416667 | 48 |
| | | | | | | | sandstone, light grey qt grains | 4 | 8.3333333 | 48 |
| | | | | | | | mylonite quartzite | 5 | 10.416667 | 48 |
| | | | | | | | white quartzite | 7 | 14.583333 | 48 |
| | | | | | | | | | | |
| Te_CC2 | 27 | 0377631E | 4012015N | 6669 | 24-27? fc:SW | El Rito | grey quartzite | 22 | 28.947368 | 76 |
| | | | | | | | grey-black banded quartzite | 8 | 10.526316 | 76 |
| | | | | | | | white quartzite | 16 | 21.052632 | 76 |
| | | | | | | | yellow-green quartzite | 12 | 15.789474 | 76 |
| | | | | | | | rose quartzite | 6 | 7.8947368 | 76 |
| | | | | | | | grey mylonite | 3 | 3.9473684 | 76 |
| | | | | | | | granite | 2 | 2.6315789 | 76 |
| | | | | | | | metavolcanic (quartzofeldspathic g | 1 | 1.3157895 | 76 |
| | | | | | | | pink very fine sandstone | 6 | 7.8947368 | 76 |
| | | | | | | | | | | |
| Te_CC3 | 45 | 0379577E | 4011488N | 6203 | 897-901 | El Rito | grey & white banded quartzite | 9 | 12.857143 | 70 |
| | | | | | | | grey quartzite | 32 | 45.714286 | 70 |
| | | | | | | | green quartzite | 14 | 20 | 70 |
| | | | | | | | white quartzite | 6 | 8.5714286 | 70 |
| | | | | | | | white-green quartzite | 4 | 5.7142857 | 70 |
| | | | | | | | granite | 3 | 4.2857143 | 70 |
| | | | | | | | sandstone | 2 | 2.8571429 | 70 |
| | | | | | | | | | | |
| Te_CC4 | 48 | 0380440E | 4012218N | 6597 | 912-915 | El Rito | grey-black banded quartzite | 7 | 5.5555556 | 126 |
| | | | | | | | grey quartzite | 42 | 33.333333 | 126 |
| | | | | | | | coarse sandstone | 23 | 18.253968 | 126 |
| | | | | | | | fine sandstone | 8 | 6.3492063 | 126 |
| | | | | | | | rose quartzite | 5 | 3.968254 | 126 |
| | | | | | | | green quartzite | 29 | 23.015873 | 126 |
| | | | | | | | green-grey banded quatzite | 3 | 2.3809524 | 126 |
| | | | | | | | shist | 2 | 1.5873016 | 126 |
| | | | | | | | grey-black banded quartzite | 7 | 5.5555556 | 126 |
| | | | | | | | | | | |
| Tr_CC1 | 59 | 037960E | 4010568N | 6164 | 978-981 | Ritito | red-black gneiss | 22 | 22.222222 | 99 |
| | | | | | | | granite | 23 | 23.232323 | 99 |
| | | | | | | | rose quartzite | 3 | 3.030303 | 99 |
| | | | | | | | grey quartzite | 8 | 8.0808081 | 99 |
| | | | | | | | white quartzite | 10 | 10.10101 | 99 |
| | | | | | | | coarse granite (porphritic?) | 6 | 6.0606061 | 99 |
| | | | | | | | black mylonite | 3 | 3.030303 | 99 |
| | | | | | | | dark grey quartzite | 15 | 15.151515 | 99 |
| | | | | | | | green mylonite | 4 | 4.040404 | 99 |
| | | | | | | | sandstone | 5 | 5.0505051 | 99 |
| | | | | | | | | | | |
| Tr_CC2 | 62 | 0379773E | 4009941N | 6082 | 988-990 | Ritito | porphritic granite | 25 | 22.321429 | 112 |
| | | | | | | | dark grey quartzite | 39 | 34.821429 | 112 |
| | | | | | | | granite | 12 | 10.714286 | 112 |
| | | | | | | | grey quartzite | 7 | 6.25 | 112 |
| | | | | | | | white quartzite | 4 | 3.5714286 | 112 |
| | | | | | | | gneiss | 12 | 10.714286 | 112 |
| | | | | | | | rose quartzite | 5 | 4.4642857 | 112 |
| | | | | | | | white-green phylite | 8 | 7.1428571 | 112 |
| | | | | | | | | | | |
| Tr_CC3 | 73 | 0364026E | 4001051N | ? | 369-370 | Ritito | tan sandstone | 23 | 19.327731 | 119 |
| | | | | | | | pink granite | 25 | 21.008403 | 119 |
| | | | | | | | white sandstone | 12 | 10.084034 | 119 |
| | | | | | | | black phyllite | 8 | 6.7226891 | 119 |
| | | | | | | | white quartzite | 3 | 2.5210084 | 119 |
| | | | | | | | salt & pepper diorite | 1 | 0.8403361 | 119 |
| | | | | | | | black & white gneiss | 2 | 1.6806723 | 119 |
| | | | | | | | biotite schist | 10 | 8.4033613 | 119 |
| | | | | | | | red(FG) granite | 14 | 11.764706 | 119 |
| | | | | | | | pink quartzite | 4 | 3.3613445 | 119 |
| | | | | | | | grey quartzite | 11 | 9.2436975 | 119 |
| | | | | | | | white-grey quartzite | 4 | 3.3613445 | 119 |
| | | | | | | | granodiorite | 2 | 1.6806723 | 119 |

Appendix 8.2. Continued

| Site # | Field Page | X-Coordinate | Y-Coordinate | Elevation(ft) | picture # | Formation | Rock Type | Count | Relative% | n |
|---|---|---|---|---|---|---|---|---|---|---|
| Tr_CC4 | 75 | 0364031E | 4001058N | ? | 373-374 | Ritito | pink granite | 19 | 13.475177 | 141 |
| | | | | | | | white sandstone | 8 | 5.6737589 | 141 |
| | | | | | | | tan sandstone | 41 | 29.078014 | 141 |
| | | | | | | | black phyllite | 11 | 7.8014184 | 141 |
| | | | | | | | white quartzite | 7 | 4.964539 | 141 |
| | | | | | | | grey quartzite | 10 | 7.0921986 | 141 |
| | | | | | | | pink quartzite | 4 | 2.8368794 | 141 |
| | | | | | | | black & white gneiss | 2 | 1.4184397 | 141 |
| | | | | | | | biotite schist | 6 | 4.2553191 | 141 |
| | | | | | | | red(FG) granite | 2 | 1.4184397 | 141 |
| | | | | | | | granodiorite | 2 | 1.4184397 | 141 |
| | | | | | | | basalt | 2 | 1.4184397 | 141 |
| | | | | | | | black quartzite | 9 | 6.3829787 | 141 |
| | | | | | | | red & black gneiss | 16 | 11.347518 | 141 |
| | | | | | | | diorite | 2 | 1.4184397 | 141 |
| | | | | | | | | | | |
| Tr_CC5 | 77 | 0363982E | 4001050N | ? | 387:388 | Ritito | pink granite | 17 | 15.315315 | 111 |
| | | | | | | | white sandstone | 11 | 9.9099099 | 111 |
| | | | | | | | tan sandstone | 14 | 12.612613 | 111 |
| | | | | | | | black phyllite | 9 | 8.1081081 | 111 |
| | | | | | | | white quartzite | 5 | 4.5045045 | 111 |
| | | | | | | | white-grey quartzite | 2 | 1.8018018 | 111 |
| | | | | | | | grey quartzite | 5 | 4.5045045 | 111 |
| | | | | | | | pink quartzite | 5 | 4.5045045 | 111 |
| | | | | | | | black & white gneiss | 3 | 2.7027027 | 111 |
| | | | | | | | biotite schist | 10 | 9.009009 | 111 |
| | | | | | | | red(FG) granite | 15 | 13.513514 | 111 |
| | | | | | | | granodiorite | 2 | 1.8018018 | 111 |
| | | | | | | | black quartzite | 8 | 7.2072072 | 111 |
| | | | | | | | red & black gneiss | 4 | 3.6036036 | 111 |
| | | | | | | | diorite | 1 | 0.9009009 | 111 |
| | | | | | | | | | | |
| Tr_CC6 | 79 | 0363981E | 4001046N | ? | 386 | Ritito | pink granite | 16 | 15.238095 | 105 |
| | | | | | | | white sandstone | 18 | 17.142857 | 105 |
| | | | | | | | tan sandstone | 12 | 11.428571 | 105 |
| | | | | | | | black phyllite | 9 | 8.5714286 | 105 |
| | | | | | | | white quartzite | 4 | 3.8095238 | 105 |
| | | | | | | | grey quartzite | 5 | 4.7619048 | 105 |
| | | | | | | | pink quartzite | 7 | 6.6666667 | 105 |
| | | | | | | | black & white gneiss | 5 | 4.7619048 | 105 |
| | | | | | | | biotite schist | 5 | 4.7619048 | 105 |
| | | | | | | | red(FG) granite | 9 | 8.5714286 | 105 |
| | | | | | | | granodiorite | 2 | 1.9047619 | 105 |
| | | | | | | | black quartzite | 3 | 2.8571429 | 105 |
| | | | | | | | red & black gneiss | 6 | 5.7142857 | 105 |
| | | | | | | | diorite | 3 | 2.8571429 | 105 |
| | | | | | | | quartz mylonite | 1 | 0.952381 | 105 |
| | | | | | | | | | | |
| Tr_CC7 | 81 | 0379597E | 4010441N | ? | 433-436 | Ritito | grey quartzite | 12 | 11.320755 | 106 |
| | | | | | | | black & white banded quartzite | 4 | 3.7735849 | 106 |
| | | | | | | | black quartzite | 16 | 15.09434 | 106 |
| | | | | | | | white quartzite | 11 | 10.377358 | 106 |
| | | | | | | | pink quartzite | 9 | 8.490566 | 106 |
| | | | | | | | granite | 12 | 11.320755 | 106 |
| | | | | | | | metagranite | 8 | 7.5471698 | 106 |
| | | | | | | | kyanite schist | 13 | 12.264151 | 106 |
| | | | | | | | tan sandstone | 1 | 0.9433962 | 106 |
| | | | | | | | red & black quartzite | 20 | 18.867925 | 106 |
| | | | | | | | | | | |
| Te_CC5 | 85 | 0379306E | 4011700N | ? | 463-464 | El Rito | metagranite | 6 | 4.5801527 | 131 |
| | | | | | | | white quartzite | 11 | 8.3969466 | 131 |
| | | | | | | | grey quartzite | 31 | 23.664122 | 131 |
| | | | | | | | green-black quartzite | 10 | 7.6335878 | 131 |
| | | | | | | | white-grey quartzite | 4 | 3.0534351 | 131 |
| | | | | | | | pink-white banded quartzite | 10 | 7.6335878 | 131 |
| | | | | | | | pink quartzite | 6 | 4.5801527 | 131 |
| | | | | | | | gneiss | 2 | 1.5267176 | 131 |
| | | | | | | | green quartzite | 32 | 24.427481 | 131 |
| | | | | | | | granite | 13 | 9.9236641 | 131 |
| | | | | | | | green-white quartzite | 3 | 2.2900763 | 131 |
| | | | | | | | pink-black quartzite | 3 | 2.2900763 | 131 |

Appendix 8.2. Continued

| Site # | Field Page | X-Coordinate | Y-Coordinate | Elevation(ft) | picture # | Formation | Rock Type | Count | Relative% | n |
|---|---|---|---|---|---|---|---|---|---|---|
| Te_CC6 | 87 | 0379399E | 4011522N | ? | 465-466 | El Rito | metagranite | 6 | 4.9180328 | 122 |
| | | | | | | | white quartzite | 5 | 4.0983607 | 122 |
| | | | | | | | grey quartzite | 28 | 22.95082 | 122 |
| | | | | | | | green-black quartzite | 7 | 5.7377049 | 122 |
| | | | | | | | white-grey quartzite | 5 | 4.0983607 | 122 |
| | | | | | | | pink-grey quartzite | 1 | 0.8196721 | 122 |
| | | | | | | | pink quartzite | 4 | 3.2786885 | 122 |
| | | | | | | | gneiss | 1 | 0.8196721 | 122 |
| | | | | | | | green quartzite | 29 | 23.770492 | 122 |
| | | | | | | | granite | 20 | 16.393443 | 122 |
| | | | | | | | green-white quartzite | 8 | 6.557377 | 122 |
| | | | | | | | pink-black quartzite | 4 | 3.2786885 | 122 |
| | | | | | | | sandstone | 4 | 3.2786885 | 122 |
| | | | | | | | | | | |
| Te_CC7 | 89 | 0379471E | 4011668N | ? | 480-481 | EL Rito | white quartzite | 9 | 7.03125 | 128 |
| | | | | | | | black quartzite | 5 | 3.90625 | 128 |
| | | | | | | | grey quartzite | 25 | 19.53125 | 128 |
| | | | | | | | green-black quartzite | 37 | 28.90625 | 128 |
| | | | | | | | white-grey quartzite | 1 | 0.78125 | 128 |
| | | | | | | | pink quartzite | 1 | 0.78125 | 128 |
| | | | | | | | schist | 2 | 1.5625 | 128 |
| | | | | | | | green quartzite | 27 | 21.09375 | 128 |
| | | | | | | | granite | 8 | 6.25 | 128 |
| | | | | | | | green-white quartzite | 3 | 2.34375 | 128 |
| | | | | | | | rhyolite tuff | 9 | 7.03125 | 128 |
| | | | | | | | sandstone | 1 | 0.78125 | 128 |
| | | | | | | | | | | |
| Te_CC8 | 91 | 0379487E | 4011637N | ? | ? | El Rito | white quartzite | 14 | 10.526316 | 133 |
| | | | | | | | green quartzite | 25 | 18.796992 | 133 |
| | | | | | | | grey quartzite | 12 | 9.0225564 | 133 |
| | | | | | | | pink quartzite | 2 | 1.5037594 | 133 |
| | | | | | | | white-black quartzite | 21 | 15.789474 | 133 |
| | | | | | | | green-black quartzite | 32 | 24.06015 | 133 |
| | | | | | | | pink-white quartzite | 1 | 0.7518797 | 133 |
| | | | | | | | pink-black quartzite | 5 | 3.7593985 | 133 |
| | | | | | | | granite | 4 | 3.0075188 | 133 |
| | | | | | | | rhyolite tuff | 5 | 3.7593985 | 133 |
| | | | | | | | green-white quartzite | 12 | 9.0225564 | 133 |
| | | | | | | | | | | |
| Te_CC9 | 95 | 0396218E | 4030479N | ? | ? | El Rito | grey quartzite | 17 | 14.655172 | 116 |
| | | | | | | | white-black banded quartzite | 35 | 30.172414 | 116 |
| | | | | | | | schist | 8 | 6.8965517 | 116 |
| | | | | | | | gneiss | 2 | 1.7241379 | 116 |
| | | | | | | | pink quartzite | 2 | 1.7241379 | 116 |
| | | | | | | | tan quartzite | 4 | 3.4482759 | 116 |
| | | | | | | | white quartzite | 26 | 22.413793 | 116 |
| | | | | | | | tan-white quartzite | 19 | 16.37931 | 116 |
| | | | | | | | green-black quartzite | 3 | 2.5862069 | 116 |
| | | | | | | | | | | |
| Te_CC10 | 97 | 0379470E | 4011426N | ? | 522 | El Rito | white quartzite | 10 | 7.5757576 | 132 |
| | | | | | | | grey quartzite | 14 | 10.606061 | 132 |
| | | | | | | | green quartzite | 20 | 15.151515 | 132 |
| | | | | | | | green-black quartzite | 34 | 25.757576 | 132 |
| | | | | | | | green-white quartzite | 6 | 4.5454545 | 132 |
| | | | | | | | white-black quartzite | 5 | 3.7878788 | 132 |
| | | | | | | | pink quartzite | 4 | 3.030303 | 132 |
| | | | | | | | pink-white quartzite | 2 | 1.5151515 | 132 |
| | | | | | | | pink-black quartzite | 6 | 4.5454545 | 132 |
| | | | | | | | granite | 8 | 6.0606061 | 132 |
| | | | | | | | rhyolite tuff | 23 | 17.424242 | 132 |
| | | | | | | | | | | |
| Te_CC11 | 115 | 0388733E | 4028522N | ? | 571 | El Rito | white quartzite | 16 | 14.545455 | 110 |
| | | | | | | | grey quartzite | 38 | 34.545455 | 110 |
| | | | | | | | black quartzite | 8 | 7.2727273 | 110 |
| | | | | | | | green-black quartzite | 1 | 0.9090909 | 110 |
| | | | | | | | white-grey quartzite | 31 | 28.181818 | 110 |
| | | | | | | | white-black quartzite | 2 | 1.8181818 | 110 |
| | | | | | | | pink quartzite | 3 | 2.7272727 | 110 |
| | | | | | | | pink-white quartzite | 1 | 0.9090909 | 110 |
| | | | | | | | pink-black quartzite | 9 | 8.1818182 | 110 |
| | | | | | | | schist | 1 | 0.9090909 | 110 |

Appendix 8.2. Continued

| Site # | Field Page | X-Coordinate | Y-Coordinate | Elevation(ft) | picture # | Formation | Rock Type | Count | Relative% | n |
|---|---|---|---|---|---|---|---|---|---|---|
| Te_CC12 | 117 | 0389009E | 4028262N | ? | 572 | El Rito | white quartzite | 34 | 25.185185 | 135 |
| | | | | | | | grey quartzite | 28 | 20.740741 | 135 |
| | | | | | | | black quartzite | 1 | 0.7407407 | 135 |
| | | | | | | | green-black quartzite | 4 | 2.962963 | 135 |
| | | | | | | | white-grey quartzite | 6 | 4.4444444 | 135 |
| | | | | | | | white-black quartzite | 27 | 20 | 135 |
| | | | | | | | pink quartzite | 7 | 5.1851852 | 135 |
| | | | | | | | pink-white quartzite | 10 | 7.4074074 | 135 |
| | | | | | | | pink-black quartzite | 7 | 5.1851852 | 135 |
| | | | | | | | schist | 11 | 8.1481481 | 135 |
| | | | | | | | | | | |
| Te_CC13 | 119 | 0388997E | 4028268N | ? | ? | El Rito | white quartzite | 10 | 10.526316 | 95 |
| | | | | | | | grey quartzite | 36 | 37.894737 | 95 |
| | | | | | | | black quartzite | 19 | 20 | 95 |
| | | | | | | | green-black quartzite | 7 | 7.3684211 | 95 |
| | | | | | | | white-grey quartzite | 2 | 2.1052632 | 95 |
| | | | | | | | white-black quartzite | 16 | 16.842105 | 95 |
| | | | | | | | pink-white quartzite | 2 | 2.1052632 | 95 |
| | | | | | | | pink-black quartzite | 2 | 2.1052632 | 95 |
| | | | | | | | schist | 1 | 1.0526316 | 95 |
| | | | | | | | | | | |
| Te_CC14 | 121 | 0389014E | 4028250N | ? | 574 | El Rito | white quartzite | 17 | 13.934426 | 122 |
| | | | | | | | grey quartzite | 33 | 27.04918 | 122 |
| | | | | | | | black quartzite | 16 | 13.114754 | 122 |
| | | | | | | | green-black quartzite | 3 | 2.4590164 | 122 |
| | | | | | | | white-black quartzite | 15 | 12.295082 | 122 |
| | | | | | | | pink-white quartzite | 3 | 2.4590164 | 122 |
| | | | | | | | pink-black quartzite | 4 | 3.2786885 | 122 |
| | | | | | | | schist | 10 | 8.1967213 | 122 |
| | | | | | | | pink quartzite | 4 | 3.2786885 | 122 |
| | | | | | | | white-grey quartzite | 16 | 13.114754 | 122 |
| | | | | | | | sandstone | 1 | 0.8196721 | 122 |
| | | | | | | | | | | |
| Te_CC15 | 123 | 0389088E | 4028207N | ? | 577 | El Rito | white quartzite | 19 | 15.447154 | 123 |
| | | | | | | | grey quartzite | 43 | 34.95935 | 123 |
| | | | | | | | black quartzite | 7 | 5.6910569 | 123 |
| | | | | | | | white-grey quartzite | 29 | 23.577236 | 123 |
| | | | | | | | white-black quartzite | 14 | 11.382114 | 123 |
| | | | | | | | pink quartzite | 1 | 0.8130081 | 123 |
| | | | | | | | pink-black quartzite | 4 | 3.2520325 | 123 |
| | | | | | | | schist | 6 | 4.8780488 | 123 |

APPENDIX 8.3. CLAST ROSE DIAGRAM DATA

| | | | | | | |
|---|---|---|---|---|---|---|
| **Appendix 8.3. Clast rose diagram data** | | | | | | |
| **Clast Counts for the El Rito Formation, North-Central, New Mexico.** | | | | | | |
| Locations are UTM NAD27, zone 13S; N = number of clasts counted in each category. | | | | | | |
| The metavolcanic, metasedimentary, and plutonic rocks, pegmatite, and vein quartz | | | | | | |
| are Proterozoic in age. | | | | | | |
| | | | | | | |
| **Location: Arroyo Seco** | 0378360E | 4011694N | | **Location: Arroyo Seco** | 0377631E | 4012015N |
| **Te_CC1** | | | | **Te_CC2** | | |
| | N | Relative % | | | N | Relative % |
| Quartzite | 39 | 81.3 | | Quartzite | 64 | 84.21 |
| Sandstone | 4 | 8.3 | | Mylonite | 4 | 5.26 |
| Mylonite | 5 | 10.4 | | Granite | 2 | 2.63 |
| *sum* | 48 | | | Sandstone | 6 | 7.89 |
| | | | | sum | 76 | |
| | | | | | | |
| | | | | | | |
| | | | | | | |
| **Location: Arroyo Seco** | 0379577E | 4011488N | | **Location: Arroyo Seco** | 0380440E | 4012218N |
| **Te_CC3** | | | | **Te_CC4** | | |
| | N | Relative % | | | N | Relative % |
| Quartzite | 65 | 92.86 | | Quartzite | 93 | 73.81 |
| Granite | 3 | 4.29 | | Sandstone | 31 | 24.60 |
| Sandstone | 2 | 2.86 | | Schist | 2 | 1.59 |
| *sum* | 70 | | | *sum* | 126 | |
| | | | | | | |
| | | | | | | |
| | | | | | | |
| | | | | | | |
| **Location: Arroyo Seco** | 0379306E | 4011700N | | **Location: Arroyo Seco** | 0379399E | 4011522N |
| **Te_CC5** | | | | **Te_CC6** | | |
| | N | Relative % | | | N | Relative % |
| Quartzite | 110 | 83.97 | | Quartzite | 91 | 74.59 |
| Granite | 19 | 14.50 | | Granite | 26 | 21.31 |
| Geniss | 2 | 1.53 | | Geniss | 1 | 0.82 |
| *sum* | 131 | | | Sandstone | 4 | 3.28 |
| | | | | *sum* | 122 | |
| | | | | | | |
| | | | | | | |
| | | | | | | |
| **Location: Arroyo Seco** | 0379471E | 4011668N | | **Location: Arroyo Seco** | 0379487E | 4011637N |
| **Te_CC7** | | | | **Te_CC8** | | |
| | N | Relative % | | | N | Relative % |
| Quartzite | 108 | 84.38 | | Quartzite | 124 | 93.23 |
| Granite | 17 | 13.28 | | Granite | 9 | 6.77 |
| Schist | 2 | 1.56 | | *sum* | 133 | |
| Sandstone | 1 | 0.78 | | | | |
| *sum* | 128 | | | | | |

Appendix 8.3. Continued

| | | | | | | |
|---|---|---|---|---|---|---|
| **Appendix 8.3. Continued** | | | | | | |
| **Location: Arroyo Seco** | 0396218E | 4030479N | | **Location: Arroyo Seco** | 0379470E | 4011426N |
| **Te_CC9** | | | | **Te_CC10** | | |
| | N | Relative % | | | N | Relative % |
| Quartzite | 106 | 91.38 | | Quartzite | 101 | 76.52 |
| Gneiss | 2 | 1.72 | | Granite | 31 | 23.48 |
| Schist | 8 | 6.90 | | *sum* | 132 | |
| *sum* | 116 | | | | | |
| | | | | | | |
| | | | | | | |
| | | | | | | |
| | | | | | | |
| **Location: Arroyo Seco** | 0388733E | 4028522N | | **Location: Arroyo Seco** | 0389009E | 4028262N |
| **Te_CC11** | | | | **Te_CC12** | | |
| | N | Relative % | | | N | Relative % |
| Quartzite | 109 | 99.09 | | Quartzite | 124 | 91.85 |
| Schist | 1 | 0.91 | | Schist | 11 | 8.15 |
| *sum* | 110 | | | *sum* | 135 | |
| | | | | | | |
| | | | | | | |
| | | | | | | |
| | | | | | | |
| | | | | | | |
| **Location: Arroyo Seco** | 0388997E | 4028268N | | **Location: Arroyo Seco** | 0389014E | 4028250N |
| **Te_CC13** | | | | **Te_CC14** | | |
| | N | Relative % | | | N | Relative % |
| Quartzite | 94 | 98.95 | | Quartzite | 111 | 90.98 |
| Schist | 1 | 1.05 | | Schist | 10 | 8.20 |
| *sum* | 95 | | | Sandstone | 1 | 0.82 |
| | | | | *sum* | 122 | |
| | | | | | | |
| | | | | | | |
| | | | | | | |
| | | | | | | |
| **Location: Arroyo Seco** | 0389088E | 4028207N | | | | |
| **Te_CC15** | | | | | | |
| | N | Relative % | | | | |
| Quartzite | 117 | 95.12 | | | | |
| Schist | 6 | 4.88 | | | | |
| *sum* | 123 | | | | | |

APPENDIX 8.4. PETROGRAPHIC SAMPLE ANALYSIS DATA

## Sample ERS34

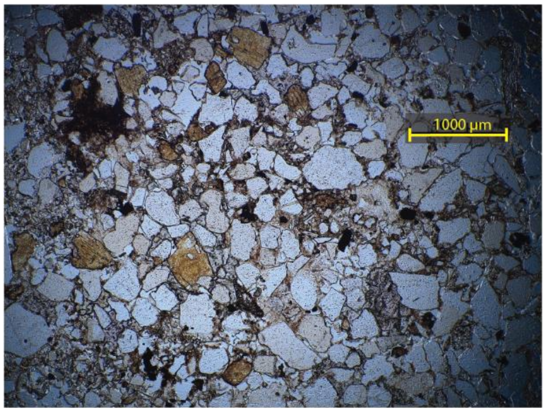


**ERS34 A:** rounded-to angular, fine-to coarse-grained sandstone

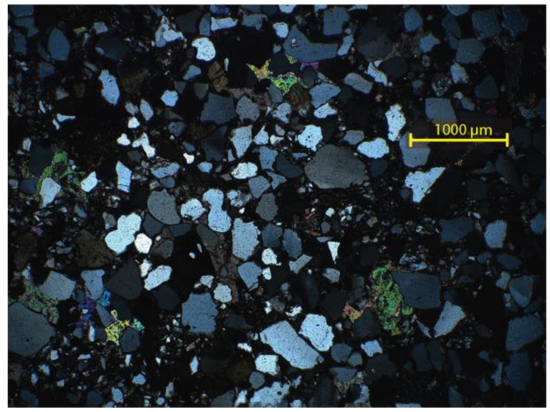


**ERS34 B:** xpl of image A

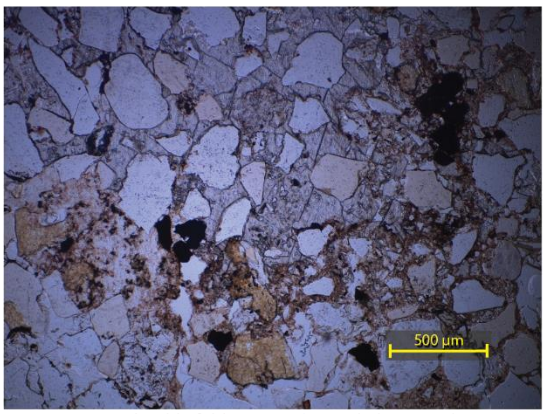


**ERS34 C:** stained k-feldspars and rounded to angular quartz clasts

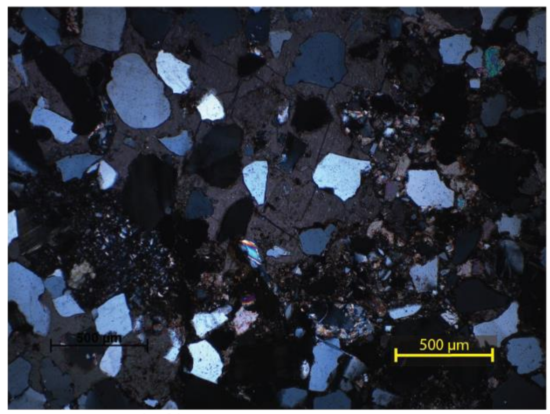


**ERS34 D:** xpl of image C

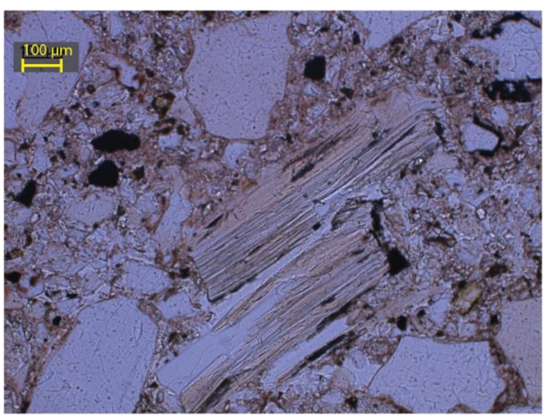


**ERS34 E:** elongate angular muscovite, and rounded to angular quartz clasts

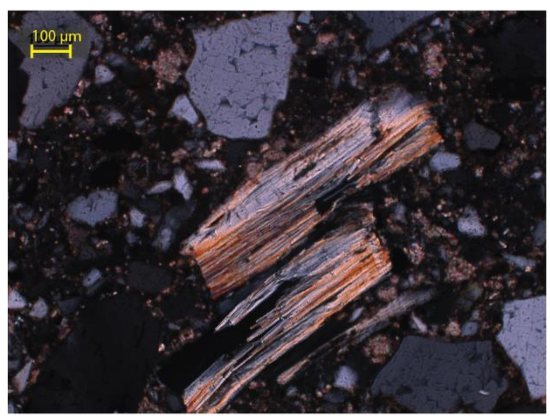


**ERS34 F:** xpl of image of E

Appendix 8.4. Continued

## Sample ERS1

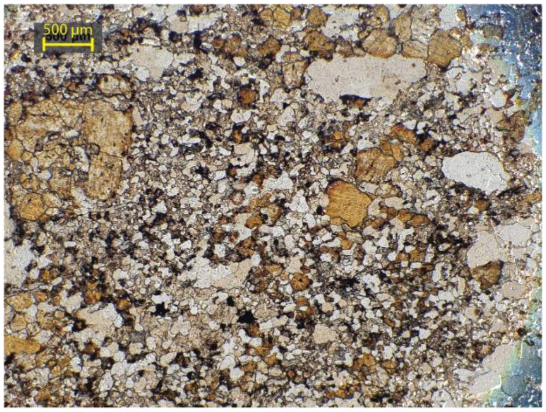


**ERS1 A:** very fine-to coarse-grained sandstone with stained k-feldspars in yellow

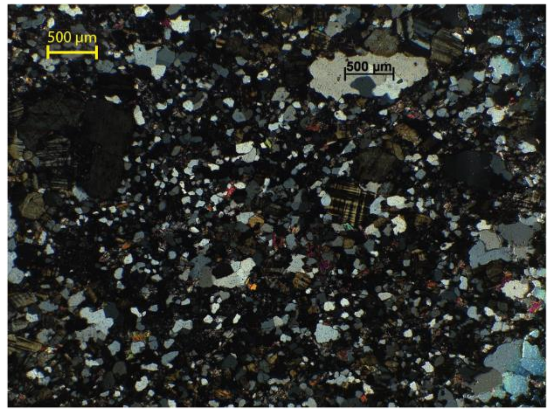


**ERS1 B:** xpl of image A

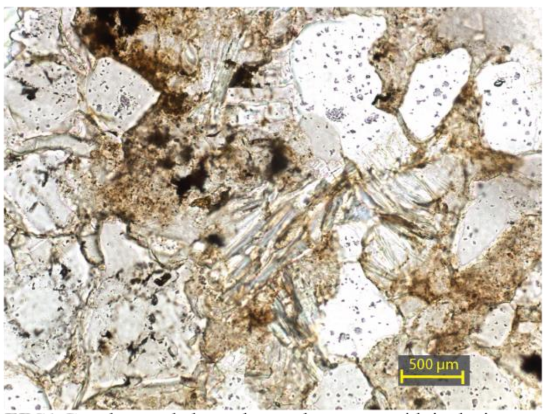


**ERS1 C:** sub-rounded to sub-angular quartz with inclusions

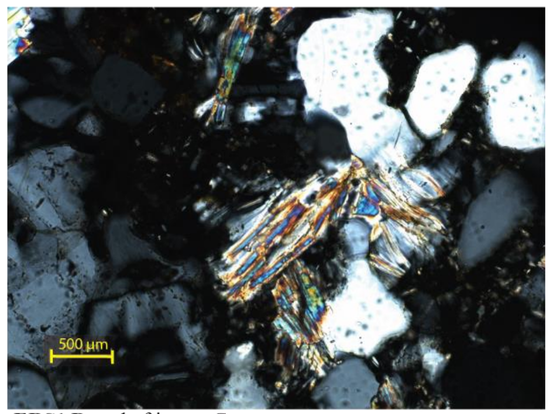


**ERS1 D:** xpl of image C

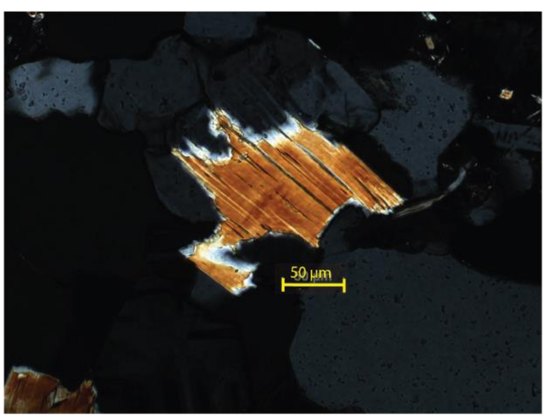


**ERS1 E:** angular muscovite

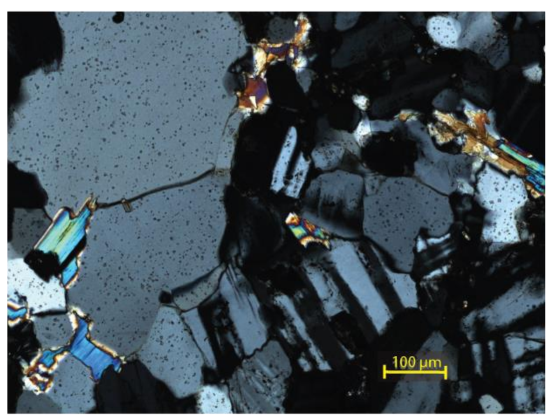


**ERS1 F:** xpl of image of sub-angular quartz, twinned plagioclase, and angular muscovite

## Sample ERE1

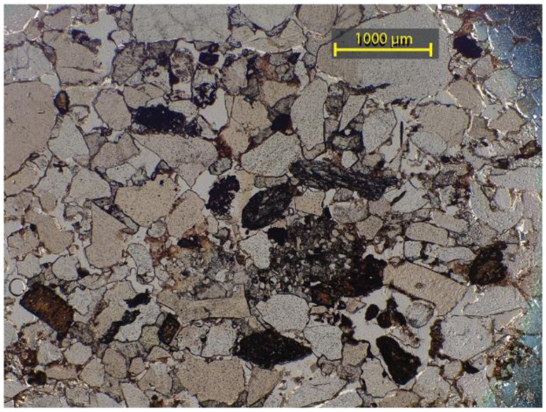


**ERE1 A:** medium-to coarse-grained sandstone

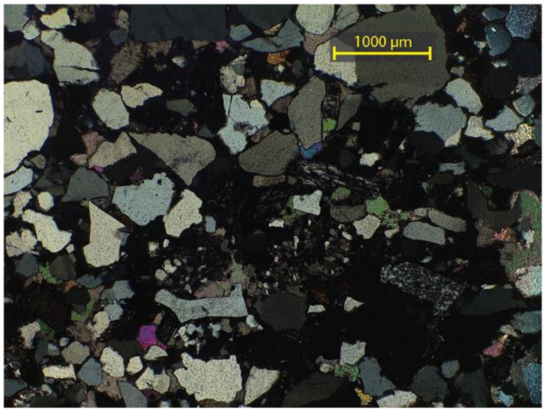


**ERE1 B:** xpl of image A

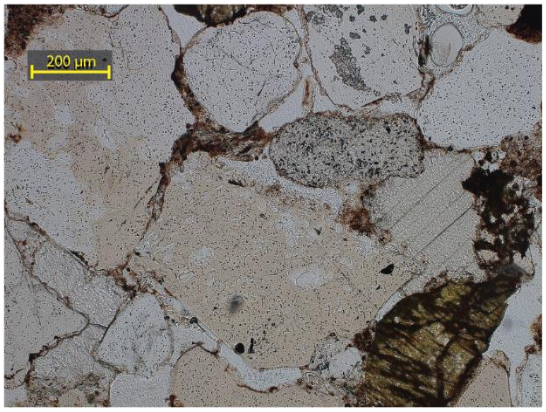


**ERE1 C:** rounded to angular clasts

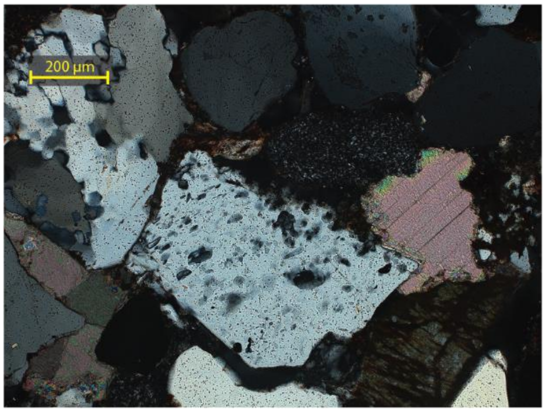


**ERE1 D:** xpl of image C

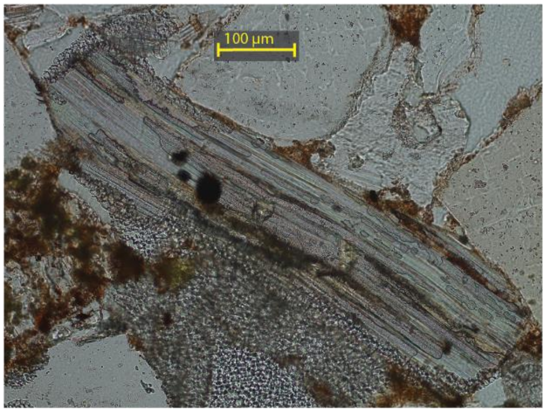


**ERE1 E:** high birefringence muscovite grain

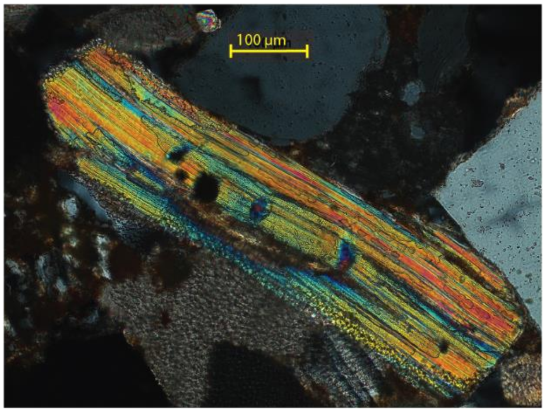


**ERE1 F:** xpl of image E

Appendix 8.4. Continued

## Sample ERE5a

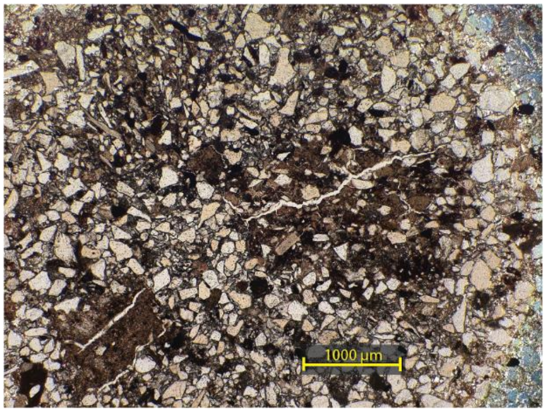


**ERE5a A:** very fine-to medium-grained sandstone

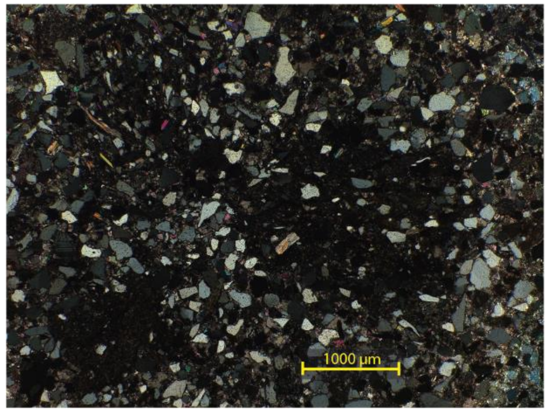


**ERE5a B:** xpl of image A

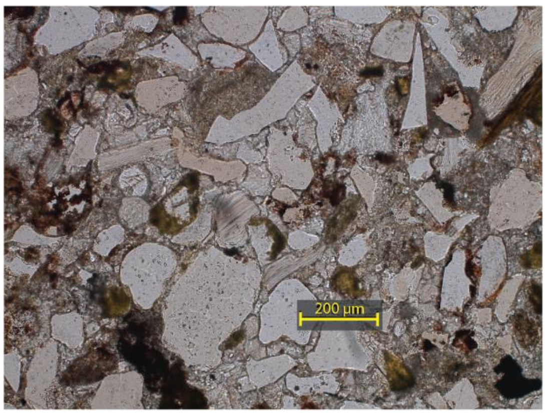


**ERE5a C:** sub-rounded to angular clasts

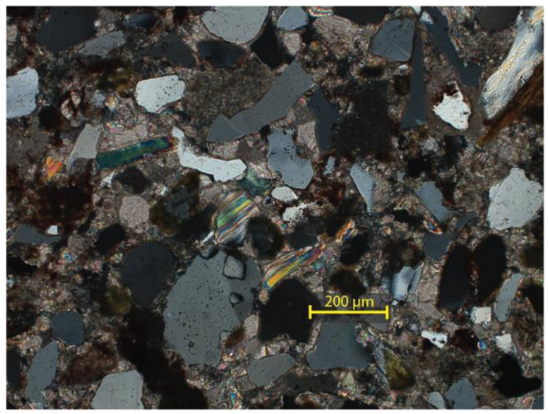


**ERE5a D:** xpl of image C

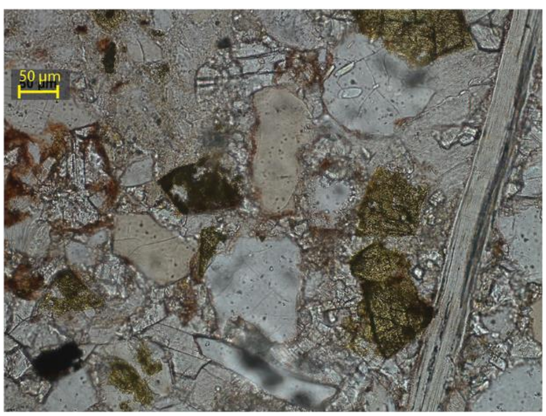


**ERE5a E:** polymorphic quartz, hemitic cement

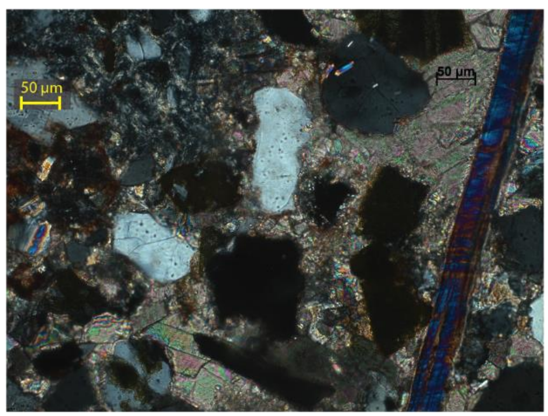


**ERE5a F:** xpl of image E

Appendix 8.4. Continued

## Sample ERE5b

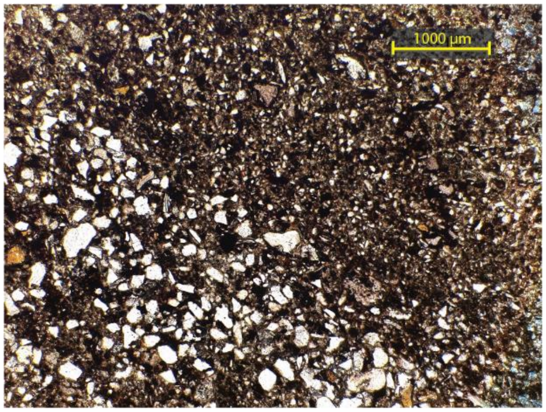


**ERE5b A:** clay rich, very fine-to medium-grained sandstone

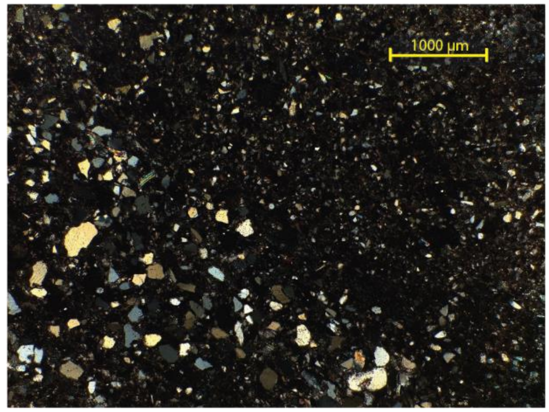


**ERE5b B:** xpl of image A

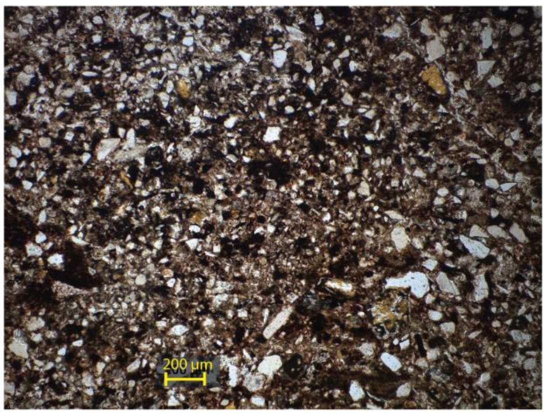


**ERE5b C:** illite dominated matrix

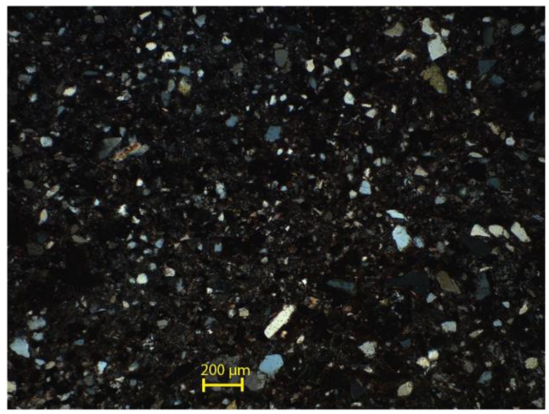


**ERE5b D:** xpl of image C

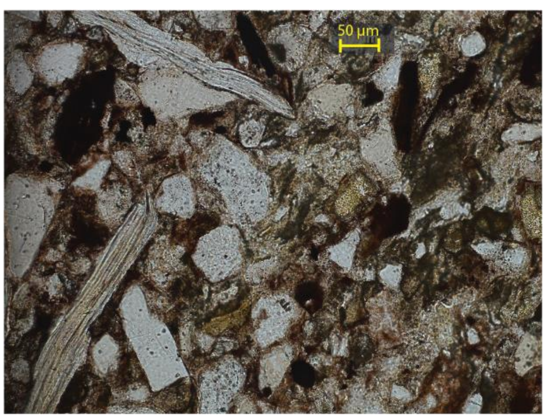


**ERE5b E:** muscovite grains, sub-rounded to angular quartz

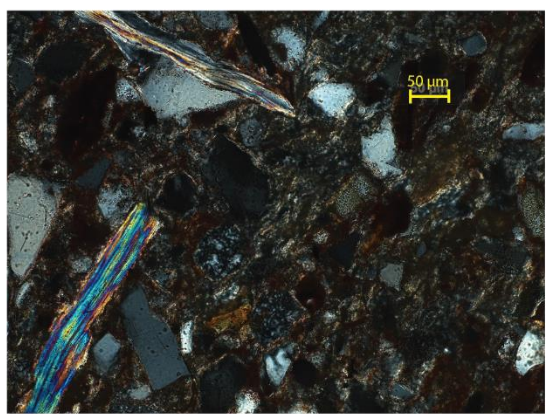


**ERE5b F:** xpl of image E

Appendix 8.4. Continued

## Sample ERE5c

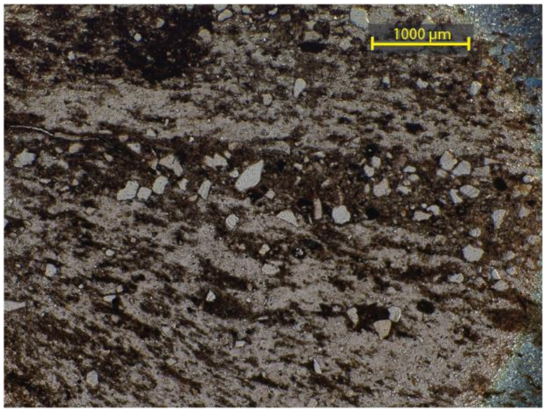


**ERE5c A:** clay rich siltstone with poorly sorted very fine-to medium-grained clasts

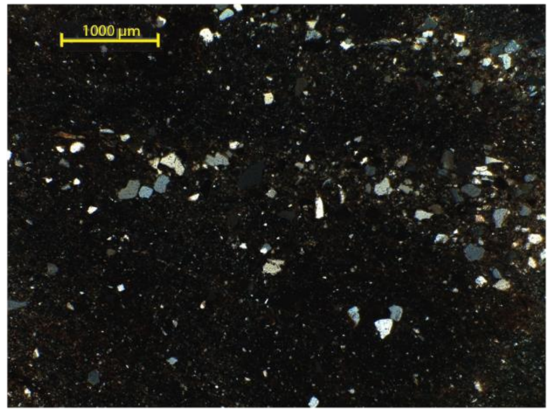


**ERE5c B:** xpl of image A

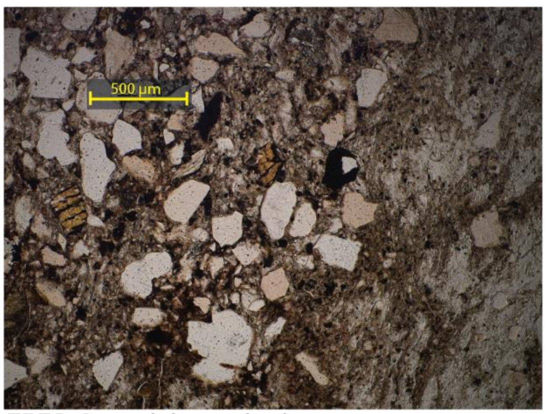


**ERE5c C:** rounded to angular clasts

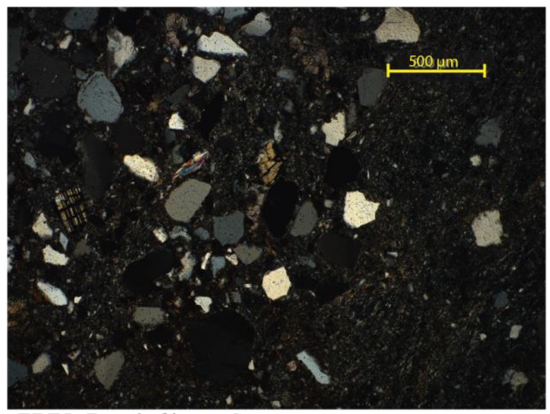


**ERE5c D:** xpl of image C

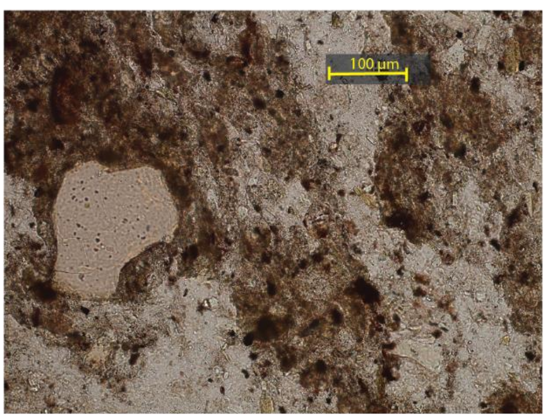


**ERE5c E:** sub-rounded quartz clast surrounded by ferrous illite clay

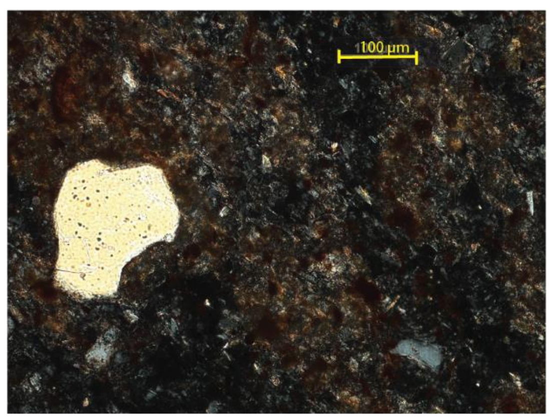


**ERE5c F:** xpl of image E

Appendix 8.4. Continued

## Sample ERE5d

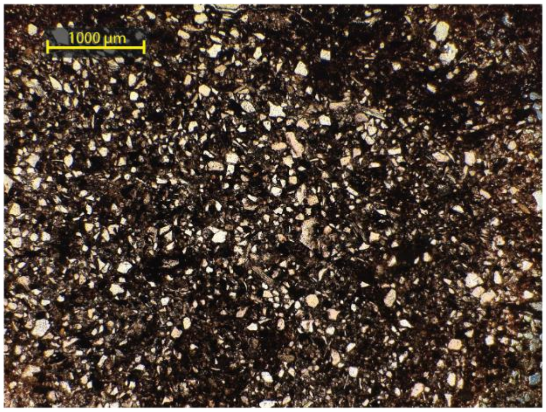


**ERE5d A:** very fine-to fine-grained, clay-dominated sandstone

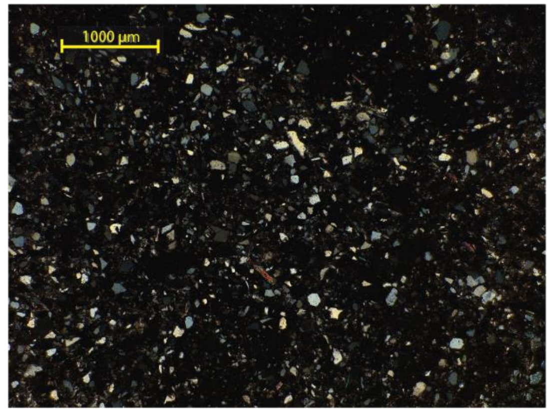


**ERE5d B:** xpl of image A


**ERE5d C:** elongate metamorphic sourced muscovite and sillmanite clasts

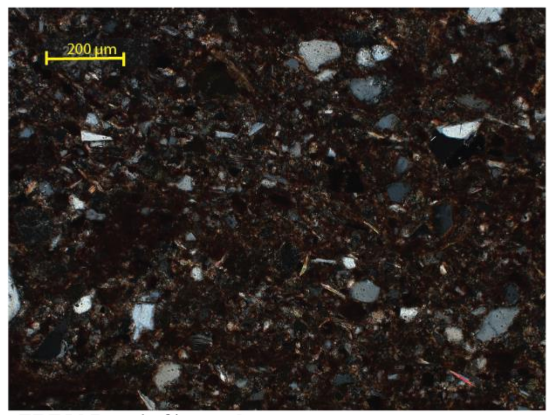


**ERE5d D:** xpl of image C

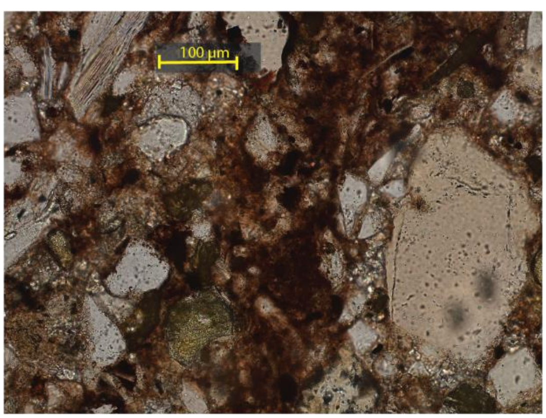


**ERE5d E:** sub-rounded to sub-angular quartz with inclusions

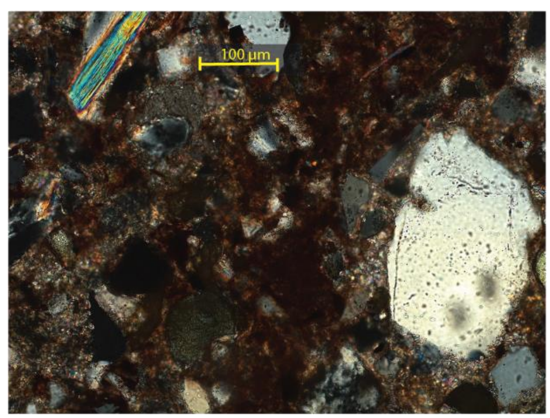


**ERE5d F:** xpl of image E

Appendix 8.4. Continued

## Ternary Diagrams

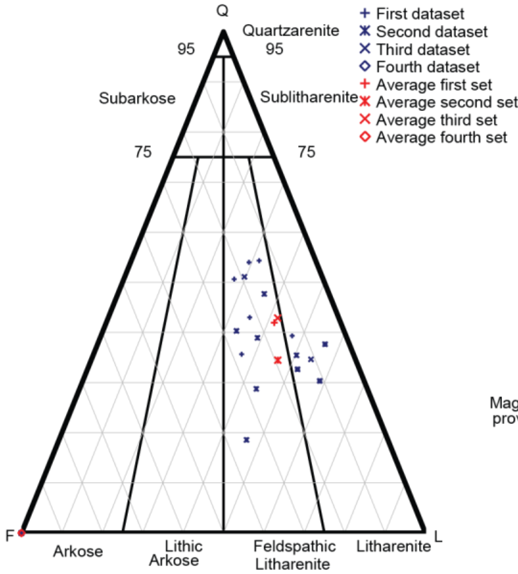


Sandstone Classification (Folk, 1980)

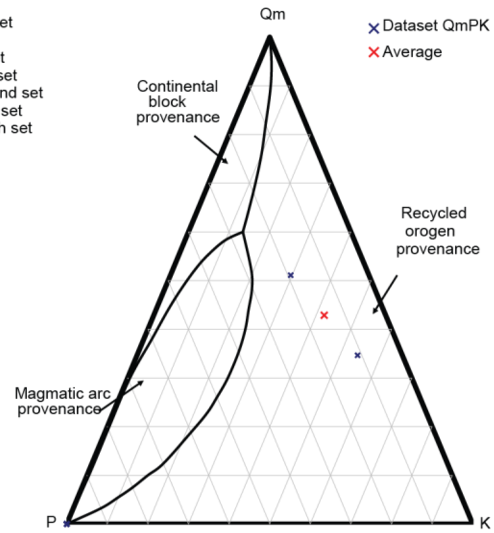


QmPK Provenance Plot (Weltje, 2006)

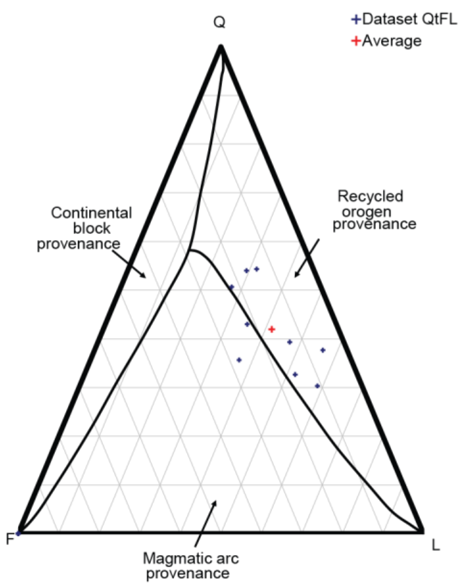


QFL Provenance Plot (Weltje, 2006)

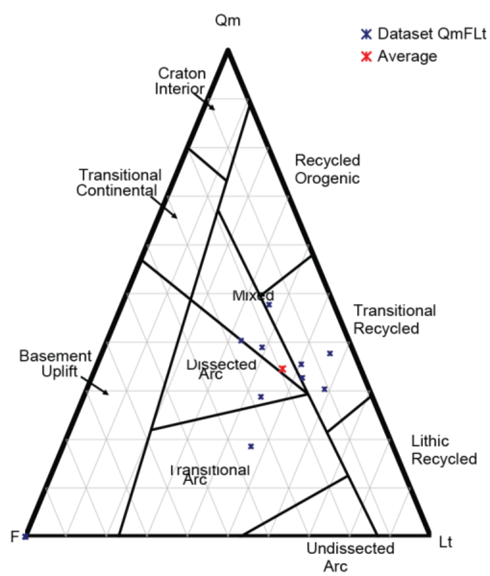


QmFLt Provenance Plot (Dickinson, 1985)

# 9. References

Abbott, J.C., Cather, S.M., and Goodwin, L.B., 1995, Paleogene synorogenic sedimentation in the Galisteo Basin related to the Tijeras-Canoncito fault system: in Bauer, P.W., Kues, B.S., Dunbar, N.W., Karlstrom, K.E., and Harrison, B., eds., Geology of the Santa Fe region: New Mexico Geological Society Guidebook 46, p. 271-278.

Ahmed Benan, C.A., and Kocurek, G., 2000, Catastrophic flooding of an aeolian dune field: Jurassic Entrada and Todilto Formations, Ghost Ranch, New Mexico, USA: Sedimentology, v. 47, p. 1069-1080.

Aldrich JR., M.J., and Dethier, D.P., 1990, Stratigraphic and tectonic evolution of the northern Espanola Basin, Rio Grande Rift, New Mexico: GSA Bulletin, v. 102, p. 1695-1705.

Armstrong, C., Dutrow, B.L., Darrell, H.J., and Thompson, R.A., 2013, Provenance of volcanic clasts from the Santa Fe Group, Culebra graben of the San Luis Basin, Colorado: A guide to tectonic evolution: in Hudson M.R., and Grauch V.J.S., eds., New Perspectives on Rio Grande Rift Basins: From Tectonics to Groundwater, GSA Special Papers, v. 494, p. 21-45.

Bachmann, O., Dungan, M.A., and Lipman, P.W., 2002, The Fishcanyon magma body, San Juan Volcanic field, Colorado: Rejuvenation and eruption of an upper-crustal batholith: Journal of Petrology, v. 43, p. 1469-1503.

Baldridge, S.W., Ferguson, J.F., Braile, L.W., Wang, B., Eckhardt, K., Evans, D., Schultz, C., Gilpin, B., Jiracek, G.R., and Biehler, S., 1994, The western margin of the Rio Grande Rift in northern New Mexico: An aborted boundary?: GSA Bulletin, v.106, p. 1538-1551.

Baldridge, W.S., 2004, Pliocene-Quaternary volcanism in New Mexico and a model for genesis of magmas in continental extension: in Mack G., and Giles, K., eds., The Geology of New Mexico: A Geologic History, New Mexico Geological Society, Special Publication, p. 313-330.

Barker, F., and Friedman, I., 1974, Precambrian metavolcanic rocks of the Tusas Mountains, New Mexico: Major elements and oxygen isotopes: New Mexico Geological Society Guidebook 25, Ghost Ranch (Central-Northern New Mexico), p. 115-117.

Barrier, L., Proust, J.N., Nalpas, T., Robin, C., and Guillocheau, F., 2010, Control of alluvial sedimentation at foreland-basin active margins: A case study from the northeastern Ebro Basin (southeastern Pyrenees, Spain): Journal of Sedimentary Research, v. 80, p. 728-749.

Bauer, P.W., and Kelson, K.I., 2004, Fault geometry and Cenozoic kinematic history of the southeastern San Luis Basin near Taos, New Mexico: New Mexico Bureau of Geology and Mineral Resources, Bulletin, v. 160, p. 79-95.

Bingler, E.C., 1974, Precambrian rocks of the Tusas Mountains: New Mexico Geological Society Guidebook 25, Ghost Ranch (Central-Northern New Mexico), p. 109-113.

Blair, T.C., 1999a, Sedimentary processes and facies of the waterlaid Anvil Spring Canyon alluvial fan, Death Valley, California: Sedimentology, v.46, p. 913-940.

Blair, T.C., 1999b, Sedimentology of the debris-flow-dominated Warm Spring Canyon alluvial fan, Death Valley, California: Sedimentology, v.46, p. 941-965.
Blair, T.C., and McPherson, J.G., 1994, Alluvial fans and their natural distinction from rivers based on morphology, hydraulic processes, sedimentary processes, and facies assemblages: Journal of Sedimentary Research, v.A64, p. 450-489.
Blakey, R. C., and Ranney, W., 2008, Ancient Landscapes of the Colorado Plateau: (Grand Canyon) Grand Canyon Association, 176 p.
Blakey, R.C., 2008, Pennsylvanian-Jurassic sedimentary basins of the Colorado Plateau and southern Rocky Mountains: in Miall, A. D., ed, The Sedimentary Basins of the United States and Canada: Sedimentary Basins of the World, v. 5, Elsevier Science, Amsterdam, p. 246-295.
Blum, M.D., and Tornqvist, T.E., 2000, Fluvial responses to climate and sea-level change: A review and look forward: Sedimentology, v. 47, p. 2-48.
Bohannon, R.G., and Parsons, T., 1995, Tectonic implications of post–30 Ma Pacific and North American relative plate motions: GSA Bulletin, v. 107, p. 937-959.
Cather, S.M., 1999, Implications of Jurassic, Cretaceous, and Proterozoic piercing lines for Laramide oblique-slip faulting in New Mexico and rotation of the Colorado Plateau, GSA Bulletin, v. 111, no. 6, p. 849-868.
Cather, S.M., 1992, Suggested revisions to the Tertiary tectonic history of north central New Mexico: New Mexico Geological society Guidebook, 43rd Field Conference, San Juan Basin IV, p. 109-122.
Cather, S.M., 2004, Laramide orogeny in central and northern New Mexico and southern Colorado: in Mack G., and Giles, K., eds., The Geology of New Mexico: A Geologic History, New Mexico Geological Society, Special Publication, p. 203-248.
Cather, S.M., Connell, S.D., Chamberlin, R.M., McIntosh, W.C., Jones, G.E., Potochnik, A.R., Lucas, S.G., and Johnson, P.S., 2008, The Chuska erg: Paleogeomorphic and paleoclimatic implications of an Oligocene sand sea on the Colorado Plateau: GSA Bulletin, v. 120, p. 13-33.
Cather, S.M., Karlstrom, K.E., Timmons, J.M., and Heizler, M.T., 2006, Palinspastic reconstruction of Proterozoic basement-related aeromagnetic features in north-central New Mexico: Implications for Mesoproterozoic to late Cenozoic tectonism: Geosphere, v. 2, no. 6, p. 299-323.
Cavazza, W., 1986, Miocene sediment dispersal in the central Espanola Basin, Rio Grande rift, New Mexico, USA: Sedimentary Geology, v. 51, p. 119-135.
Chamberlain, C.P., Mix, H.T., Mulch, A., Hren, M.T., Kent-Corson, M.L., Davis, S.J., Horton, T.W., and Graham, S.A., 2012, The Cenozoic climatic and topographic evolution of the western North American Cordillera: American Journal of Science, v. 112, p. 213-262.
Chapin, C.E., and Cather, S.M., 1994, Tectonic setting of the axial basins of the northern and central Rio Grande Rift: in Keller G.R., Cather S.M., eds., Basins of the Rio Grande Rift: Structure, Stratigraphy, and Tectonic Setting, GSA Special Papers, v.291, p. 5-25.
Chapin, C.E., McIntosh, W.C., and Chamberlin, R.M., 2004, The late Eocene-Oligocene peak of Cenozoic volcanism in southwestern New Mexico: in Mack G., and Giles,

K., eds., The Geology of New Mexico: A Geologic History, New Mexico Geological Society, Special Publication, p. 271-293.
Copeland, P., Murphy, M.A., Dupre, W.R., and Lapen, T.J., 2011, Oligocene Laramide deformation in southern New Mexico and its implications for Farallon plate geodynamics: Geosphere, v. 7, p. 1209-1219.
Czamanske, G. K., Foland, K. A., Kubacher, F. A., and Allen, J. C., 1990, The $^{40}Ar/^{39}Ar$ chronology of caldera formation, intrusive activity and Mo-ore deposition near Questa, New Mexico: New Mexico Geological Society, 41st Field Conference, Guidebook, p. 355- 358.
Davis, S.J., Mix, H.T., Wiegand, B.A., Carroll, A.R., and Chamberlain, C.P., 2009, Synorogenic evolution of large-scale drainage patterns: Isotope paleohydrology of sequential Laramide basins, American Journal of Science, v. 309, p. 549-602.
Davis, S.J., Wiegand, D.A., Carroll, A.R., and Chamberlain, C.P., 2008, The effect of drainage reorganization on paleoaltimetry studies: An example from the Paleogene Laramide foreland: Earth and Planetary Science Letters, v. 275, p.258-268.
De Almeida, R.P., Janikian, L., Fragoso-Cesar, A.R.S., and Marconato, A., 2009, Evolution of a rift basin dominated by subaerial deposits: The Guaritas Rift, early Cambrian, Southern Brazil: Sedimentary Geology, v. 217, p. 30-51.
DeCelles, P.G., 2004, Late Jurassic to Eocene evolution of the Cordilleran thrust belt and foreland basin system, western USA: American Journal of Science, v. 304, p. 105-168.
DeCelles, P.G., and Giles, K.A., 1996, Foreland basin systems: Basin Research, v. 8, p. 105-123.
DeCelles, P.G., and Langford, R.P., 1983, Two new methods of paleocurrent determination from trough cross-stratification: Journal of Sedimentary Petrology, v. 53, p.0629-0642.
Dechene, H.R., Engelhardt, D.W., and Woodward, L.A., 1981, Palynologic evidence for the age of the Abiquiu formation, north-central New Mexico: GSA Bulletin, v. 92. P. 993-998.
Devore, M.L., and Pigg, K.B., 2010, Floristic composition and comparison in of middle Eocene to late Eocene and Oligocene floras in North America: Bulletin of Geosciences, v. 85, p. 111-134.
Dickinson, W.R., 1970, Interpreting detrital modes of greywacke and arkose: Journal of Sedimentary Petrology, v. 40, p. 695-707.
Dickinson, W.R., 1988, Provenance and sediment dispersal in relation to paleotectonics and paleogeography of sedimentary basins: in K. L. Kleinspehn et al. eds., New Perspectives in Basin Analysis, p. 3-25.
Dickinson, W.R., and Suczek, C.A., 1979, Plate tectonics and sandstone compositions: AAPG Bulletin, v. 63, p. 2164-2182.
Dickinson, W.R., Klute, M.A., Hayes, M.J., Janecke, S.U., Lundin, E.R., McKittrick, M.A., and Olivares, M.D., 1988, Paleogeographic and paleotectonics setting of Laramide sedimentary basins in the central Rocky Mountain region: GSA Bulletin, v. 100, p. 1023-1039.

Dickinson, W.R., Lawton, T.F., and Inman, K.F., 1986, Sandstone detrital modes, central Utah foreland region: Stratigraphic record of Cretaceous-Paleocene tectonic evolution: Journal of Sedimentary Petrology, v. 56, p. 276-293.

Disbrow, A. E. and Stoll, W. C., 1957, Geology of the Cerrillos area, Santa Fe County, New Mexico: New Mexico Bureau of Mines and Mineral Resources, Bulletin 48, 73 p.

Dunbar, J.A., and Cook, R.W., 2003, Palinspastic reconstruction of structure maps: an automated finite element approach with heterogeneous strain: Journal of Structural Geology, v. 26, p. 11021-1036.

Eberth, D.A., and Miall, A.D., 1991, Stratigraphy, sedimentology and evolution of a vertebrate-bearing, braided to anastomosed fluvial system, Cutler Formation (Permian-Pennsylvanian), north-central New Mexico: Sedimentary Geology, v. 72, p. 225-252.

Erickson, S.G., Hardy, S., and Suppe, J., 2000, Sequential restoration and unstraining of structural cross sections: Applications to extensional terranes: AAPG Bulletin, v. 84, p. 234-249.

Erskine, D. W. and Smith, G. A., 1993, Compositional characterization of volcanic products from a primarily sedimentary record: GSA Bulletin, v. 105, p. 1214-1222.

Erslev, E.A., 2001, Multistage, multidirectional Tertiary shortening and compression in north-central New Mexico: GSA Bulletin, v. 113, p. 63-74.

Fan, M., Quade, J., Dettman D., and DeCelles, P.G., 2011, Widespread basement erosion during the late Paleocene – early Eocene in the Laramide Rocky Mountains inferred from $^{87}Sr/^{86}Sr$ ratios of freshwater bivalve fossils: GSA Bulletin, v.123, p. 2069-2082.

Fan, M., Quade, J., Dettman, D., and DeCelles, P.G., 2011, Widespread basement erosion during the late Paleocene–early Eocene in the Laramide Rocky Mountains inferred from 87Sr/86Sr ratios of freshwater bivalve fossils: GSA Bulletin, v. 123, p. 2069-2082.

Flowers, R. M., and Farley K.A., 2012, Apatite 4He/3He and (U-Th)/He evidence for an ancient Grand Canyon. Science 338, 1616

Folk, R.L., 1980. Petrology of Sedimentary Rocks: Austin, Texas, Hemphill Publishing Company, 182 p.

Formento-Trigilio, M.L., and Pazzaglia, F.J., 1998, Tectonic geomorphology of the Sierra Nacimiento: Traditional and new techniques in assessing long-term landscape evolution in the southern Rocky Mountains: The Journal of Geology, v. 106, p. 433-453.

Frankel, K.L., and Pazzaglia, 2006, Mountain fronts, base-level fall, and landscape evolution: Insights from the southern Rocky Mountains: in Willett, S. D., Hovius, N., Brandon, M. T., and Fisher, D., eds., Tectonics, Climate, and Landscape Evolution, GSA Special Papers, v. 398, p. 419-434.

Freer, C.M., 2010, Investigation of the deformation history in reactivated Laramide asymmetric anticlines in north-central New Mexico: An investigation of an alternative geometry for Laramide structures and its role in guiding Miocene extension: Master’s thesis, University of Houston, Houston, Texas, 125 p.

Fuentes, F., DeCelles, P.G., Constenius, K.N., and Gehrels, G.E., 2011, Evolution of the Cordilleran foreland basin system in northwestern Montana, U.S.A.: GSA Bulletin, v.123, p. 507-533.

Galloway, W.E., and Hobday, D.K., 1996a, Alluvial Fans, Chapter 3: Terrigenous Clastic Depositional Systems, Second edition, Springer-Verlag, p. 29-59.

Galloway, W.E., and Hobday, D.K., 1996b, Fluvial Systems, Chapter 4: Terrigenous clastic depositional systems, Second edition, Springer-Verlag, p. 60-90.

Galloway, W.E., Whiteaker, T.L., and Ganey-Curry, P., 2011, History of Cenozoic North American drainage basin evolution, sediment yield, and accumulation in the Gulf of Mexico Basin: Geosphere, v. 7, p. 938-973.

Gardner, J. N., Goff, f., Garcia, S., and Hagan, R. C., 1986, Stratigraphic relations and lithologic variations in the Jemez volcanic field: Journal of Geophysical Research, v. 91, p. 1763- 1778. (Gardner et al., 1986)

Ghosh, P., 2000, Estimation of channel sinuosity from paleocurrent data: A method using fractal geometry; Journal of Sedimentary Research, v. 70, p. 449-455.

Goff, F., and Gardner, J.N., 2004, Late Cenozoic geochronology of volcanism and mineralization in the Jemez Mountains and Valles Caldera, north central New Mexico: in Mack G., and Giles, K., eds., The Geology of New Mexico: A Geologic History, New Mexico Geological Society, Special Publication, p. 295-312.

Goff, F., Gardner, J. N., and Valentine, G. A., 1990, Geology of St. Peter's Dome area, Jemez Mountains, New Mexico: New Mexico Bureau of Mines and Mineral Resources, Geologic Map 69, scale 1:24,000.

Golombek, M.P., McGill, G.E., and Brown, L., 1983, Tectonic and geologic evolution of the Espanola Basin, Rio Grande Rift: Structure, rate of extension, and relation to the state of stress in the western United States: in: P. Morgan and B.H. Baker, eds., Processes of Continental Rifting, Tectonphysics, v.94, p. 483-507.

Gonzalez, M.A., and Dethier, D.P., 1991, Geology along a margin of the Colorado Plateau and Rio Grande Rift, north-central New Mexico: roadlog and field-stop discussions to accompany Field-Trip # 3 of the Rocky Mountain/South-Central sections annual meeting of the GSA in Albuquerque, New Mexico, New Mexico Bureau of Mines and Mineral Resources Open-File Report 374, 79 p.

Gorham, T.W., and Ingersoll, R.V., 1979, Evolution of the Eocene Galisteo Basin, north-central New Mexico: New Mexico Geologic Society Guidebook 30, p. 219-224.

Goteti, R., Becene, A., Sussman, A., and Lewis, C., 2013, Three-dimensional finite-element modeling of fault interactions in rift-scale normal fault systems: Implications for the late Cenozoic Rio Grande Rift of north-central New Mexico: in Hudson M.R., and Grauch V.J.S., eds., New Perspectives on Rio Grande Rift Basins: From Tectonics to Groundwater, GSA Special Papers, v. 494, p. 157-184.

Gregory, K.M., and Chase, C.G., 1994, Tectonic and climatic significance of the late Eocene low-relief high-level geomorphic surface, Colorado: Journal of Geophysical Research, v. 99, p. 20,141-20,160.

Gries, R.R., 1990, Rocky Mountain foreland structures: changes in compression direction through time: Petroleum and tectonics in mobile belts, Proceedings of the 4th IFP Exploration and Production Research Conference, p. 129-147.

Hamilton, J.S., 2009, A new multistage model for the Late Mesozoic to present tectonic evolution of north-central New Mexico: Master's thesis, University of Houston, Houston, Texas, 84 p.

Hampton, B.A., and Horton B.K., 2007, Sheetflow fluvial processes in a rapidly subsiding basin, Altiplano plateau, Bolivia: Sedimentology, v. 54, p. 1121-1147.

Heller, P.L., Mathers, G., Dueker, K., and Foreman, B., 2012, Far-traveled latest Cretaceous–Paleocene conglomerates of the Southern Rocky Mountains, USA: Record of transient Laramide tectonism: GSA Bulletin, v. 125, p. 490-498.

Holbrook, J., Scott, R.W., and Oboh-Ikuenobe, F.E., 2006, Base-level buffers and buttresses: A model for the upstream versus downstream control on fluvial geometry and architecture within sequences: Journal of Sedimentary Research, v. 76, p. 162-174.

Horton, B.K., Constenius, K.N., and DeCelles, P.G., 2004, Tectonic control on coarse-grained foreland-basin sequences: An example from the Cordilleran foreland basin, Utah: Geology, v. 32, p. 637-640.

Hudson, M.R., and Grauch, V.J.S., 2013, Introduction to GSA Special Papers 494: in Hudson M.R., and Grauch V.J.S., eds., New Perspectives on Rio Grande Rift Basins: From Tectonics to Groundwater, GSA Special Papers, v. 494, p. v-xii.

Hunt, A.P., and Kelley, S.A., 2010, Ghost Ranch and vicinity: Carson National Forest: in L.Greer, ed., , The Geology of Nothern New Mexico's Parks, Monuments, and Public Lands, New Mexico Bureau of Geology and Mineral Resources, Soccorro, New Mexico, USA, p. 112-124.

Ingersoll, R.V., 2001, Structural and stratigraphic evolution of the Rio Grande Rift, northern New Mexico and southern Colorado: International Geology Review, v. 43, p. 867-891.

Ingersoll, R.V., and Cavazza, W., 1991, Reconstruction of Oligo-Miocene volcaniclastic dispersal patterns in north-central New Mexico using sandstone petrofacies, in Fisher R.V., Smith G.A., eds., Sedimentation in Volcanic Settings: SEPM Special Publication 45, p. 227–236.

Ingersoll, R.V., Bullard, T.F., Ford, R.L., Grimm, J.P., Pickle, J.D., and Sares, S.W., 1984, The effect of grain size on detrital modes: A test of the Gazzi–Dickinson point-counting method: Journal of Sedimentary Petrology, v. 54, p. 103–116.

Ingersoll, R.V., Cavazza, W., Baldridge, W.S., and Shafiqullah, Mohammed, 1990, Cenozoic sedimentation and paleotectonics of north-central New Mexico: Implications for initiation and evolution of the Rio Grande Rift: GSA Bulletin, v. 102. p. 1288-1296.

Johnson, C. M., Czamanske, G. K., and Lipman, P. W., 1989, Geochemistry of intrusive rocks associated with the Latir volcanic field, New Mexico, and contrast between evolution of plutonic and volcanic rocks: Contributions to Mineralogy and Petrology, v. 103, p. 90-109.

K.E. Karlstrom, K.E., Coblentz, D., Dueker, K., Ouimet, W., Kirby, E., Van Wijk, J., Schmandt, B., Kelley, S., Lazear, G., Crossey, L.J., Crow, R., Aslan, A., Darling, A., Aster, R., MacCarthy, J., Hansen, S.M., Stachnik, J., Stockli, D.F., Garcia, R.V., Hoffman, M., McKeon, R., Feldman, J., Heizler, M., Donahue, M.S., and the CREST Working Group, 2012, Mantle-driven dynamic uplift of the Rocky

Mountains and Colorado Plateau and its surface response: Toward a unified hypothesis, Lithosphere, v. 4, p. 3-22.

Karlstrom, K.E., Amato, J.M., Williams, M.L., Heizler, M., Shaw, C.A., Read, A.S., and Bauer, P., 2004, Proterozoic tectonic evolution of the New Mexico region: A synthesis: in Mack G., and Giles, K., eds., The Geology of New Mexico: A Geologic History, New Mexico Geological Society, Special Publication, p. 1-34.

Karlstrom, K.E., and Daniel, C.G., 1993, Restoration of Laramide right-lateral strike slip in northern New Mexico by using Proterozoic percing points: Tectonic implications from the Proterozoic to the Cenozoic: Geology, v. 21, p. 1139-1142.

Kelley, S.A., Kempter, K.A., McIntosh, W.C., Maldonado, F., Smith, G.A., Connell, S.D., Koning, D.J., and Whiteis, J., 2013, Syndepositional deformation and provenance of Oligocene to Lower Miocene sedimentary rocks along the western margin of the Rio Grande Rift, Jemez Mountains, New Mexico: in Hudson M.R., and Grauch V.J.S., eds., New Perspectives on Rio Grande Rift Basins: From Tectonics to Groundwater, GSA Special Papers, v. 494, p. 101-123.

Kelley, S.A., Lawrence, J.R., and Osburn, G.R., 2005, Preliminary Geologic Map of the Youngsville Quadrangle, Rio Arriba County, New Mexico: New Mexico Bureau of Geology and Mineral Resources, Open-File Digital Geologic Map OF-GM 106, scale 1:24,000. 1 pamphlet, 16p.

Kelley, S.A., Lawrence, J.R., Zeigler, K.E., Osburn, G.R., and Lucas, S.G., 2006, Preliminary Geologic Map of the Arroyo del Agua Quadrangle, Rio Arriba County, New Mexico: New Mexico Bureau of Geology and Mineral Resources, Open-File Digital Geologic Map OF-GM 124, scale 1:24,000. 1 pamphlet, 17 p.

Kelley, S.A., Osburn, G.R., Ferguson, C., Kempter, K., and Osburn, M., 2004, Preliminary Geologic Map of the Seven Springs Quadrangle, Sandoval and Rio Arriba Counties, New Mexico: New Mexico Bureau of Geology and Mineral Resources, Open-File Digital Geologic Map OF-GM 88, scale 1:24,000. 1 pamphlet, 11 p.

Kelley, S.A., Osburn, G.R., Ferguson, C., Moore, J., and Kempter, K., 2005, Preliminary Geologic Map of the Cañones Quadrangle, Rio Arriba County, New Mexico: New Mexico Bureau of Geology and Mineral Resources, Open-File Digital Geologic Map OF-GM 107, scale 1:24,000. 1 pamphlet, 16 p.

Kelley, V.C., 1978, Geology of the Espanola Basin, New Mexico, New Mexico Bureau of Geology and Mineral Resources, Geologic Map 48, scale 1:125,000.

Kelley, V.C., 1979, Geomorphology of the Espanola Basin: New Mexico Geologic Society Guidebook 30, p. 281-288.

Kellogg K.S., 1999. Neogene basins of the northern Rio Grande Rift: partitioning and asymmetry inherited from Laramide and older uplifts. Tectonophysics. 305: 141-152.

Kempter, K., Kelley, S.A., Goff, F., and Rampey, M., 2004, Preliminary Geologic Map of the Polvadera Peak Quadrangle, Rio Arriba County, New Mexico: New Mexico Bureau of Geology and Mineral Resources, Open-File Digital Geologic Map OF-GM 96, scale 1:24,000. 1 pamphlet, 10 p.

Kempter, K., Kelley, S.A., Koning, D.J., Ferguson, C., Osburn, G.R., and Fluk, L., 2005, Preliminary Geologic Map of the Vallecitos Quadrangle, Rio Arriba County, New

Mexico: New Mexico Bureau of Geology and Mineral Resources, Open-File Digital Geologic Map OF-GM 108, scale 1:24,000. 1 pamphlet, 14p.
Kempter, K., Koning, D.J., and Karlstrom, K.E., 2008, Preliminary Geologic Map of the Valle Grande Peak Quadrangle, Rio Arriba County, New Mexico: New Mexico Bureau of Geology and Mineral Resources, Open-File Digital Geologic Map OF-GM 180, scale 1:24,000. 1 pamphlet, 27p.
Kempter, K., Zeigler, K., Koning, D., and Lucas, S., 2007, Geologic Map of the Canjilon SE Quadrangle, Rio Arriba County, New Mexico: New Mexico Bureau of Geology and Mineral Resources, Open-File Digital Geologic Map OF-GM 150, scale 1:24,000. 1 pamphlet, 35 p.
Koning, D.J., and Connell, S.D., 2012, The evolution of the Rio Grande: in Welch, S., Bland, D., eds., Lite Geology, New Mexico Bureau of Geology and Mineral Resources, v. 32, p. 1-6.
Koning, D.J., Grauch, V.J.S., Connell, S.D., Ferguson, J., McIntosh, W.C., Slate, J.L., Wan, E., and Baldridge, S.W., 2013, Structure and tectonic evolution of the eastern Española Basin, Rio Grande Rift, north-central New Mexico: in Hudson M.R., and Grauch V.J.S., eds., New Perspectives on Rio Grande Rift Basins: From Tectonics to Groundwater, GSA Special Papers, v. 494, p. 185-219.
Koning, D.J., Kelley, S.A., Zeigler, K.E., and Lucas, S.G., 2006, Preliminary Geologic Map of the Ghost Ranch Quadrangle, Rio Arriba County, New Mexico: New Mexico Bureau of Geology and Mineral Resources, Open-File Digital Geologic Map OF-GM 127, scale 1:24,000. 1 pamphlet, 23 p.
Koning, D.J., May, J., Aby, S., and Horning, R., 2004, Preliminary Geologic Map of the Mendanales Quadrangle, Rio Arriba County, New Mexico: New Mexico Bureau of Geology and Mineral Resources, Open-File Digital Geologic Map OF-GM 89, scale 1:24,000. 1 pamphlet, 33 p.
Koning, D.J., Smith, G.A., and Aby, S., 2008, Preliminary Geologic Map of the El Rito Quadrangle, Rio Arriba County, New Mexico: New Mexico Bureau of Geology and Mineral Resources, Open-File Digital Geologic Map OF-GM 166, scale 1:24,000. 1 pamphlet, 31 p.
Kukulski, R.B., Hubbard, S.M., Moslow, T.F., and Raines, M.K., 2013, Basin-scale stratigraphic architecture of upstream fluvial deposits: Jurassic-Cretaceous foredeep, Alberta Basin, Canada, Journal of Sedimentary Research, v. 83, p. 704-722.
Lawrence, J.R., Kelley, S.A., and Rampey, M., 2004, Preliminary Geologic Map of the Cerro del Grant Quadrangle, Rio Arriba and Sandoval Counties, New Mexico: New Mexico Bureau of Geology and Mineral Resources, Open-File Digital Geologic Map OF-GM 87, scale 1:24,000.
Lawton, T.F., 2008, Laramide sedimentary basins: In Miall, A. D., ed, The Sedimentary Basins of the United States and Canada: Sedimentary Basins of the World, v. 5, Elsevier Science, Amsterdam, p. 429-446.
Lawton, T.F., and McMillan, N.J., 1999, Arc abandonment as a cause for passive continental rifting: Comparison of the Jurassic Mexican Borderland rift and the Cenozoic Rio Grande Rift, Geology, v. 27, p. 779-782.

Lawton, T.F., and Trexler Jr., J.H., 1991, Piggyback basin in the Sevier orogenic belt, Utah: Implications for development of the thrust wedge, Geology, v. 19, p. 827-830.
Leeder, M.R., 2011, Tectonic sedimentology: sediment systems deciphering global to local tectonics, Sedimentology, v. 58, p. 2-56.
Lindsey, D.A., Langer, W.H., and Van Gosen, B.S., 2007, Using pebble lithology and roundness to interpret gravel provenance in piedmont fluvial systems of the Rocky Mountains, USA: Sedimentary Geology, v. 199, p. 223-232.
Lipman, P. W. and Reed, J. C., Jr., 1989, Geologic Map of the Latir Volcanic Field and Adjacent Areas, Northern New Mexico: U.S. Geological Survey, Miscellaneous Investigations Series Map 1-1907, scale 1:48,000.
Lipman, P. W., I 975a, Evolution of the Platoro Caldera Complex and Related Volcanic Rocks, Southeastern San Juan Mountains, Colorado: U.S. Geological Survey, Professional Paper 852, 128 p.
Lisenbee, A.L., 2013, Multi-stage Laramide deformation in the area of the southern Santa Fe embayment (Rio Grande Rift), north-central New Mexico: in Hudson M.R., and Grauch V.J.S., eds., New Perspectives on Rio Grande Rift Basins: From Tectonics to Groundwater, GSA Special Papers, v. 494, p. 239-260.
Logsdon, M.J., 1981, A preliminary basin analysis of the El Rito Formation (Eocene), north-central New Mexico: GSA Bulletin, v. 92. p. 968-975.
Lucas, S.G., and Abbott, J.C., 1997, Stratigraphy and tectonic implications of Paleogene strata in the Laramide Galisteo Basin, north-central New Mexico: New Mexico Geology, v. 19, p. 89-95.
Lucas, S.G., and Ingersoll, R.V., 1981, Cenozoic continental deposits of New Mexico: An overview: GSA Bulletin, v. 92, p. 917-932.
Mack, G.H., Seager, W.R., and Kieling, J., 1994, Late Oligocene and Miocene faulting and sedimentation, and evolution of the southern Rio Grande Rift, New Mexico, USA: Sedimentary Geology, v. 92, p. 79-96.
Magnani, M.B., Miller, K.C., Levander, A., and Karlstrom, K., 2004, The Yavapai-Mazatzal boundary: A long-lived tectonic element in the lithosphere of southwestern North America: GSA Bulletin, v. 116, p. 1137-1142.
Maldonado, F., and Kelley, S.A., 2009, Revisions to the stratigraphic nomenclature of the Abiquiu formation, Abiquiu and contiguous areas, north-central New Mexico: New Mexico Geology, v.31, no.1, p.3-8.
Maldonado, F., Miggins, D.P., Budahan, J.R., and Spell, T., 2013, Deformational and erosional history for the Abiquiu and contiguous area, north-central New Mexico: Implications for formation of the Abiquiu embayment and a discussion of new geochronological and geochemical analysis: in Hudson M.R., and Grauch V.J.S., eds., New Perspectives on Rio Grande Rift Basins: From Tectonics to Groundwater, GSA Special Papers, v. 494, p. 125-155.
Maldonado, Florian, 2008, Geologic Map of the Abiquiu Quadrangle, Rio Arriba County, New Mexico:U.S. Geological Survey Scientific Investigations Map 2998,1 sheet, scale 1:24,000, 1 pamphlet, 21 p.

Maynard, S. R., Martin, K. W., Nelson, C. J., and Schutz, J. L., 1990, Geology and gold mineralization of the Ortiz Mountains, Santa Fe County, New Mexico: Mining Engineering, v. 42, p. 1007- 1011.

McMillan, M.E., Angevine, C.L., and Heller, P.L., 2002, Postdepositional tilt of the Miocene-Pliocene Ogallala Group on the western Great Plains: Evidence of late Cenozoic uplift of the Rocky Mountains: Geology, v. 30, p. 63-66.

McMillan, M.E., Heller, P.L., and Wing, S.L., 2006, History and causes of post-Laramide relief in the Rocky Mountain orogenic Plateau: GSA Bulletin, v. 118, p. 393-405.

McMillan, N.J., 2004, Magmatic record of Laramide subduction and the transition to Tertiary extension: Upper Cretaceous through Eocene igneous rocks of New Mexico: in Mack G., and Giles, K., eds., The Geology of New Mexico: A Geologic History, New Mexico Geological Society, Special Publication, p. 249-270.

Miall, A. D., Catuneanu, O, Vakarelov, B, and Post, R, 2008, The Western Interior Basin: In Miall, A. D., (ed), The Sedimentary Basins of the United States and Canada: Sedimentary Basins of the World, v. 5, Elsevier Science, Amsterdam, p. 329-362.

Miller, K.G., Browing, J.V., Aubry, M.P., Wade, B.S., Katz, M.E., Kulpecz, A.A., and Wright, J.D., 2008, Eocene–Oligocene global climate and sea-level changes: St. Stephens Quarry, Alabama: GSA Bulletin, v. 120, p. 34-53.

Minor, S.A, Hudson, M.R., Caine, J.S., and Thompson, R.A., 2013, Oblique transfer of extensional strain between basins of the middle Rio Grande Rift, New Mexico: Fault kinematic and paleostress constraints: in Hudson M.R., and Grauch V.J.S., eds., New Perspectives on Rio Grande Rift Basins: From Tectonics to Groundwater, GSA Special Papers, v. 494, p. 345-382.

Moucha, R., Forte, A.M., Rowley, D.B., Mitrovica, J.X., Simmons, N.A., and Grand, S.P., 2008, Mantle convection and the recent evolution of the Colorado Plateau and the Rio Grande Rift valley: Geology, v.36, p.439-442.

O’Keeffe, K.A., 2014, Geometry and kinematics of the Cañones Fault and the effects of lithology on the distributions of strain within the Cañones Fault damage zone: Master’s thesis, University of Houston, Houston, Texas, 90 p.

Pigg, K.B., and Devore, M.L., 2010, Floristic composition and variation in late Paleocene to early Eocene floras in North America: Bulletin of Geosciences, v. 85, p. 135-154.

Rasskazov, S.V., Yasnygina, T.A., Fefelov, N.N., and Saranina, E.V., 2010, Geochemical evolution of middle–late Cenozoic magmatism in the northern part of the Rio Grande Rift, Western United States: Russian Journal of Pacific Geology, v. 4, p. 13-40.

Ridgway, K.D., Trop, J.M., and Jones, D.E., 1999, Petrology and provenance of the Neogene Usibelli group and Nenana gravel: Implications for the denudation history of the central Alaska Range: Journal of Sedimentary Research, v. 69, p. 1262-1275.

Roberts, G.G, White, N.J., Martin-Brandis, G.L., and Crosby, A.G., 2012, An uplift history of the Colorado Plateau and its surroundings from inverse modeling of longitudinal river profiles: Tectonics, v. 31, TC4022.

Roca, X., and Nadon, G.C., 2007, Tectonic controls on the sequence stratigraphy of nonmarine retroarc foreland basin fills: Insights from the upper Jurassic of central Utah, USA: Journal of Sedimentary Research, v. 77, p. 239-255.

Sauer, R. R., 1999, Petrochemistry and geochronology of plutons relative to tectonics in the San Pedro-Ortiz porphyry belt, New Mexico: M.S. thesis, Boulder, University of Colorado, 115 p.

Saylor, J., DeCelles, P., Gehrels, G., Murphy, M., Zhang, R., and Kapp, P., 2010, Basin formation in the High Himalaya by arc-parallel extension and tectonic damming: Zhada Basin, southwestern Tibet: Tectonics, v. 29, p. TC1004.

Scholle, P.A., 2003, Geologic Map of New Mexico: New Mexico Bureau of Geology and Mineral Resources, scale 1:500,000.

Seager, W.R., Mack, G.H., and Lawton, T.F., 1997, Structural kinematics and depositional history of a Laramide uplift-basin pair in southern New Mexico: Implications for development of intraforeland basins: GSA Bulletin, v. 109, p. 1389-1401.

Smith, G. A., Moore, J. D., and Mcintosh, W. C., 2002, Assessing roles of volcanism and basin subsidence in causing Oligocene-lower Miocene sedimentation in the northern Rio Grande Rift, New Mexico: Journal of Sedimentary Research, v. 72, p. 836-848.

Smith, G.A., 2000, Recognition and significance of streamflow-dominated piedmont facies in extensional basins: Basin Research, v. 12, p. 399-411.

Smith, G.A., 2004, Middle to late Cenozoic development of the Rio Grande Rift and adjacent regions in northern New Mexico: in Mack G., and Giles, K., eds., The Geology of New Mexico: A Geologic History, New Mexico Geological Society, Special Publication, p. 331-358.

Smith, G.A., and Huckell, B.B., 2005, The geological and geoarchaeological significance of Cerro Pedernal, Rio Arriba County, New Mexico: New Mexico Geological Society Guidebook 56, Geology of the Chama Basin, p. 425-431.

Smith, G.A., Moore, J.D., and McIntosh, W.C, 2002, Assessing roles of volcanism and basin subsidence in causing Oligocene-lower Miocene sedimentation in the northern Rio Grande Rift, New Mexico, U.S.A., Journal of Sedimentary Research, v.72, No. 6, p. 836-848.

Smith, R. L., Bailey, R. A., and Ross, C. S., 1970, Geologic Map of the Jemez Mountains, New Mexico: U.S. Geological Survey, Miscellaneous Investigation Map 1-57 1, scale I: 125,000.

Stearns, C. E., 1953, Early Tertiary volcanism in the Galisteo-Tongue area, north central New Mexico: American Journal of Science, v. 25 1, p. 415-452.

Sun, M.S. and Baldwin, B., 1958, Volcanic Rocks of the Cienega Area, Santa Fe County, New Mexico: New Mexico Bureau of Mines and Mineral Resources, Bulletin 54, 80 p.

Thompson, R. A., Johnson, C. M., and Mehnert, H. H., 1991 , Oligocene basaltic volcanism of the northern Rio Grande Rift; San Luis Hills, Colorado: Journal of Geophysical Research, v. 96, p. 13,577-13,592.

Timmer, R., Woodward, L., Kempter, K., Kelley, S.A., Osburn, G.B., Osburn, M., Buffler, R., and Lawrence, J.R., 2006, Preliminary Geologic Map of the Jarosa

Quadrangle, Rio Arriba County, New Mexico: New Mexico Bureau of Geology and Mineral Resources, Open-File Digital Geologic Map OF-GM 128, scale 1:24,000. 1 pamphlet, 27 p.

Tomlinson, D.W., Copeland, P., Murphy, M.A., and Lapen, T.J., 2013, Oligocene shortening in the Little Burro Mountains of southwest New Mexico: Rocky Mountain Geology, v. 48, p. 169-183.

Vakarelov, B.K., and Ainsworth, R.B., 2013, A hierarchical approach to architectural classification in marginal-marine systems: Bridging the gap between sedimentology and sequence stratigraphy: AAPG Bulletin, v. 97, p. 1121-1161.

Vazzana, M.E., and Ingersoll, R.V., 1981, Stratigraphy, sedimentology, petrology, and basin analysis of the Abiquiu Formation (Oligocene-Miocene), north-central New Mexico: GSA Bulletin, v.92, Part I, p. 990-992.

Wallace, A. R., 1995, Cenozoic rift-related sedimentation and faulting, northern Culebra Range, southern Colorado: New Mexico Geological Society, 46th Field Conference, Guidebook, p. 147-153.

Wawrzyniec, T.F., Geissman, J.W., Melker, M.D., and Hubbard, M., 2002 Dextral shear along the eastern margin of the Colorado Plateau: A kinematic link between Laramide contraction and Rio Grande rifting (Ca. 75–13 Ma): The Journal of Geology, v. 110, p. 305-324.

Wells, N.A., 2000, Are there better alternatives to standard rose diagrams?: Journal of Sedimentary Research, v.70, p.37-46.

Weltje, G.J., 2006, Ternary sandstone composition and provenance: an evaluation of the ‘‘Dickinson model’’: Geological Society of London, Special Publications, v. 264, p. 79–99.

Whittaker, A.C., Cowie, P.A., Attal, M., Tucker, G.E., and Roberts, G.P., 2007, Bedrock channel adjustment to tectonic forcing: Implications for predicting river incision rates: Geology, v. 35, p. 103-106.

Wohl, E.E., Anthony, D.J., Madsen, S.W., and Thompson, D.M., 1996, A comparison of surface sampling methods for coarse fluvial sediments: Water Resources Research, v. 32, p. 3219-3226.

WoldeGabriel, G., Koning, D.J., Broxton, D., and Warren, R.G., 2013, Chronology of volcanism, tectonics, and sedimentation near the western boundary fault of the Española Basin, Rio Grande Rift, New Mexico: in Hudson M.R., and Grauch V.J.S., eds., New Perspectives on Rio Grande Rift Basins: From Tectonics to Groundwater, GSA Special Papers, v. 494, p. 221-238.

WoldeGabriel, G., Laughlin, A. W., Dethier, D. P., and Heizler, M., 1996, Temporal and geochemical trends of lavas in White Rock Canyon and the Pajarito Plateau, Jemez volcanic field, New Mexico, USA: New Mexico Geological Society, 47th Field Conference, Guidebook, p. 25 1-262.

Woodward, L.A., 1974, Tectonics of central-northern New Mexico: New Mexico Geological Society Guidebook 25, Ghost Ranch (Central-Northern New Mexico), p. 123-129.

Woodward, L.A., Martinez, R., DeChene, H.R., Schumacher, O.L., and Reed, R.K., 1974, Precambrian rocks of the southern Sierra Nacimiento New Mexico: New

Mexico Geological Society Guidebook 25, Ghost Ranch (Central-Northern New Mexico), p. 95-99.

Woodward, W.A., Kaufman, W.H., and Anderson, J.B., Nacimiento Fault and related structures, northern New Mexico: GSA Bulletin, v. 83, p. 2383-2396.

Yin, A., and Ingersoll, R.V., 1997, A model for evolution of Laramide axial basins in the southern Rocky Mountains, U.S.A., International Geology Review, v. 39, p. 1113-1123.

Zachos, J., Pagani, M., Sloan, L., Thomas, E., and Billups, K., 2001, Trends, rhythms, and aberrations in global climate 65 Ma to present, Science, v. 292, p. 686-693.

Zahid, K.M., and Barbeau, JR., D.L., 2011, constructing sandstone province and classification ternary diagrams using and electronic spreadsheet: Journal of Sedimentary Research, v. 81, p. 702-707.

Zimmerer, M.J., and McIntosh, W.C., 2012, The geochronology of volcanic and plutonic rocks at the Questa caldera: Constraints on the origin of caldera-related silicic magmas: GSA Bulletin, v. 124, p. 1394-1408.